2015-11

Investigation of Photopolymer-based Holographic Optical Elements for Solar Applications

Hoda Akbari
Technological University Dublin, hodaakbari@gmail.com

INVESTIGATION OF PHOTOPOLYMER-BASED HOLOGRAPHIC OPTICAL ELEMENTS FOR SOLAR APPLICATIONS

Hoda Akbari, B.Sc.

A thesis submitted for the degree of Doctor of Philosophy to the

Dublin Institute of Technology

Supervisors:

Dr. Suzanne Martin, Dr. Izabela Naydenova

Centre for Industrial and Engineering Optics,

School of Physics,

College of Sciences and Health

Dublin Institute of Technology

November 2015

ABSTRACT

The aim of this research was to explore the potential of photopolymer Holographic Optical Elements (HOE) for use in the collection of light from a moving source, such as the sun, and its direction into a fixed detector/convertor for application in solar concentrators. In order to increase the acceptance angle and the wavelength range of operation of the holographic device, low spatial frequency holographic recording was explored. The challenge was to record high diffraction efficiency HOEs at this spatial frequency, since it requires a material with relatively fast monomer diffusion. The acrylamide-based photopolymer developed at the Centre for Industrial and Engineering Optics has been selected, because it has previously shown such diffusion properties. In order to achieve large acceptance angle, the theoretical modelling of the angular and wavelength selectivity of the HOEs was carried out. The theoretical results confirmed that the gratings with just a few hundred lines per mili meter were of most interest in this study because the selectivity is lower.

The next challenge was to fabricate off-axis holographic spherical and cylindrical lenses with large range of operation in the photopolymer. This was achieved by stacking a number of gratings and focusing elements on top of each other. The stacked devices were characterised in two ways: (i) the regular Bragg diffraction characteristics of the stack devices were measured (ii) a set up was constructed to analyse their performance in a non-tracking system with a moving source and fixed detector/converter. The results show significant improvement for the collection of light from the higher angles.

The effect of using the HOE elements with unpolarised light has also been explored. For the first time, the photopolymer was used to fabricate a combined element with symmetrically arranged off axis lens elements in order to maximise the collection area and avoid unwanted diffraction of light away from the solar cell. The combined device was tested using a solar simulator and c-Si solar cell. The maximum 60% increase was achieved.

DECLARATION

I certify that this thesis which I now submit for examination for the award of **Doctor of Philosophy**, is entirely my own work and has not been taken from the work of others, save and to the extent that such work has been cited and acknowledged within the text of my work.

This thesis was prepared according to the regulations for postgraduate study by research of the Dublin Institute of Technology and has not been submitted in whole or in part for another award in any other third level institution. The work reported on in this thesis conforms to the principles and requirements of the DIT's guidelines for ethics in research.

The Dublin Institute of Technology has permission to keep, lend or copy this thesis in whole or in part, on condition that any such use of the material of the thesis is duly acknowledged.

Candidate: **Hoda Akbari**

Signature _____ Date _____

KNOWLEDGEMENTS

I would like to take this opportunity to thank a number of people, who gave suggestions, encouraged me with their valuable advices and assistance.

First and foremost I would like to express my deepest appreciation to my supervisors, Dr. Suzanne Martin and Dr. Izabela Naydenova, for all of their endless support, knowledge and encouragement throughout the past four years.

I would like to express my gratitude to say a huge thank you to Dr. Sarah Mc Comark, Dr. Hind Ahmed and Dr. Manus Kennedy who have always been extremely helpful with their support and knowledge and help me through this research.

I'm very grateful to all my colleagues and friends the Centre for Industrial and Engineering Optics, especially Prof. Vincent Toal, Dr. Emilia Mihaylova, Dr. Jacinta Brown, Dr. Dervil Cody, Dr. Mohesh Moothanchery, Dr. Lina Persechini, Dr. Monika Zawadzka, Dr.Bakary Diarra, Dr. Subhash Chandra, Ms. Amanda Creane, Ms. Tatsiana Mikulchyk, Ms. Sabad e Gul and Mr Sanjay Keshri for their technical advice and assistance.

I would like to thank all staff and researchers in the FOCAS Research Institute, School of Physics and Dublin Energy Lab for their full cooperation and help, and providing excellent research facilities.

Also I would like to acknowledge the DIT Fiosraigh Self-funded Scholarship Scheme, School of Physics and the COST action for providing travel grants.

I would like to say a big thank you to all of the great people that I have met and friends I have made in the past ten years. Especial thanks toAbed Motaghi, Fatemeh Karimi,

Gary Carey, Ayda Esfandyari and Aritra Gosh and many, many more friends and family which I cannot list all the names here.

Last but not least, I would like to thank my parents, Rostam and Afsar, for their love and support throughout my life. Thank you both for giving me strength to reach for stars and chase my dreams. I would specially like to say big thanks to my amazing brothers, Hamid and Amir, who provided me with much needed diversion, and constant support over the course of my studies, I will always be indebted.

This thesis is only begging of my journey ….

TABLE OF CONTENTS

TABLE OF FIGURE

CHAPTER SUMMARY

Chapter 1 describes the basic principles of holographic recording. The different types of recording media available for holography are also discussed, as well as outlining some of the main applications of holography which are of interest.

Chapter 2reviews the development of Holographic Optical Elements (HOEs) and outlines the main motivation and aims of this research.

Chapter 3 describes the theoretical simulations of the variation of the diffraction efficiency of gratings with angle and wavelength under different conditions and modelling results are presented.

Chapter 4describes the recording set up and the measurement techniques used to fabricate and characterize low spatial frequency holographic gratings and holographic optical elements. Optimum recording conditions are identified.

Chapter 5presentthe characterization of spherical/cylindrical HOEs is in terms of diffraction efficiency, angular selectivity and wavelength selectivity.

Chapter 6studies devices fabricated in photopolymer by multiplexing a small number of high diffraction efficiency gratings/HOEs to give a larger angular working range , This chapter also deals with issues around using gratings as a device in solar collection including polarization, multiplexing, directing onto a single location.

Chapter 7tests the holographic concentrators in use with silicon solar cells and compares the performance of solar cells with and without HOEs in place.

Chapter 8summarises the main conclusions from the PhD research, and discuss some potential areas for future work. The outputs resulting from the dissemination of the research are also presented.

1 Holography

1.1 General introduction to holography

The technique of holography, records the complete phase information of the light scattered by an object as well as the intensity distribution. In photography only the intensity distribution of the light from original object is recorded, in other words, information about the relative optical paths to different parts of the object is lost and this is the reason why a photograph of a three dimensional image appears as two dimensional [1].

The roots of holographic imaging were started in X-ray crystallography by Wolfke in 1920 [2] and were continued by Bragg [3,4]. One of Bragg's achievements was to form the image of the structure of the crystal lattice by recording the diffraction pattern which guides the development of the Bragg X-ray microscope. Since unwanted phase information was also obtained his method was limited. In 1948, Denis Gabor carried on Bragg's work [5–8]. His aim was to obtain an improvement in the resolution in electron microscopy. Gabor suggested a new method to obtain the image of an object from the diffraction pattern produced by the object. His method is also known as in-line holography. He was awarded a Nobel Prize for his work in year 1971.

After Gabor, in mid 1960's, Leith and Upatnieks successfully solved the problem for separating the twin image observed in in-line holography by inventing the off-axis reference beam technique [9,10]. After the invention of the laser by T.Maiman in 1960 [11], they have successfully demonstrated that three-dimensional image can be generated by illuminating a photographic plate by using laser light. At the time, laser

was first powerful source of coherent light in order to record the holograms of an object with considerable depth [12].

1.2 Holographic process

A hologram forms when the photosensitive medium is exposed to an interference pattern formed by mixing the object beam and the reference beam. After recording, when the hologram is illuminated with the same reference beam, the diffracted light will be diffracted in such a way that the object wave is reproduced. This is because; during recording the optical properties of the photosensitive medium vary depending on the intensity of the interference pattern.

The holographic process can be divided in two steps; the first step is when a hologram is recorded using a reference wave coherent with the light scattered or diffracted by an object, so that information about the amplitude and phase of these waves is retained; then from this recorded interference pattern an image of the original object can be reconstructed using just the reference wave [13]. There are many types of holograms, depending on the recording geometry they can be classified as transmission or reflection holograms, depending on the thickness of the recording medium relative to the spatial frequencies that are recorded they can be divided as thin or thick holograms and depending on whether amplitude or phase information is recorded they are known as amplitude or phase holograms.

1.2.1 Transmission holograms

In a transmission hologram an object beam and a reference beam are incident on the holographic photo sensitive medium from the same side. The image can be reconstructed when the object beam is blocked and the hologram is illuminated with the same reference beam. In slanted transmission grating, the two recording beams are incident at different angles with respect to the recording layer's surface and as a result the interference fringes are not perpendicular (nor parallel) to the surface of the recording medium; whereas in unslanted holographic gratings, the two beams have equal incident angles and the interference fringes are perpendicular to the surface of the recording medium. Transmission holographic gratings have been used in this research since they have several advantages to be used in solar application for example they can be designed to re-direct and focus the light with high efficiency. Due to the fact that the reference wave must be transmitted through the hologram in order for the image to be reconstructed, this type of holograms are called transmission hologram.

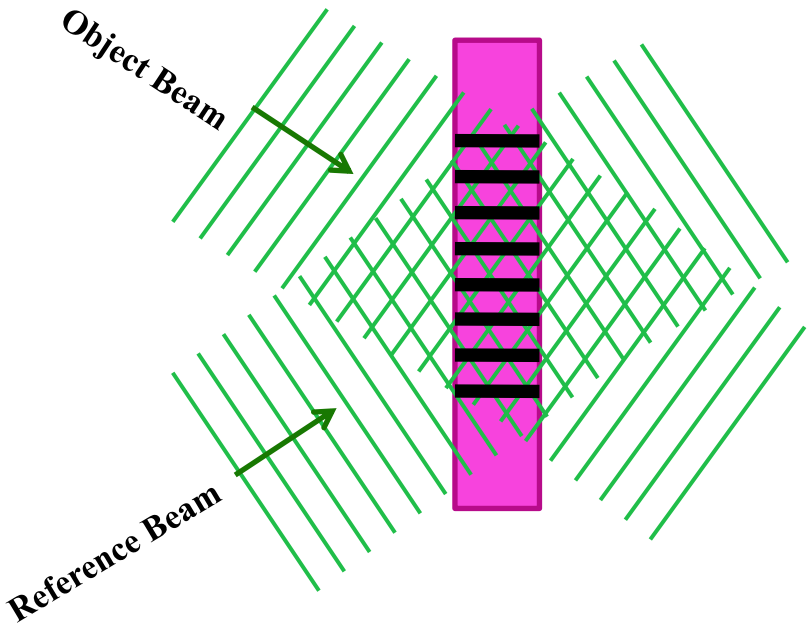

Figure 1-1 Recording of a transmission hologram in a photosensitive medium

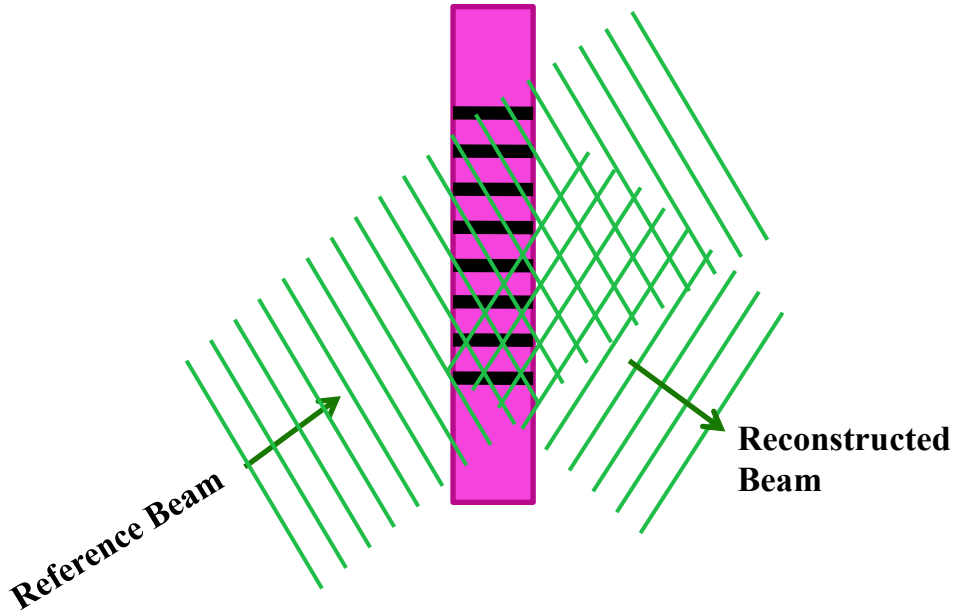

Figure 1-2 Reconstruction from a transmission hologram recorded in a photosensitive medium

1.2.2 Reflection holograms

In a reflection hologram an object beam and a reference beam interfere on the holographic photosensitive medium from the opposite sides. Thus, the interference fringes are formed nearly parallel to the surface of the recording medium. During the reconstruction process, the object beam is blocked and the hologram is illuminated by light from the same side of the photo sensitive medium as the viewer. A hologram recorded in reflection mode can produce a visible image when reconstructed using the white light since they can act as spectral filters. Reflection mode recording can be useful in solar applications where reflective elements are needed and where there is a need to separate some spectral components. In photopolymer material the efficiency tends to be lower than for transmission gratings mainly because of the high spatial frequency.

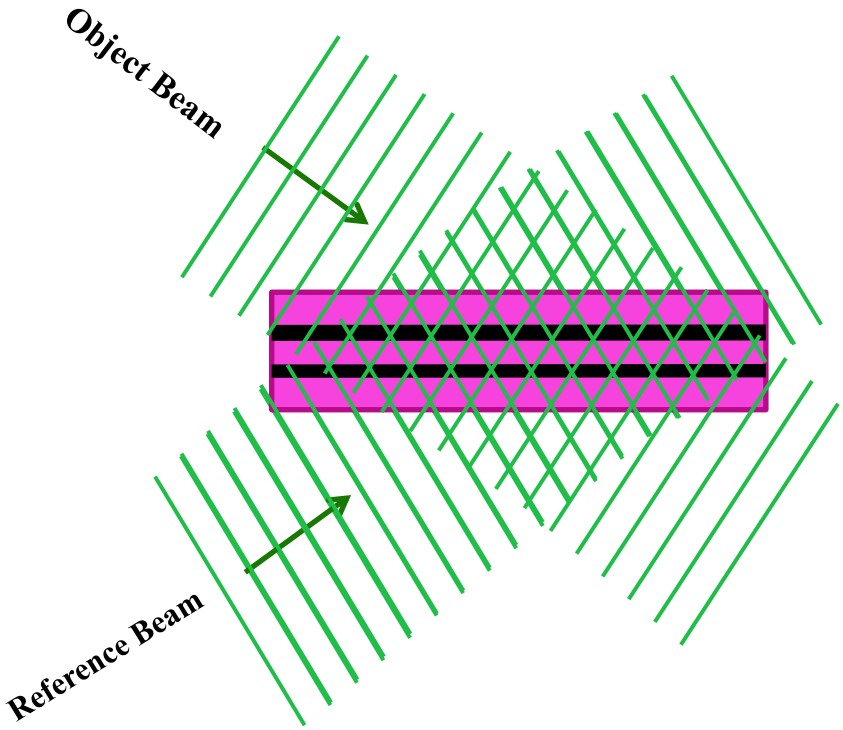

Figure 1-3 Recording of reflection hologram in photosensitive medium

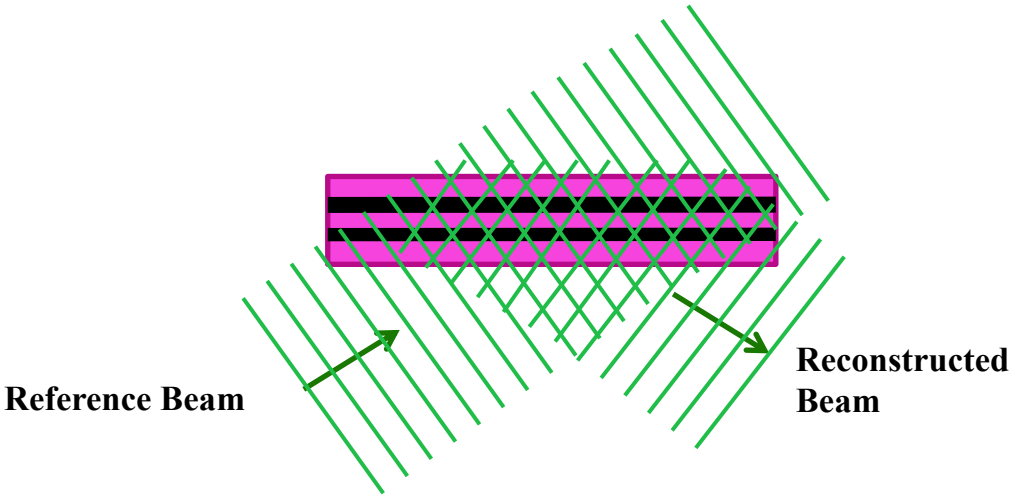

Figure 1-4 Reconstruction from reflection hologram recorded in photosensitive medium

1.2.3 Thin holograms

Holograms can be classified as thin (plane) or thick (volume) holograms depending on the thickness of the recording materials and the fringe spacing of the recorded gratings.

Usually if the thickness of the recording material is smaller than the average spacing of the interference fringes, the holograms are known as thin holograms.

Parameter Q can be used in order to classify whether a hologram is thin or thick, parameter Q can be defined by equation 1.1:

$$Q = \frac{2\pi\lambda d}{n_0 \Lambda^2} \qquad \text{Equation 1.1}$$

Where λ is the wavelength, d is the thickness of the recording medium, n_0 is the refractive index of the recording material and Λ is the fringe spacing.

Therefore, gratings with the value of Q<1 are considered as thin while the grating with the value of Q>1 are considered thick holograms [1,7].

1.2.4 Thick holograms

When analysing the diffraction of light by thick gratings, it is necessary to consider that the diffraction efficiency can be very high and the incident wave intensity decreases, as they propagate through the grating. The coupled wave theory was developed by Kogelnik to solve this problem [14] and gives the angular and wavelength selectivities for all types of holograms, transmission or reflection, amplitude or phase, with slanted or unslanted fringe planes.

A particular interest is the ability of thick holograms to convert light into the useful reconstructed wave (characterized by the diffraction efficiency) and the angular dependence of diffraction efficiency as the incident light deviates from the Bragg angle.

Coupled wave theory is based on the assumption that monochromatic incident light at the Bragg angle is S and P polarized. Only two light waves travel through the gratings; the incident reference wave, and the outgoing signal wave, which obey the Bragg condition[14]. Kogelnik predicts the relationship between incident angle and diffraction efficiency in thick gratings, for specific conditions [14].

For gratings that are not over-modulated there is a maximum at the Bragg angle and the width of the peak depends on grating thickness and spatial frequency.

Interaction of light with the grating fringes will occur as it travels through the volume grating. There are several factors which determine how much light is diffracted into each order, including grating thickness, fringe contrast, and whether the Bragg condition is met [15]. Maximum diffraction efficiency will be obtained when the reconstruction beam is incident on the grating at a particular angle of incidence θ, called the Bragg angle. In the case of unslanted transmission grating, the Bragg condition is given by equation 1.2 [16,17]:

$$m\lambda = 2\Lambda \sin\theta \qquad \text{Equation 1.2}$$

where θ is the Bragg angle defined as the angle that the incident beam makes with the fringe plane in the recording medium. For thick gratings m=1.

Kogelnik theory yields equations which can be used to relate the diffraction efficiency of the grating to a number of parameters. Equation 1.3 presents the diffraction

efficiency, η, of unslanted transmission grating when it is illuminated at the Bragg angle:

$$\eta = \sin^2\left[\frac{d\pi n_1}{\cos\theta_1 \lambda}\right] \qquad \text{Equation 1.3}$$

Where d is grating thickness, n_1 is refractive index modulation, θ_1 is the Bragg angle of incidence and λ is the wavelength of the reconstructed beam.

According to Kogelnik's theory, the off-Bragg parameter (ξ) can be calculated using equation 1.5, allowing us to model how the diffraction efficiency varies with angle of incidence, near the Bragg angle (equation 1.4). This allows us to observe how grating thickness and spatial frequency affect the angular selectivity of an individual grating:

$$\eta = \frac{\sin^2\sqrt{\left(\xi^2 + \upsilon^2\right)}}{\left(1 + \frac{\xi^2}{\upsilon^2}\right)} \qquad \text{Equation 1.4}$$

The parameters ξ and υ are defined as:

$$\xi = \Delta\theta \frac{kd}{2} \qquad \text{Equation 1.5}$$

$$\upsilon = \frac{\pi n_1 d}{\lambda \cos\theta} \qquad \text{Equation 1.6}$$

where d is the thickness of the grating, n_1 is the refractive index modulation; λ is the wavelength of the reconstructed beam; Δθ is the deviation from the Bragg angle and **k** is interference fringe vector, normal to the fringes with a magnitude $k = 2\pi$/spatial period. Equation 1.4 will be used in chapter 3 for the theoretical modelling of angular selectivity of the diffracted elements.

Thick holograms have a narrow angular bandwidth and a narrow spectral bandwidth. They can be used to redirect and focus the incident beam. Thin holograms tend to have lower diffraction efficiency with a large angular bandwidth and spectral bandwidth and

they can be used in some applications requiring a broader angular bandwidth [18]. For solar applications where a large spectral and angular bandwidth is needed a very 'thin' grating with very high efficiency would be the ideal.

1.2.5 Amplitude and phase holograms

Holograms can be categorised as amplitude or phase holograms depending on the type of changes of the photosensitive recording medium during the recording of the hologram. The hologram is amplitude hologram when the amplitude transmittance depends on the recording intensity, where in phase hologram the thickness or refractive index of the hologram is depending on the recording intensity. Amplitude holograms have several disadvantages for example they have lower efficiency compared to phase holograms. This is because amplitude holograms rely on absorption of the light therefore some part of the energy of the reading beam must be lost during the reconstruction. This can also cause heating.

In this research, most photopolymer devices fall into the categories of thick, phase transmission holograms.

1.3 Holographic recording materials

There are several types of holographic recording materials such as silver halide emulsions, dichromated gelatin, photoresists, photochromics, photothermoplastics, photodicroics, photorefractives and photopolymers. The recording material is chosen to best fit the requirements of the holographic application. Ideal holographic recording materials must be sensitive to the recording wavelength, achieve high spatial resolution,

have low noise, have a linear transfer response, large dynamic range, good environmental stability, self-developing and be relatively inexpensive [1,18].

1.3.1 Silver Halide Emulsion

Silver Halide materials are the oldest and the most popular holographic recording media because of their advantages [1,19–21]; they are highly sensitive with low scattering ; they can be sensitised for a number of different recording wavelengths, have high stability after recording and have relatively long pre-recording shelf life. These materials can be used to record phase, amplitude and colour holograms. The main disadvantage of this material is that it requires wet processing, which can introduce variations; they are not re-usable and are relatively expensive which make them unsuitable for certain applications.

Kim et al. used Silver Halide Sensitized Gelatine (SHSG) emulsion from Slavich, commercial manufacturing company, to record transmission holographic optical elements (HOEs). High quality and large format HOEs can be produced in SHSG by using a laser with wavelengths anywhere within the visible spectrum [22].

The dependence of wavelength selectivity of holographic solar concentrators recorded on silver halide plate (PFG-01) has been investigated by Ghosh et al.[23].The theoretical results are compared with experimental results for a range of refractive index modulation. The results show that change in depth of refractive index modulation of holocons cause the exhibits maximum diffraction efficiency in various wavelengths of the spectrum. Advantages of using Holocons for concentrated photovoltaic system due to twin function of dispersion as well as concentration are explored.

1.3.2 Dichromated Gelatin (DCG):

Dichromated gelatin has been used in holography since the late 1960s. It's known as an almost ideal recording material for volume phase holograms since it has the following advantages: large refractive index modulation capability (as large as 0.08), high diffraction efficiency, high resolution, low noise and high optical quality [24]. DCG materials are suitable for reflection holography since they can achieve spatial resolutions as high as 5000 l/mm. However the main drawback of DCG is that the layer fabrication can be complicated and working with this material is time consuming as wet processing is required before and after recording.

Gelatin is water absorbing and has been used in water vapor sensors [25], it can swell or shrink depending on the level of humidity in the environment.

Holograms recorded in dichromated gelatin (DCG) are usually sealed with a glass plate and an epoxy glue to protect the holograms from moisture in the environment. A method to improve the stability of sealed DCG holograms is proposed by Liu et al. [26]. Investigation of wavelength properties of the sealed DCG holograms has been carried out by exposing to different temperature and humidity environments conditions.

Number of on-axis and off-axis cylindrical holographic lens recorded in dichromated gelatin emulsion (PFG-04) and their angular and chromatic selectivity is described by Bañares-Palacios et al. [27]. The performance of a volume transmission holographic solar concentrator has been reported [27]. It was found that off-axis lens has a better performance when the incident light goes out of the Bragg condition however it has higher chromatic dispersion. The diffraction efficiency lower than 40%, was achieved. The optical concentration ratio was measured 1.94 and 1.67 for on-axis and off-axis lens respectively.

1.3.3 Photothermoplastics

Thermoplastic materials have been used in holographic interferometry for non-destructive testing applications or can be used to record surface relief holograms when it is combined with a photoconductor and charged to a high voltage. On exposure to heat, the thermoplastic material is softened. The main advantage of these materials is that they don't require wet processing, can be re-used several times and also they have practically high sensitivity over the whole visible spectrum, however they are expensive to purchase and less available commercially in recent times. The material can then be deformed via a spatially varying electrostatic field. When it is cooled, the pattern is fixed and a surface modulation is achieved. The holograms can be erased simply by heating the thermoplastic to a higher temperature [28,29]. Currently, American company "Tavex" is the commercial producer of thermoplastic cameras which included the holograms with area of 32 x 32 mm. Used holograms has special features such as: spectral sensitivity between 400-800 nm, capability of 3000 write erase cycles, shelf life of more than 10 years [30,31]. To the best of my knowledge, this type of material has not been used in solar concentrators. This can be explained by the fact that in this material the hologram will be erased on the exposure to the high temperature.

1.3.4 Photoresists

Photoresists are thin light sensitive organic films which produce a surface relief hologram on exposure to UV and blue light. They are widely used in the electronics industry because of their ability to produce very small surface features. Positive and negative are the two types of photoresist. For negative photoresists, the exposed areas become insoluble and unexposed areas are dissolved away by a developer after

exposure. Long exposure time is required for negative photoresist material in order to be sure that the exposed photoresist adheres to the substrate during development. Positive photoresists are preferable where the exposed area is soluble and unexposed area is dissolved during the development. The main disadvantage of these materials is the need for chemical development. A spatial resolution of up to 1500 l/mm is achievable and the scattering is low [32,33]. To the best of my knowledge, this type of material has not been used in solar application.

1.3.5 Photochromics

Photchromics have a property of reversible colour change when it is illuminated with light i.e. the optical density and hence the absorption of the material is modulated [1,30,33–36]. This allows them to record amplitude holograms. Although this effect is reversible, the lifetime of these materials is limited. They can achieve high resolution, they are self-developed and can be re-used several times but low sensitivity and low diffraction efficiencies are the main drawbacks of these material [1,30,37–39].

1.3.6 Photopolymer

Photopolymers can be used to record volume phase holograms which have many applications among which are real-time holographic interferometry [40], holographic optical elements [41–43] and holographic data storage [44–46]. They are one of the most promising material for holographic applications due to their properties such as relatively high sensitivity, real-time image development, self-processing, large dynamic range, good image stability, high diffraction efficiency and relatively low cost; however

disadvantages include the relatively short shelf life of the prepared materials and the fact that the material cannot be recycled [47–49]. The recording material used in this research is self-processing acrylamide-based photopolymer which has been developed at the Centre for Industrial and Engineering Optics. Due to the fact that the present work is using acrylamide-based photopolymer materials, their recording process are described in more details below.

The main composition of an acrylamide-based photopolymer consists of two monomers (Acrylamide and NN'methylenebisacrylamide), an electron donor (Triethanolamine TEA), a dye sensitizer (Erythrosine B, sensitive at 532nm) and a binder (Polyvinylalcohol) which keeps all of the components suspended [50–52].

The main advantages of acrylamaide-based photopolymer compared to other recording materials which has been mentioned before is that there are no further steps such as heating or illuminating with UV-light required after the recording process and also all the components in acrylamide-based photopolymer are water soluble.

1.4 Photopolymerisation

This process consists of three steps: initiation, propagation and termination. In this reaction photons of light are absorbed by photosensitive dye molecules and it will make a dye molecule excited to a singlet energy state [18].

$$DYE + h\upsilon \rightarrow DYE_1 *$$ (Excited Singlet state)

The energy of the molecule in an excited singlet state can be released by returning quickly back to the ground state and emitting light of a longer wavelength via fluorescence process, or by energy transfer to another molecule (electron donor such as, TEA), this process called fluorescence quenching.

$$DYE *_1 \rightarrow DYE + h\upsilon$$ (Fluorescence)

$$DYE *_1 + TEA \rightarrow DYE + TEA$$

$$DYE *_1 + TEA \rightarrow DYE + TEA *$$ (Fluorescence quenching)

The exited dye molecule can be converted to a more stable triplet state dye molecule through inter system crossing.

$$DYE *_1 \rightarrow DYE *_3$$ (Inter-system crossing)

The produced triplet state dye molecule can reacts with the electron donor (TEA) to produce a free radical.

$$DYE *_3 + TEA \rightarrow DYE \bullet + TEA \bullet$$ (Free radical production)

These radicals can react with the monomers (M) to initiate the polymersation process.

$$TEA \bullet + M \rightarrow TEA - M \bullet$$ (Initiating step)

The growing chain continues via propagation when this radical monomer attacks another monomer molecule.

$$TEA-M\bullet \rightarrow TEA(M)_2\bullet$$ (Propagation step)

The chain size will continue increasing until a termination process occurs. The termination can occur due to two processes:

$$TEA-M_n\bullet + TEA-M_m\bullet \rightarrow TEA-(M)_{nm}-TEA$$ (Combination)

$$TEA-M_n\bullet + TEA-M_m\bullet \rightarrow TEA-(M)_n + TEA-(M)_m$$ (Disproportionation)

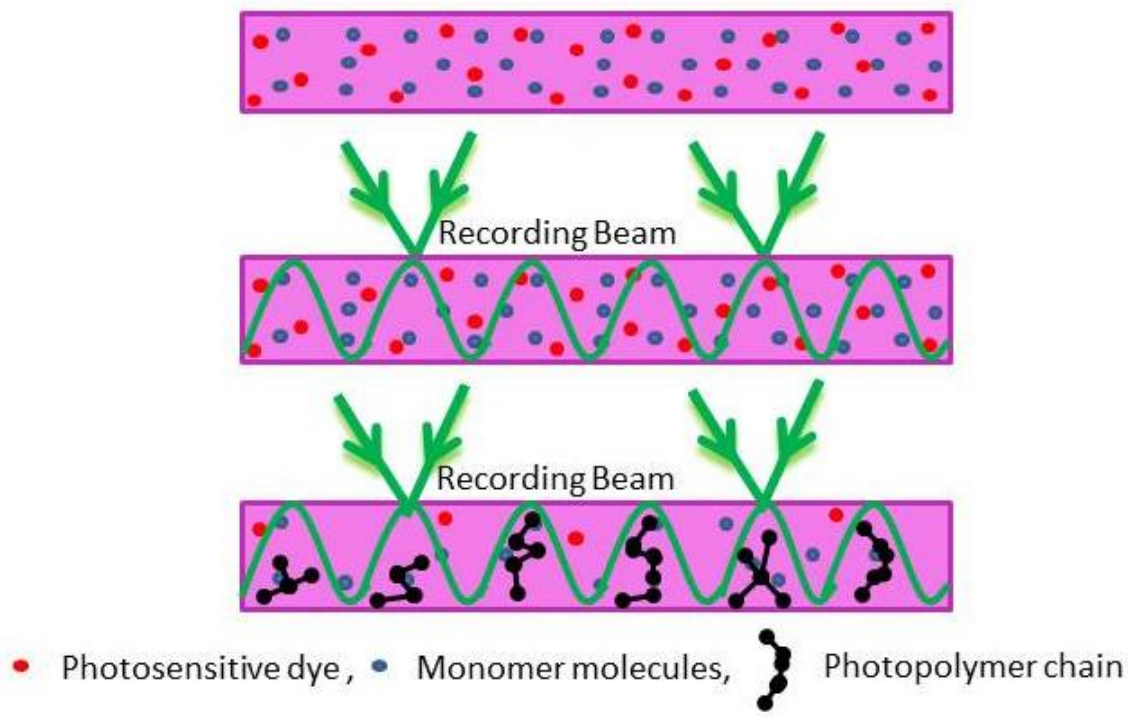

Figure 1-5 Photopolymer recording process

Figure 1.5 shows the photopolymer recording process, initially in a photopolymer layer there is uniform distribution of photosensitive dye and monomer molecules throughout the volume. When it is exposed to the light pattern, the dye absorbs the light in the bright fringes, the monomer photopolymerisation begins. This involves the monomer molecules linking together and forming polymer chains in the exposed area. Diffusion processes also occur and a refractive index change results.

Currently accepted models describe the recorded pattern formation as a result of changes in the density and the molecular polarizability, which accompany polymerisation. The magnitude of the refractive index change is also dependent on the achieved chain length, which depends on the rate at which the photons are delivered. Higher recording intensity leads to faster polymerisation rate and the formation of shorter polymer chains, while lower recording intensities result in longer chains[53].

The diffusion models [54–60]predict that the dynamics and properties of the recorded holographic grating (refractive index spatial profile and modulation) are determined by the balance between the polymerisation rate and monomer diffusion rate. Both parameters are strongly dependent on the chemical composition of the photopolymer system. Information about their ratio is necessary for the determination of the optimal conditions for holographic recording, especially at the low spatial, frequencies used in this work.

Two different regimes of holographic recording at given spatial frequency can be distinguished with respect to the ratio of the diffusion and polymerisation rate. When the polymerisation rate is slower than the diffusion rate, the grating profile closely resembles the sinusoidal recording interference pattern and a high saturation value of the refractive index modulation can be achieved. When the monomer diffusion rate is slower than the polymerisation rate deviation from the sinusoidal profile of the grating

is observed and the diffraction efficiency at saturation is lower. The monomer diffusion rate is characteristic for a given photopolymer system. In a simplified picture when the diffusion dependence on the degree of polymerization is not considered, the diffusion time is constant at given spatial frequency. The polymerisation rate, however, depends on the recording intensity. By changing the recording intensity one can control the polymerisation rate and in such a way to switch between the two regimes – relatively slow diffusion compared to the polymerisation rate at high intensity and relatively fast diffusion when the intensity and the polymerisation rate are low. Thus in order to achieve high diffraction efficiency at low spatial frequency of recording one expects that relatively low recording intensity will be required.

In materials in which the diffusion of monomers is very slow, the response at low spatial frequency will be very limited even with low intensity of recording.

The acrylamide based photopolymer presented in this thesis is characterised by fast diffusion rate[61] and this allows for the recording of high diffraction efficiency gratings even in the low spatial frequency range of 100-300 l/mm. As it has been already established, such low spatial frequencies are preferable when devices with larger acceptance angle (broad angular and wavelength selectivity curves) are sought.

1.5 Major applications of holography

Holography is huge field for many years and the range of holographic applications has extended by the technique of producing three dimension images of applications in display holograms [62], data storage [44,63], holographic optical elements [24,40,41,64–67], LCD displays [68–70], Head-up displays (HUDs) [71,72], holographic optical tweezers [73–75] , holographic sensors [76–78], optical Metrology and industrial applications [79,80] and many other applications. Some of the applications are briefly described below.

1.5.1 Display holograms

Small display holograms have become commonplace on credit cards and passports, licenses, banknotes and tickets for security and also can be used to create holographic images of important historical artefacts in the museums [81–83]. Large format holographic displays are widely used in advertising, mostly in form of rainbow holograms and small embossed holograms. In general there are two types of display holograms: the first type can be viewed by white light and the other type would require a laser light for reconstruction [30].

This technology can be implemented by creating holograms on a flat surface which are capable of diffracting light beams at different wavelength and intensity in various directions, in a controlled manner. The light beams are generated through a light modulation system arranged in a specific geometry and the holographic screen makes the necessary optical transformation to compose these beams into a perfectly continuous 3D view.

Largest photorefractive 3D display(4 × 4 inches in size)have recently reported by Savas Tay et al. [84]. This can be recorded within a few minutes, viewed for several hours

without the need for refreshing, and can be completely erased and updated with new images when desired [84].

Photorefractive polymers need to have numerous properties such as: 100% diffraction efficiency, fast writing time, hours of image persistence, rapid erasure, and large area and capable of recording and displaying new images every few minutes.

Photopolymer materials and silver halide are the most common recording material for display holograms due to their advantages.

1.5.2 Holographic data storage (HDS)

Currently the main commercially data storage media is CDs, DVDs and hard disk drives where in CDs, DVDs the information is stored as optical changes on the surface of the recording medium [85] and in hard disk drives the information is stored as a distinct magnetic state. However in terms of increasing the storage capacity of media, both types are reaching their physical limits[86]. The maximal possible data density of these hard disks is approximately 100 Gbit/cm^2[87]. The big challenge in multi media market is to increase the magnitude of storage requirements of data storage. One possibility to achieve is have smaller spot sizes by decreasing the wavelength of the laser in order to increase the storage capacities for DVDs and/or using a higher numerical aperture [88] or by adding more layers to the disk.

Holographic Data Storage (HDS) made it possible to increase the storage capacity of hard disc drives by storing a large number of holograms in the same place as the data can be stored throughout the three-dimensional volume of a recording medium. Unlike DVDs and hard disk drives, where data are recorded and recovered on the surface of a

medium, holographic data storage systems store data throughout the three-dimensional volume of a recording medium.

An advantage of a holographic memory compared to a conventional storage medium is, that the entire data page can be reconstructed at one time. Another unique feature of HDS systems is their content-addressability. The pattern for a specific data page can be sent over the object beam, if the stored holograms are illuminated with this beam, all reference beams will be reconstructed. The intensity of these reference beams is proportional to the similarity of the stored data pages and the specific data page sent with the object beam. The reference beam with the highest intensity belongs to the data page which matches closest to the search pattern.

The most suited material for HDS require having several physical properties, such as a large dynamic range, high photosensitivity, undergo no dimensional changes and be capable of forming thick layers. Photopolymers and photorefractive materials appear to be ideal recording material for HDS. However, photorefractive materials are reported to have low photosensitivity, while they have following features: the recorded holograms are rewriteable, large refractive index modulation can be achieved, and also the material does not suffer from shrinkage during recording. Unlike photorefractives, photopolymers demonstrate high photosensitivity. However, photopolymers also face problems such as thickness limitations (approximately 1mm) and shrinkage.
Holographic recording in thick material is essential for HDS, currently many research groups investigating the stability of photopolymers and photopolymer composites for HDS [89–96].

A Japanese based company, Optware, has developed a new method of holographic storage called collinear holography in 2005 [17]. Instead of separate signal and

reference beams to create the interference pattern, they used a collinear approach by aligning the two laser beams into a single beam of coaxial light to create data fringes.

An American company, InPhase Technologies carried out several significant technical milestones in commercialising photopolymer based HDS systems. InPhase was the first company to release the prototype of holographic disc-drive in 2008 [97].

Many other commercial companies have been involved in development of possibilities of commercialising HDS; such as IBM, PulseTec, General Electric and Sony are [98], however is still unclear how the commercial application of this technology will evolve.

1.5.3 Digital holographic microscopy

Microscopy is used broadly to study phase objects or imaging purposes in biology [99–101] and medicine[102] and makes it possible to visualize and quantify transparent objects with variation in thickness or refractive index [30,99]. However, most designs do not exhibit sufficient spatial resolution for imaging bacteria.

Grebenyuk et al. recently propose the advantages of off-axis partially coherent digital holographic microscopy (DHM) with a comparatively simple optical scheme. Theoretical and experimental analysis of the off-axis imaging process in this microscope is presented in [103].

DHM is excellent tool for investigation of microbial motility, however most of the design cannot image the bacteria due to poor spatial resolution. Kuhn et al., proposed an off-axis Mach-Zehnder design of a holographic microscope has a spatial resolution of better than 800 nm and the ability to resolve bacterial samples at varying densities over

a 380 μm × 380 μm × 600 μm with three-dimensional field of view. In addition, the design is capable to resolved the larger organisms in details such as protozoa [104].

1.5.4 Holographic Optical Tweezers

Optical tweezer are rapidly growing research area since their introduction in 1986 by Ashkin, Dziedzic, Bjorkholm and Chu as a technique for trapping and manipulate a large number of object at the same time with scale ranging from nanometers to millimetres in wide range of application in biology [105] and physical science [106].

Holographic optical tweezers use computer-generated diffractive optical elements to diffract a single collimated input laser beam into desired output of beams with individual direction which is focused into an optical trap. This approach can be used for precise shaping and directing of optical wavefronts in three-dimensional configurations [107–109]. Such a device can be used to study mechanical properties of an object which are bound together by elastic forces[110]. Recently, holographic optical tweezers are used in biology application to understand the change in mechanical properties of tissues when a disease occurred [111–113].

1.5.5 Holographic sensor:

Holograms can be designed to detect and quantify certain molecules or environmental changes. The operation of holographic sensors is mostly due to physical or chemical changes in the holograms, such as changing temperature, humidity, pressure which cause a change in the refractive index modulation of the hologram or change in fringe

spacing of the recorded holograms. These changes usually lead to a visual change in the holographic images for example change in colour which can be detected by human eyes. Currently the IEO centre has developed prototypes humidity and temperature and pressure holographic sensors [77,114–117].

(a) **(b)**

Figure 1-6 a) The IEO holographic humidity sensor as the relative humidity is increased from 20-60 % and b) The IEO holographic pressure sensor as the pressure is increased from 10 N/cm^2-50 N/cm^2

In the recent years, holographic sensor technologies are studied for applications in the medical field. Patients with diabetes, cardiac problems, kidney disorders or high blood pressure could benefit from the development of new hologram technology[76,118–122]. Currently, the research groups are developing prototype smartphone-based test for diabetic patient to monitor glucose levels and urinary tract infections. The device allows diabetes patients to self- monitor their blood-sugar levels from home.

1.6 Conclusions

In this chapter, a brief overview of the field of holography has been given. The principles behind holographic recording, the different classifications of holograms, the main holographic recording media and the mechanism of holographic recording in photopolymers have been outlined. In addition to a number of holographic applications briefly described, another application of holography is Holographic Optical Elements (HOEs), since in this research holographic optical elements are fabricated, and this application will be described in more details in the next chapter.

References:

1. Hariharan P. Optical Holography: Principles, Techniques, and Applications. Optical Engineering. 1997. p. 1267.

2. Wolfke M. uber die moglichkeit de optischen abbildung von molecular gittern. 1920.

3. Bragg w. The x-ray microscope. Nature. 1939;149(3782):470.

4. Bragg w. A new type of x-ray microscope. Nature. 1939;143(3625):678.

5. Gabor D. A new microscopic principle. Nature. 1948;161(4098):777.

6. Bragg WL. Microscopy by reconstructed wave-fronts. Nature. 1950;166(4218):399–400.

7. Hecht E. Optics. Optics. 1998.

8. Gabor D. Microscopy by Reconstructed Wave Fronts: II. Proceedings of the Physical Society. Section B. 2002. p. 449–69.

9. Leith EN, Upatnieks J. Reconstructed Wavefronts and Communication Theory. Journal of the Optical Society of America. 1962. p. 1123.

10. Leith EN, Upatnieks J. Wavefront Reconstruction with Continuous-Tone Objects. Journal of the Optical Society of America. 1963. p. 1377.

11. Maiman TH. Stimulated Optical Radiation in Ruby. Nature [Internet]. 1960 Aug 6 [cited 2014 Dec 26];187(4736):493–4. Available from: http://dx.doi.org/10.1038/187493a0

12. Leith EN, Upatnieks J Wavefront Reconstruction with Diffused Illumination and Three-Dimensional Objects. Journal of the Optical Society of America. 1964. p. 1295.

13. Pavani K. Holographic Liquid Crystal Devices. Dublin Institute of Technology; 2008.

14. Kogelnik H. Coupled wave theory for thick hologram gratings. Bell Syst Tech J. 1969;48(9):2909–47.

15. Barden SC, Arns JA, Colburn WS. Volume-phase holographic gratings and their potential for astronomical applications. Proc SPIE Vol 3355. 1998;3355:866–76.

16. Bragg WL. The Structure of Some Crystals as Indicated by Their Diffraction of X-rays. Proceedings of the Royal Society A: Mathematical, Physical and Engineering Sciences. 1913. p. 248–77.

17. Jenkins F.A. Fundamental of Optic. ApplOpt. 1975;14(3):593–601.

18. Jallapuram R. Obtimization of an acrylamide-based photopolymer for reflection holographic recording. Dublin Institute of Technology; 2005.

19. Lawrence J. R. OFT and SJT. Photopolymer holographic recording material. Optik (Stuttg). 2001;112:449–63.

20. Collados MV, Arias I, García A, Atencia J, Quintanilla M. Silver halide sensitized gelatin process effects in holographic lenses recorded on Slavich PFG-01 plates. Appl Opt. 2003;42(5):805–10.

21. Osanlou A, Snashall E, Osanlou O, Osanlou R, Mirlis E, Shi L, et al. High sensitive materials in medical holographic microscopy. IOP Conf Ser Mater Sci Eng. IOP Publishing; 2015 Feb 17;74(1):012012.

22. Kim JM, Choi BS, Kim SI, Kim JM, Bjelkhagen HI, Phillips NJ. Holographic optical elements recorded in silver halide sensitized gelatin emulsions. Part I. Transmission holographic optical elements. Appl Opt. 2001;40(5):622–32.

23. Ghosh A, Nirala AK, Yadav HL. Dependence of wavelength selectivity of holographic PV concentrator on processing parameters. Opt - Int J Light Electron Opt. 2015 Mar;126(6):622–5.

24. Chang BJ, Leonard CD. Dichromated gelatin for the fabrication of holographic optical elements. Appl Opt. 1979;18(14):2407–17.

25. Calixto S, Andres M V. Water Vapor Sensors Based on the Swelling of Relief Gelatin Gratings. Adv Mater Sci Eng. 2015;2015(Article ID 584324):1–5.

26. Liu Y, Li W, Ding Q, Yan Z. Wavelength properties of DCG holograms under the conditions of different temperature and humidity. In: Jin G, Zhuang S, Liu J, editors. International Symposium on Optoelectronic Technology and Application 2014. International Society for Optics and Photonics; 2014. p. 929514.

27. Bañares-Palacios P, Álvarez-Álvarez S, Marín-Sáez J, Collados M-V, Chemisana D, Atencia J. Broadband behavior of transmission volume holographic optical elements for solar concentration. Opt Express. 2015 Jun 1;23(11):A671–81.

28. Urbach JC, Meier RW. Properties and limitations of hologram recording materials. Appl Opt. 1969;8(11):2269–81.

29. Urbach J. Thermoplastic Hologram Recording, in Holographic Recording Materials, Topics in applied physics. ed. H. M. . Springer; 1977. 20, Vol. p.

30. Toal V. Introduction to Holography. CRC Press; 2011. 502 p.

31. Tavex America I. Holocamera. 2013.

32. Muhammad-Sukki F, Abu-Bakar SH, Ramirez-Iniguez R, McMeekin SG, Stewart BG, Sarmah N, et al. Mirror symmetrical dielectric totally internally reflecting concentrator for building integrated photovoltaic systems. Appl Energy. Elsevier Ltd; 2014;113:32–40.

33. Blanche P-A. Field guide to holography. 2014.

34. Watson J. Basics of holography. Optics and Lasers in Engineering.2004.p.475–6.

35. Ranaghan MJ, Greco JA, Wagner NL, Grewal R, Rangarajan R, Koscielecki JF, et al. Photochromic Bacteriorhodopsin Mutant with High Holographic Efficiency and Enhanced Stability via a Putative Self-Repair Mechanism. ACS Appl Mater Interfaces. American Chemical Society; 2014 Feb 26;6(4):2799–808.

36. Bianco A, Pariani G, Colella L, Castagna R, Bertarelli C. High performances photochromic polyurethanes for phase and amplitude optical elements. Advanced Photonics 2015. Washington, D.C.: OSA; 2015. p. NS1A.4.

37. Martin S. A new photopolymer recording material for holographic applications: photochemical and holographic studies towards an optimized system. Doctoral. 1995.

38. Lawrence J. Diffusion based grating formation in a photopolymer material. Masters. 2002.

39. Ishii N, Kato T, Abe J. A real-time dynamic holographic material using a fast photochromic molecule. Sci Rep. Nature Publishing Group; 2012 Nov 8;2.

40. Guntake S., Toal V., Martin S. Holographically recorded diffractive optical elements for holographic and electronic speckle pattern interferometry. ApplOpt. 2002;41(35):7475–9.

41. Gallego S, Marquez a, Fernandez R, Piera a, Martinez FJ, Ortuno M, et al. Analysis of the fabrication of diffractive optical elements in photopolymers. Opt Photonics Inf Process Vii. 2013;8855:1–8.

42. Guntaka SR, Toal V, Martin S. Holographically recorded photopolymer diffractive optical element for holographic and electronic speckle-pattern interferometry. Appl Opt. 2002;41(35):7475–9.

43. Akbari H, Naydenova I, Martin S. Using acrylamide-based photopolymers for fabrication of holographic optical elements in solar energy applications. Appl Opt. OSA; 2014;53(7):1343–53.

44. Sherif H, Naydenova I, Martin S, McGinn C, Toal V. Characterization of an acrylamide-based photopolymer for data storage utilizing holographic angular multiplexing. J Opt A Pure Appl Opt. 2005;7(5):255–60.

45. Sherif H, Naydenova I, Martin S, McGinn C, Berger G, Denz C, et al. Study of an acrylamide-based photopolymer for use as a holographic data storage medium [Internet]. Opto-Ireland 2005: Photonic Engineering. 2005. p. 305–13. Available from: ISIP:000231203600030

46. Ortuño M, Gallego S, Márquez A, Neipp C, Pascual I, Beléndez A. Biophotopol: A Sustainable Photopolymer for Holographic Data Storage Applications. Materials (Basel). 2012;5(5):772–83.

47. Jenney JA. Holographic Recording with Photopolymers. J Opt Soc Am. OSA; 1970 Sep 1;60(9):1155.

48. Coufal HJ, Psaltis D, Sincerbox GT, editors. Holographic Data Storage [Internet]. Berlin, Heidelberg: Springer Berlin Heidelberg; 2000 [cited 2015 May 5]. Available from: http://link.springer.com/10.1007/978-3-540-47864-5

49. Ortuño M, Fernández E, Gallego S, Beléndez A, Pascual I. New photopolymer holographic recording material with sustainable design. Opt Express. 2007;15(19):12425–35.

50. Naydenova IG, Martin S, Toal V. Photopolymers: beyond the standard approach to photosensitisation. Journal of the European Optical Society - Rapid publications. 2009.

51. Martin S. Characterization of an acrylamide-based dry photopolymer holographic recording material. Opt Eng. 1994;33(12):3942.

52. Blaya S, Carretero L, Mallavia R, Fimia A, Madrigal RF, Ulibarrena M, et al. Optimization of an acrylamide-based dry film used for holographic recording. Appl Opt. 1998 Nov 10;37(32):7604–10.

53. Tomlinson W, Kaminow I, Chandross E, Fork R. Photoinduced refractive index increase in poly (methylmethacrylate) and its applications. Appl Phys Lett [Internet]. 1970; Available from: http://link.aip.org/link/?APPLAB/16/486/1

54. Zhao G, Mouroulis P. Diffusion Model of Hologram Formation in Dry Photopolymer Materials. Journal of Modern Optics. 1994. p. 1929–39.

55. Moreau V, Renotte Y, Lion Y. Characterization of dupont photopolymer: determination of kinetic parameters in a diffusion model. Appl Opt. 2002;41(17):3427–35.

56. Colvin VL, Larson RG, Harris AL, Schilling ML. Quantitative model of volume hologram formation in photopolymers. J Appl Phys. 1997;81(9):5913–23.

57. Jin Hyuk Kwon, Hyo Chang Hwang and KCW. Analysis of temporal behavior of beams diffracted by volume gratings formed in photopolymers. J Opt Soc Am B 16. 1999;16(10):1651–7.

58. Piazzolla S, Jenkins BK. Holographic grating formation in photopolymers. Opt Lett. 1996;21(14):1075–7.

59. Wu S-D, Glytsis EN. Holographic grating formation in photopolymers: analysis and experimental results based on a nonlocal diffusion model and rigorous coupled-wave analysis. Journal of the Optical Society of America B. 2003. p. 1177.

60. Tsvetanka Babeva, Izabela Naydenova, Dana Mackey, Suzanne Martin and VT. Two-way diffusion model for short-exposure holographic grating formation in acrylamide-based photopolymer. J Opt Soc Am B 27. 2010;27(2):197–203.

61. Naydenova I, Jallapuram R, Howard R, Martin S, Toal V. Investigation of the diffusion processes in a self-processing acrylamide-based photopolymer system. Appl Opt. 2004;43(14):2900–5.

62. Kaura SK, Chhachhia DP, Aggarwal AK. Interferometric moiré pattern encoded security holograms. J Opt A Pure Appl Opt. IOP Publishing; 2006 Jan 1;8(1):67–71.

63. Leith EN, Kozma A, Upatnieks J, Marks J, Massey N. Holographic data storage in three-dimensional media. Appl Opt. 1966;5(8):1303–11.

64. Mohan NK, Islam QT, K. Rastogi P. Recent developments in holographic optical elements (HOEs). Opt Lasers Eng. 2006;44(9):871–80.

65. De L. A two step method for recording holographic optical elements with partially coherent light. 1991;22(3):135–40.

66. Bokor N, Davidson N. Curved holographic optical elements for diffuse light collimation and concentration. Proc CAOL'2003 1st Int Conf Adv Optoelectron Lasers Jontly with 1st Work Precis Oscil Electron Opt (IEEE Cat No03EX715). 2003;1(September):91–8.

67. Kim JM, Choi BS, Choi YS, Kim JM, Bjelkhagen HI, Phillips NJ. Holographic optical elements recorded in silver halide sensitized gelatin emulsions. Part 2. Reflection holographic optical elements. Appl Opt. 2002;41(8):1522–33.

68. Sabnis RW. Color filter technology for liquid crystal displays. Displays. 1999;20(3):119–29.

69. Tsuda K. Colour filters for LCDs. Displays. 1993. p. 115–24.

70. Biles J. Holographic Color Filters for LCDs. SID. 1994;94(Digest):403–6.

71. R R A. Syms. Practical Volume Holography. Oxford University; 1990.

72. McCauley DG, Simpson CE, Murbach WJ. Holographic Optical Elements for Visual Display Applications. Appl Opt. 1973;12(2).

73. Dufresne ER, Grier DG. Optical tweezer arrays and optical substrates created with diffractive optics. Rev Sci Instrum. 1998;69(5):1974.

74. Dufresne ER, Spalding GC, Dearing MT, Sheets SA, Grier DG. Computer-generated holographic optical tweezer arrays. Rev Sci Instrum. 2001;72(3):1810–6.

75. Plewa J, Tanner E, Mueth DM, Grier DG. Processing carbon nanotubes with holographic optical tweezers. Optics Express. 2004. p. 1978.

76. Yetisen AK, Naydenova I, da Cruz Vasconcellos F, Blyth J, Lowe CR. Holographic sensors: three-dimensional analyte-sensitive nanostructures and their applications. Chem Rev. American Chemical Society; 2014 Oct 22;114(20):10654–96.

77. Naydenova I, Jallapuram R, Toal V, Martin S. Characterisation of the humidity and temperature responses of a reflection hologram recorded in acrylamide-based photopolymer. Sensors Actuators, B Chem. 2009;139(1):35–8.

78. Cody D, Mihaylova E, O'Neill L, Babeva T, Awala H, Retoux R, et al. Effect of zeolite nanoparticles on the optical properties of diacetone acrylamide-based photopolymer. Opt Mater (Amst). Elsevier B.V.; 2014;37:181–7.

79. Smigielski P, Meyrueis P, Dubourg M. Effective Practical Use Of Holography And Related Technologies In Industry. In: Grosmann MH, Meyrueis P, editors. 2nd European Congress on Optics Applied to Metrology. International Society for Optics and Photonics; 1980. p. 213–23.

80. HOLO3 [Internet]. [cited 2015 Dec 14]. Available from: http://www.holo3.com/optical-measurement.html

81. Bjelkhagen HI, Osanlou A. Color holography for museums: bringing the artifacts back to the people. In: Bjelkhagen HI, editor. SPIE OPTO. International Society for Optics and Photonics; 2011. p. 79570B – 79570B – 7.

82. Bjelkhagen HI. Color holography: recent improvements and applications. In: Bjelkhagen HI, Bove VM, editors. SPIE OPTO. International Society for Optics and Photonics; 2013. p. 86440L.

83. Stephan Reichelt, Ralf Haussler, Norbert Leister, Gerald Futterer HS and AS. Advances in Lasers and Electro Optics. Costa N, Cartaxo A, editors. InTech; 2010. Chapter 29 p.

84. Tay S, Blanche P-A, Voorakaranam R, Tunç A V, Lin W, Rokutanda S, et al. An updatable holographic three-dimensional display. Nature. Nature Publishing Group; 2008 Feb 7;451(7179):694–8.

85. Mansuripur M. The Physical Principles of Magneto-optical Recording. Cambridge: Cambridge University Press; 1995.

86. Thompson D a, Best JS. The future of magnetic data storage technology. IBM J Res Dev. 2000;44(3):311–22.

87. S. C. Esener, M. H. Kryder, W. D. Doyle, M. Keshner, M. Mansuripur and DAT. The Future of Data Storage Technologies. International Technology Research Institute; 1999.

88. Osato K, Ichimura I, Maeda F, Yamamoto K, Kasami Y. Progress in optical disk recording with over 20 GB of capacity. 2000 Opt Data Storage Conf Dig (Cat No00TH8491). 2000;

89. Jallapuram R, Naydenova I, Martin S, Howard R, Toal V, Frohmann S, et al. Acrylamide-based photopolymer for microholographic data storage. Opt Mater (Amst). 2006;28(12):1329–33.

90. Lin SH, Hsu KY, Chen W-Z, Whang WT. Phenanthrenequinone-doped poly(methyl methacrylate) photopolymer bulk for volume holographic data storage. Opt Lett. Optical Society of America; 2000 Apr 1;25(7):451.

91. Sherif H, Naydenova I, Martin S, McGinn C, Toal V. Characterisation of an Acrylamide-based Photopolymer for Data Storage Utilizing Holographic Angular Multiplexing. Articles. 2005.

92. Fernández E, Ortuño M, Gallego S, García C, Beléndez A, Pascual I. Comparison of peristrophic multiplexing and a combination of angular and peristrophic holographic multiplexing in a thick PVA/acrylamide photopolymer for data storage. Appl Opt. Optical Society of America; 2007 Aug 1;46(22):5368.

93. Sheridan JT, Gleeson MR, Close CE, Kelly J V. Optical response of photopolymer materials for holographic data storage applications. J Nanosci Nanotechnol. 2007 Jan;7(1):232–42.

94. Carre C, Lougnot D-J. Optimization of self-processing photopolymers as holographic storage material taking into account application requirements. In: Lessard RA, editor. SPIE's 1996 International Symposium on Optical Science, Engineering, and Instrumentation. International Society for Optics and Photonics; 1996. p. 137–41.

95. Guattari F, Maire G, Contreras K, Arnaud C, Pauliat G, Roosen G, et al. Balanced homodyne detection of Bragg microholograms in photopolymer for data storage. Opt Express. 2007 Mar 5;15(5):2234–43.

96. Psaltis D, Levene M, Pu A, Barbastathis G, Curtis K. Holographic storage using shift multiplexing. Opt Lett. Optical Society of America; 1995 Apr 1;20(7):782.

97. Tapestry 300r. http://www.inphase-technologies.com/downloads/pdf/products/2007. TapestryProductBrochure.

98. Sheridan JT. Characterizing and designing photopolymer materials. SPIE Newsroom [Internet]. Society of Photo-Optical Instrumentation Engineers; 2009. Available from: http://dx.doi.org/10.1117/2.1200909.1764

99. Garcia-Sucerquia J. Color lensless digital holographic microscopy with micrometer resolution. Opt Lett. Optical Society of America; 2012 May 14;37(10):1724.

100. Marquet P, Depeursinge C, Magistretti PJ. Review of quantitative phase-digital holographic microscopy: promising novel imaging technique to resolve neuronal network activity and identify cellular biomarkers of psychiatric disorders. Neurophotonics. International Society for Optics and Photonics; 2014 Oct 1;1(2):020901.

101. Wallace JK, Rider S, Serabyn E, Kühn J, Liewer K, Deming J, et al. Robust, compact implementation of an off-axis digital holographic microscope. Opt Express. Optical Society of America; 2015 Jun 29;23(13):17367–78.

102. Emery Y, Cuche E, Colomb T, Depeursinge C, Rappaz B, Marquet P, et al. DHM (Digital Holography Microscope) for imaging cells. J Phys Conf Ser. IOP Publishing; 2007 Apr 1;61(1):1317–21.

103. Grebenyuk AA, Tarakanchikova Y V, Ryabukho VP. An off-axis digital holographic microscope with quasimonochromatic partially spatially coherent illumination in transmission. J Opt. IOP Publishing; 2014 Oct 1;16(10):105301.

104. Kühn J, Niraula B, Liewer K, Kent Wallace J, Serabyn E, Graff E, et al. A Mach-Zender digital holographic microscope with sub-micrometer resolution for imaging and tracking of marine micro-organisms. Rev Sci Instrum. 2014 Dec;85(12):123113.

105. Rigler R, Orrit M, Basché T. Single Molecule Spectroscopy. Berlin, Heidelberg: Springer Berlin Heidelberg; 2001.

106. Grier DG. Optical tweezers in colloid and interface science. Curr Opin Colloid Interface Sci. 1997 Jun;2(3):264–70.

107. Grier DG. A revolution in optical manipulation. Nature. 2003 Aug 14;424(6950):810–6.

108. Roichman Y, Grier DG. Three-dimensional holographic ring traps. In: Andrews DL, Galvez EJ, Nienhuis G, editors. Complex Light and Optical Forces Edited by Andrews. 2007. p. 64830F – 64830F – 5.

109. Dufresne ER, Spalding GC, Dearing MT, Sheets SA, Grier DG. Computer-generated holographic optical tweezer arrays. Rev Sci Instrum. AIP Publishing; 2001 Mar 1;72(3):1810.

110. Sun B, Roichman Y, Grier DG. Theory of holographic optical trapping. Opt Express. Optical Society of America; 2008 Sep 19;16(20):15765.

111. Remmerbach TW, Wottawah F, Dietrich J, Lincoln B, Wittekind C, Guck J. Oral cancer diagnosis by mechanical phenotyping. Cancer Res. 2009 Mar 1;69(5):1728–32.

112. Volpe G. Optical Tweezers: Methods and Applications, edited by Miles J. Padgett, Justin Molloy and David McGloin. Contemp Phys. Taylor & Francis; 2011 Jul 10;52(4):379–80.

113. Ramser K, Hanstorp D. Optical manipulation for single-cell studies. J Biophotonics. 2010 Apr;3(4):187–206.

114. Naydenova I, Jallapuram R, Toal V, Martin S. A visual indication of environmental humidity using a color changing hologram recorded in a self-developing photopolymer. Appl Phys Lett. 2008;92(3).

115. Bavigadda V, Mihaylova E, Jallapuram R, Toal V. Vibration phase mapping using holographic optical element-based electronic speckle pattern interferometry. Opt Lasers Eng. 2012;50(8):1161–7.

116. Bavigadda V, Jallapuram R, Toal V, Mihaylova E. Vibration Phase Measurements using Holographic Optical Elements. Articles. Optics Letters; 2010;35(19):3273–5.

117. M. Zawadzka, T. Mikulchyk, D. Cody, S. Martin, E. Mihaylova, A. K. Yetisen JL, Martinez-Hurtado, H. Butt, H. Awala, S. Mintova, S. H. Yun IN. Photonic Materials for Sensing, Biosensing, And Display Devices. Photonic Materials for Holographic Sensing. Springer; 2015.

118. Yetisen AK. Holographic Sensors. Cham: Springer International Publishing; 2015.

119. Marshall AJ, Young DS, Blyth J, Kabilan S, Lowe CR. Metabolite-sensitive holographic biosensors. Anal Chem. 2004 Mar 1;76(5):1518–23.

120. Bhatta D, Christie G, Madrigal-González B, Blyth J, Lowe CR. Holographic sensors for the detection of bacterial spores. Biosens Bioelectron. 2007 Nov 30;23(4):520–7.

121. Farandos NM, Yetisen AK, Monteiro MJ, Lowe CR, Yun SH. Contact lens sensors in ocular diagnostics. Adv Healthc Mater. 2015 Apr 22;4(6):792–810.

122. Yetisen AK, Butt H, da Cruz Vasconcellos F, Montelongo Y, Davidson CAB, Blyth J, et al. Light-Directed Writing of Chemically Tunable Narrow-Band Holographic Sensors. Adv Opt Mater. 2014 Mar 2;2(3):250–4.

2 Holographic Optical Elements

2.1 Introduction

The amount of energy from the sun that reaches the earth through the earth atmosphere is about 174 PW [1]. If the energy from the sun could be converted into usable energy such as electricity, this could produce few times more energy than world needs. Currently the world energy usage is 13 TW per year; this is presently supplied by conventional energy resources such as fossil fuels and nuclear. By the year 2050 this value is projected to triple to approximately 30 TW [2,3]. Solar energy has the capability to provide a clean and sustainable energy supply in the future as the sun is abundant availability source on earth and the fossil fuel resource is depleting rapidly, it is important to find a technology which can meet the ever increasing demand of energy.

A number of researchers all over the world are focusing to improve the use of holographic techniques in solar applications and have suggested and successfully demonstrated working designs over last few years due to their potential to collect light from a large area and focus or re-direct the light onto a smaller area and increase the efficiency of Photovoltaic (PV) devices.

As discussed in chapter 1, there is a wide range of holographic recording media and depending on their advantages and disadvantages they can be the subject of much study for many holographic applications. HOEs are just one type of Diffractive Optical Element (DOE) and similar diffractive structures can also be made using non-holographic methods such as direct lithography, moulding and stamping processes. Although the production processes are different, the principle of operation is identical, the diffractive element changes the path of the incident light through diffraction at the

sub micron structures, and these structures have been designed to produce a particular output such as focused, deflected or patterned light.

This thesis concerns the development of a HOE device that aims to improve the efficiency of solar energy concentration onto solar cell.

HOEs are suited to use as solar concentrators because of several unique features such as capability to diffract light at large offset angle, Bragg selectivity, flexible design and the potential to create multiplexed gratings. Concentrating systems have been developed to concentrate the sun light from a large area into small area which can reduce the cost of solar energy, as they can replace a large area of expensive photovoltaic cells. Depending on the geometry they can be classified as mirror (reflection) or lenses (focussing).The aim of this research is to explore the potential of using photopolymer Holographic Optical Elements (HOE) to collect light from a large area and focus it onto a small detector / solar cell. For solar applications, this should work efficiently for as broad a range of incident angles as possible.

In this chapter, a review of the development of holographic optical elements is presented, in order to present the current state-of-the-art in this area. Recent research in the field of using Holographic Optical Elements in solar application is discussed, as well as outlining the main motivation for this research. Finally, the aims of the PhD research project are presented.

2.2 Holographic Optical Elements in solar applications

HOEs can offer significant advantages in many applications as they are thin, flat and lightweight and can be easily reproducible by embossing or in the case of volume DOE by exposing photosensitive materials such as photopolymer. Their advantages make them attractive in many applications and areas for example in optical sensors [4–8], fibre-optics [9–11], optical scanners [12–15], optical disk pick-up heads [16,17]as well as holographic concentrators [18–42]. Holographic concentrators are discussed further below. HOEs can function as gratings, lenses, beam splitter, spectral filter, shear elements, mirror, birefringent elements, multi-function elements, etc.

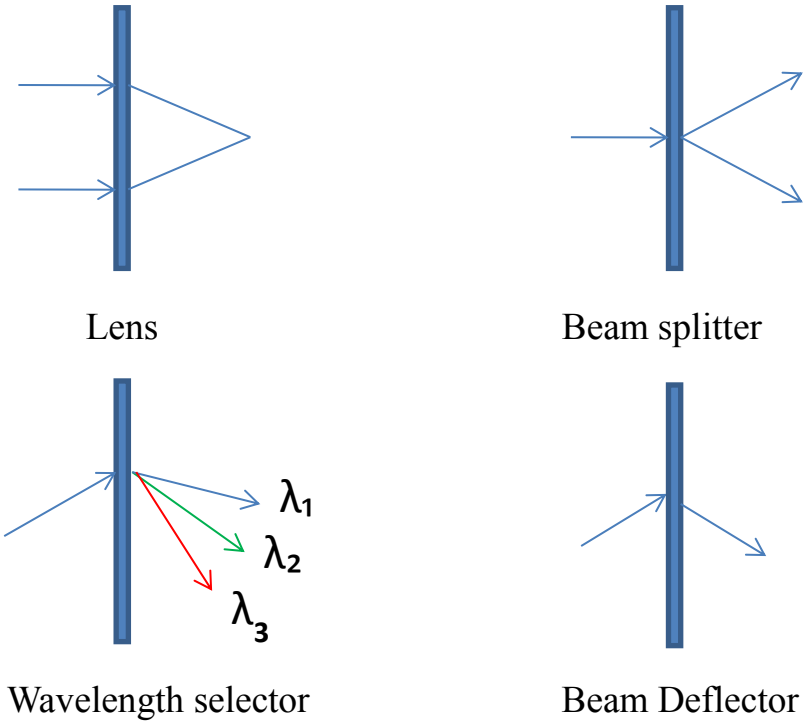

Figure 2-1 Holographic Optical Element functions examples

In general the HOEs can be classified as two different types depending on their effect on the incident light:

- Non focussing elements: optical elements that are used simply to redirect or split the light;
- Focussing elements: optical elements that produce a converging wavefront, having the same effect as spherical or cylindrical lenses and mirrors. The focal length of the focussing elements can vary depending on the devices; they can have a dual role in solar collectors by focusing the light and redirecting the beam[43].

Diffractive optics is subfield of physical optics which includes refraction, reflection and diffraction processes. Any light concentrator can be replaced by a holographic optical element such as lens, diffraction grating, and mirror. HOEs can be defined as diffractive structures that are recorded holographically by interfering at least two incident beams.

One of the key features of holographic elements is their ability to simultaneously perform multiple functions such as: concentration and spectral beam splitting filter all in the same area of the HOE. The HOE can be made with large numerical aperture in a very lightweight photosensitive material. HOEs are relatively cheaper to be manufactured as there is no grinding or polishing of optical glass required [44].

The development of the HOEs started with the imaging properties in mid 1960 [45,46]. The theoretical analysis and understanding of the diffraction behaviour of volume or thick HOEs was advanced significantly by Kogelnik's coupled wave theory which modelled the behaviour of thick volume gratings[47]. The couple wave theory was improved by Loewen et al. [48], Gaylord et al. [49], Moharam et al.[50].

In 1971, Lin and Doherty proposed the method where HOEs were recorded with He-Ne laser and reconstructed with blue argon laser [51]. Reconstruction of the holograms at different wavelength changes the scale of reconstruction and magnifies/de-magnifies the object field. This method was introduced based on Gabor's proposal on the potential of

holography technique to magnify the object [52]. Following up on that, the fabrication of hololens was developed by Silvennoinen and Jaaskelaine [53] where 488nm laser was used for the recording the holograms and it was reconstructed using a 628 nm.

In 1986, Herzig [54] reported two step methods for recording of high efficiency off-axis HOE for near infrared. HOE were recorded in visible (514 nm) using dichromated gelatin on Kodak 649 F photosensitive material and reconstructed in infrared (800 nm). In this method all the wavelength dependent parameters such as Bragg angle, focal length and astigmatism required careful control. This method can be applied to fabricate aberration free holographic lenses for semiconductor laser at 800 nm. This can be extended to 1500 nm by changing the recording parameters. The experimental results showed that the lens with focal length of 300 mm can be produced with an aperture of about 15 mm and the diameter of the diffracted spot at 800 nm was found to be 40 μm. This method can be used in many applications such as focusing deflectors for laser printers and focusing gratings for diode-laser spectrum analysers.

A computer design tool was proposed by Awatsuji et al. in 2001[55,56]to fabricate a HOE light concentrator taking into account the wavelength shift. The design had capability to analyse reconstruction and imaging characteristic and provided easier operation for the users to simulate and obtain the required parameters. In 2002, Matsuura et al. presented an optimum HOE lens recorded by visible laser beams for an infrared two-dimensional vertical cavity surface emitting laser (VCSEL) array. The hologram computer-aided design tool was used for designing holograms and analysing their reconstruction and imaging characteristics. The optimum HOE had high diffraction efficiency and a small amount of aberration. This design can be used to fabricate optical elements for application in parallel optical interconnects and optical computing [57].

2.3 Holographic Optical Elements in solar applications

During the last year numbers of other researchers have demonstrated novel designs of holographic optical elements for use in solar applications including volume transmission phase holograms, spherical lenses and cylindrical lenses. Particularly, the most recent ones suggested avoiding the tracking system.

In order to design a holographic solar concentrator, the position of the sun at different times of the day and year needs to be considered. In 1982, Ludman suggested HOEs could be used in solar applications because they have the capability to redirect, concentrate or block the incident light [58].

Dispersive and concentrating devices (DISCO) based on volume phase transmission gratings has been introduced by Bloss et al in 1982 and intended for solar applications. Figure 2.2 shows the main concept of this method. Volume HOEs are suitable for multiplexing; a range of HOEs with various angles between the recording beams can be recorded in one photosensitive layer and this allows spatial separation of the red and the blue spectral ranges of sunlight into different areas. Three solar cell systems with various band gaps and multiplexed HOEs were tested [59]. In this design, the incoming solar radiations are focused and redirected into solar cell 1 and 2. The performance of the PV generator system is increased using DISCO system which separates the spectral regions. The maximum conversion efficiency with the all three band gaps that can be achieved was 42% while the concentration ratio (c= 100) for diffracted wavelengths was about.

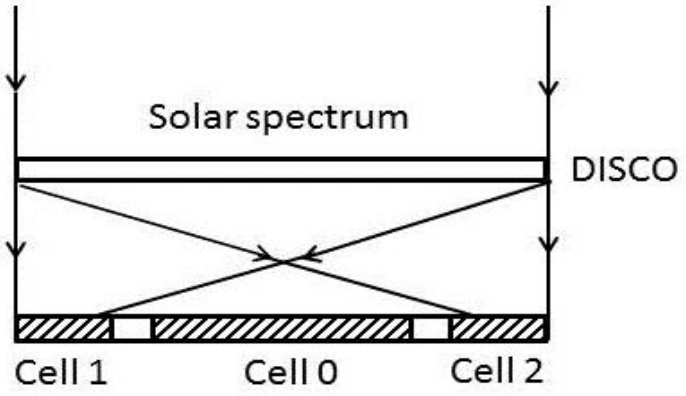

Figure 2-2 DISCO system using three solar cells with different band gaps

One commercial example is Prism Solar Technologies; this company manufacture a solar cell concentrator incorporating an HOE. Using Holographic Planar Concentrator (HPC) has many advantages such as: the ability to collect both direct and diffuse sunlight without tracking and also it reduced the cost of PV module by replacing the PV cells material with low cost holographic concentrating elements. Figure 2.3 is reproduced from [18] shows the side view of holographic planar concentrator. The sunlight is reflected and concentrated onto the photovoltaic cell (PV) with all components supported by a substrate. Where A_{PVC} is the area of the PV cell, A_H is the hologram area, d is the thickness of the substrate, n_1 is the refractive index of the substrate, n_2 is the refractive index of the cover glass over the hologram, θ_{inc} and θ_{diff} are the incident and diffracted angles relative to a normal to the substrate.

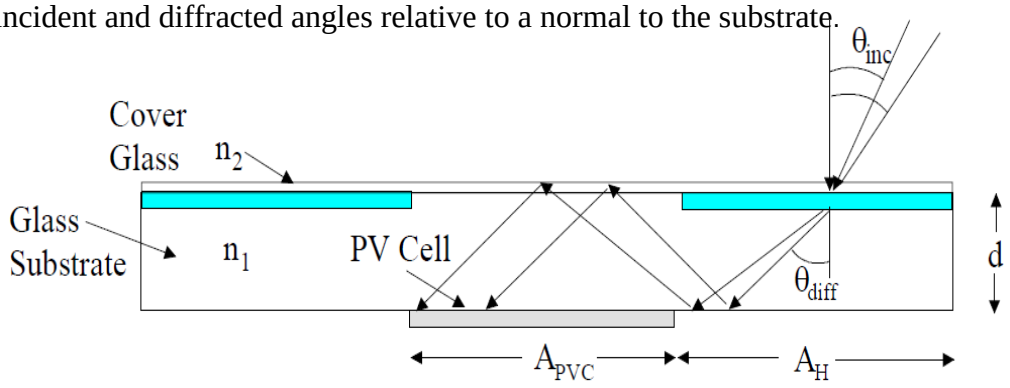

Figure 2-3 Schematic side view of a holographic planar concentrator

HOEs have also been used in collection of light and demonstrated by increasing the light collection from fluorescence-based biochips[60]. The HOEs increased the transmitted fluorescence intensity and also served to filter out the undesired wavelengths. This was possible due to their high angular selectivity the diffracted intensity of the HOE was measured to be about 50% of that of the incident beam. The diffraction efficiency was relatively low due to a complexity of the recording process that covers a large spatial frequency range (0-2800 lines/mm). The transmitted light intensity distributions were acquired on the CCD, with and without the HOE, with the fluorescing spot located over the centre of the HOE. It was found that the HOE gave an enhancement efficiency of approximately 4 times.

Holographic solar concentrators have been theoretically modelled [61] and several useful aspects of holographic gratings have been investigated for use in these applications. The basic relationships for designing holographic elements have also been presented. This is helpful to improve the design and fabrication of new devices.

The Holographic Planar Concentrator (HPC) concept is distinguished from the Holographic lens concentrator. Transparent plates with gratings recorded on surface or within the plate result in diffracted light being guided by total internal reflection to a reduced area of solar cell collector attached to the plate [62–64]. A similar technology has commercially demonstrated by Prism Solar Technologies.

The design and optimization of photopolymer based holographic solar concentrators was recently reported in [25]. The authors demonstrated the recording of a broad band spectrally splitting holographic solar concentrator in HoloMer photopolymer material with an efficiency of 70% and an average efficiency of 56.6% for a wavelength range

from 633nm to 442 nm. The recorded elements showed a narrow angular selectivity hence tracking would be required for an effective photovoltaic concentrator system.

A simple technique to realize a compact with large angle collection solar energy concentrator using a volume holographic element is presented in [22]. In this study PQ doped PMMA photopolymer was used to record volume holograms. The theoretical modelling of the HOE predicts up to a fivefold increase in concentration of energy per unit area of photovoltaic material. This means the collection area of the volume hologram is 5 times that the area of the solar cell. The experimental results show that the collected angle can be significantly increased from 0.01 degree to 6 degrees. Figure 2.4, taken from the recent publication [22], show the optical design for proposed volume holographic concentrator.

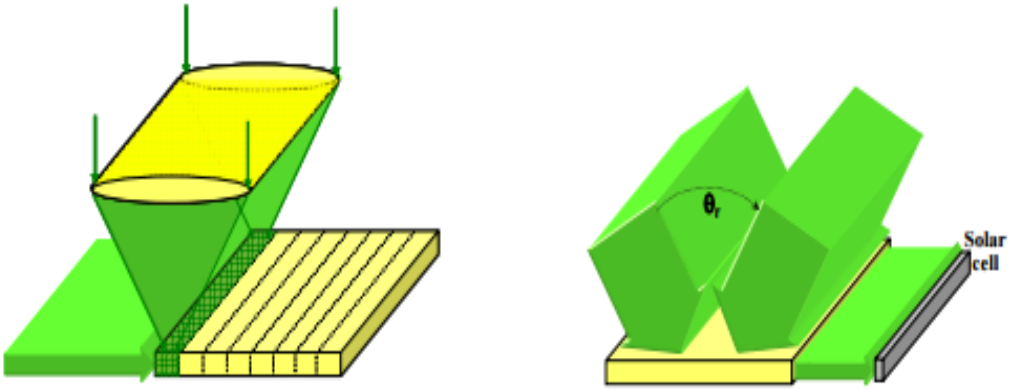

(a) (b)

Figure 2-4 Illustration of Optical Design a) recording geometry and b) configuration of volume holographic concentrator.

A solar radiation receiver as shown in figure 2.5 is described in [27]. This combined system uses a holographic film to concentrate the solar radiation and to optimize the efficiency of the sensor. The advantage of using combined solar receiver is that there is no tracking system required. In the proposed design, there is no need for solar tracking

as more efficient utilization solar radiation influencing the 1 m^2 surface. However, the complexity of the production is one of the disadvantages.

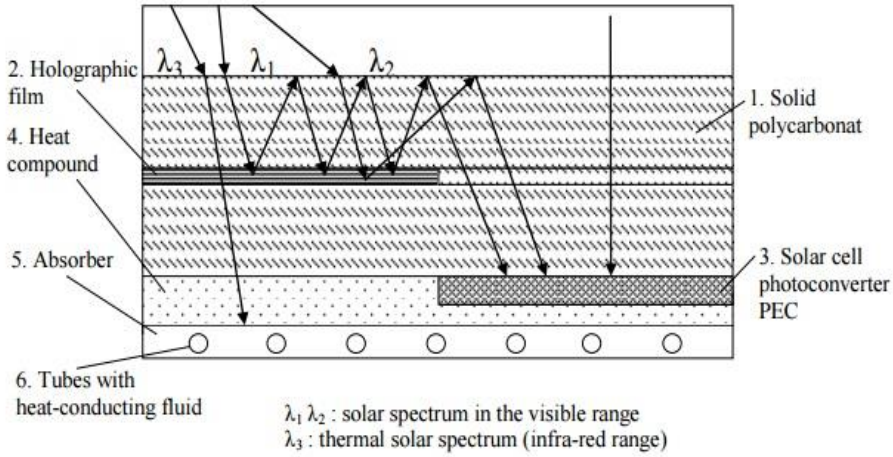

Figure 2-5 Schematic view of the combined receiver

Currently there is not much commercial use, possibly due to lack of suitable material, device complexity and producer processes. However, commercial materials have begun to become available; this leads to recent solar research[65,66].

2.4 Recent research in solar application

In 2013, Altmeyer et al. demonstrated the potential of multiplexing of thick transmission holograms in photopolymer [67]. The variation of the diffraction efficiency of the multiplexed grating respect to the angle of incidence and the wavelength are theoretically shown. The experimental results of the angular acceptance of the single and four multiplexed holograms are compared with the simulation results. The maximum diffraction efficiency of 60% was achieved for the layer with the thickness of 16 micron. This demonstrates the potential for recording multiple high

efficiency elements in photopolymer layer. However further work is required to design combinations of elements that direct the light in single direction.

The most recent applications of HOE in solar systems are briefly reviewed in the following section. In 2015, Sreebha et al. [68] have reported preliminary results on recording transmission holographic optical elements in silver halide. The wavelength selectivity and focusing properties of a holographic lens was used to design a concentrator for solar application. The fabricated holographic lenses were coupled with dye sensitized solar cells in order to measure the efficiency enhancement of the device. It was stated that fabricated holographic lens has achieved 32.9% energy enhancement using the HOE in place while the dye cells were only collecting the yellow radiation of the simulator light source. However tracking would be required in a usable device as the enhancement is just at one angle and it is challenging to mass produce silver halide.

Bañares Palacios et al.[69]in 2015 reported the development of ray tracing techniques to analyse the energy performance of holographic optical elements as solar concentrators. Holographic lenses were recorded in dichromated gelatin with on-axis and off-axis focusing effect. A maximum optical efficiency of 40% was achieved for each recorded lens. It was found that the on-axis lens achieved 16.1% higher average concentration ratio compared to off-axis lens. Comparisons of the experimental and theoretical results for each holographic lens were performed and reported in details for both chromatic and angular selectivity. This work is very interesting because of the detailed analysis of the working device on and off the Bragg angle. However, the concentration ratio for the lenses is very low (approximately 2).

Some systems use tracking as well as holographic elements, for example holographic solar application described in [26] uses a sensor and feedback system to maintain 0.5

degree tracking accuracy with one-axis tracking holographic planar concentrators (HPCs). It was found that in the polar one-axis tracking HPC system the efficiency increases by 43.8% compared to non-tracking HPC systems due to high optical efficiency and higher levels of irradiance in overall module.

HOEs have also been used for radiant control in buildings to facilitate the optimization of energy use for heating, cooling and day lighting in the past decades [40,70].

2.5 Motivation for development of Holographic Optical Elements for solar applications

From the above discussion it is clear that more research in this field is needed. In our investigation, a mass-producible inexpensive material is used. The focus is on making low spatial frequency elements in order to increase the working range and testing the HOE devices with broadband source.

The collection of light from a moving source (such as a sun) which exhibits a broad spectral range of wavelengths is a complex task. HOEs have the potential to perform a range of functions in one element thus providing a solution to this problem, possibly without the need for tracking or mechanical movement. For the collection of light from a moving source, slanted, high efficiency gratings can provide an efficient means to re-direct light from many directions into one location where it can be converted. A careful design was priority to ensure that the collection of light is at single location. This is why volume gratings and photopolymers are of particular interest. Holographic optical elements can be designed to act as on or off axis focusing elements. Figure 2.6 shows

the schematic diagram of a light beam being focused by an on-axis and off-axis focusing HOE element recorded on a photopolymer layer.

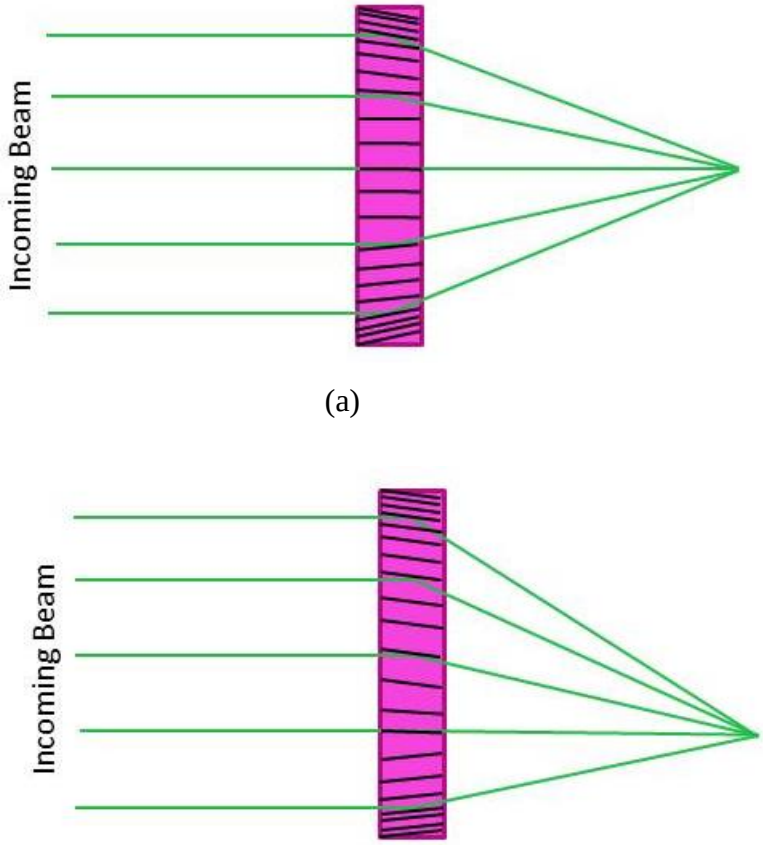

Figure 2-6 Reconstruction of a) on-axis HOE and b) off-axis HOE recorded in photopolymer layer

Such slanted gratings can be produced relatively easily by holographic recording in a photopolymer. This involves creation of a grating in the volume of a layer of polymer by interfering beams of light to produce the required refractive index distribution. The slant angle can be very high, and fringes can even be produced parallel to the plane of the medium (reflection holograms). Higher orders are suppressed by the sinusoidal nature of the interference pattern that creates the grating. The absence of higher orders

is an advantage over binary and multilevel surface gratings; an added advantage is that since the refractive index variation is produced in the volume of the material not the surface, devices can be protected with a plastic cover without affecting performance. Assuming the HOEs can be produced at low cost the key technical challenges are in providing a significant concentration factor so that smaller areas of PV can be used and maintaining this over a range of incident angles in order to limit the need for tracking.

This work focuses on optimization of the holographic recording in photopolymer to maximize their applicability to solar collection. Figure 2.7 illustrates the concept of the holographic concentrators using off-axis holographic lens. The incoming solar radiation is focused and redirected on solar cells utilize HOE.

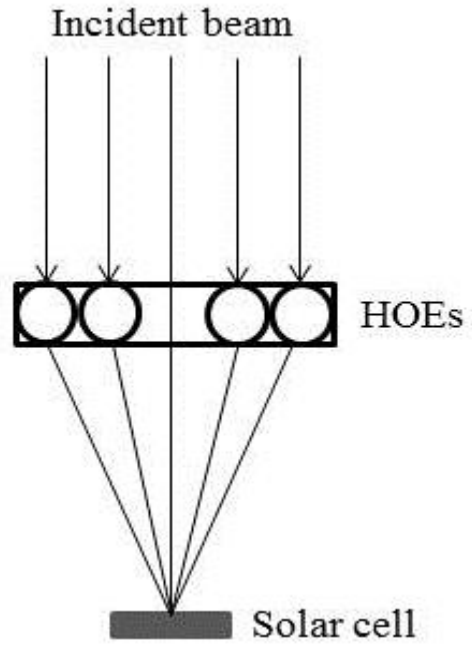

Figure 2-7 illustration of the concept

2.6 Research objectives

- To model the angular and wavelength selectivity of holographic optical elements at typical thicknesses for highly efficient recording in acrylamide based photopolymer in order to identify the conditions which will maximize the operational angular range of the individual elements.

- To develop and record protocol for recording highly efficient holographic optical elements at appropriate spatial frequencies, exposure energy and thickness in order to find the optimum recording parameters.

- To characterize a range of spherical and cylindrical focusing elements on plastic or glass substrate.

- To develop a combined device to be used in solar collection applications and demonstrate the capability of the acrylamide-based photopolymer for holographic concentrator, specifically to collect the light from a large angle and concentrate it on small centre part of c-Si solar cells.

- To test the performance of acrylamide-based photopolymer devices in use with c-Si solar cells.

2.7 Conclusion

In this chapter, the history of the development of holographic optical elements has been summarised. Following this, a review of the developments made to date in using holographic techniques in solar application has been given. This was done in order to introduce the research presented here, which is the fabrication of holographic optical elements with large range of operation to be used in solar applications. The motivation behind this is to develop a photopolymer holographic concentrator with the large range of operation, in order to reduce the size of detectors for collection of the energy. Also the main objectives of the research are listed.

References:

1. Saha P. Modern Climatology. Allied Publishers; 2012. 376 p.

2. Zweibel K. The Terawatt Challenge for Thin-Film PV. NREL Technical Report. 2005.

3. Green MA. Third generation photovoltaics: Solar cells for 2020 and beyond. Physica E: Low-Dimensional Systems and Nanostructures. 2002. p. 65–70.

4. Marshall AJ, Young DS, Blyth J, Kabilan S, Lowe CR. Metabolite-sensitive holographic biosensors. Anal Chem. 2004 Mar 1;76(5):1518–23.

5. Bhatta D, Christie G, Madrigal-González B, Blyth J, Lowe CR. Holographic sensors for the detection of bacterial spores. Biosens Bioelectron. 2007 Nov 30;23(4):520–7.

6. Naydenova I, Jallapuram R, Toal V, Martin S. A visual indication of environmental humidity using a color changing hologram recorded in a self-developing photopolymer. Appl Phys Lett. 2008;92(3).

7. Naydenova I, Jallapuram R, Toal V, Martin S. Characterisation of the humidity and temperature responses of a reflection hologram recorded in acrylamide-based photopolymer. Sensors Actuators, B Chem. 2009;139(1):35–8.

8. Leite E, Naydenova I, Mintova S, Leclercq L, Toal V. Photopolymerizable Nanocomposites for Holographic Recording and Sensor Application. Appl Opt. 2010;49(19):3652–60.

9. Battey DE, Slater JB, Wludyka R, Owen H, Pallister DM, Morris MD. Axial Transmissive f/1.8 Imaging Raman Spectrograph with Volume-Phase Holographic Filter and Grating. Appl Spectrosc. Society for Applied Spectroscopy; 1993 Nov 1;47(11):1913–9.

10. Sudarshanam VS, Pappu S V. Holographic optical element based single-mode hybrid fiber optic interferometer for realizing zero-order fringe. Fiber Integr Opt. Taylor & Francis Group; 1992 Jan 13;11(1):71–83.

11. Trolinger JD, Lal RB, Batra AK. Holographic instrumentation for monitoring crystal growth in space. In: Grover CP, editor. San Dieg - DL Tentative. International Society for Optics and Photonics; 1991. p. 151–65.

12. Kim T, Kim YS, Jang SH. Recent Progress on Three-dimensional Imaging System using Optical Scanning Holography. Digital Holography and Three-Dimensional Imaging. Washington, D.C.: OSA; 2013. p. DW4A.1.

13. Salvador M, Prauzner J, Salvador M, Prauzner J, Köber S, Köber S, et al. Three-dimensional holographic imaging of living tissue using a highly sensitive photorefractive polymer device. Opt Express. 2009;17(14):11834–49.

14. Cheng CCK. High-performance horizontal side scanner using holographic technology. In: Tsai YT, Kung T-M, Larsen J, editors. Asia Pacific Symposium on Optoelectronics '98. International Society for Optics and Photonics; 1998. p. 257–62.

15. Herzig HP, Dandliker R. Holographic optical scanning elements with minimum aberrations. Appl Opt [Internet]. 1988 Nov 15 [cited 2015 May 26];27(22):4739–46. Available from: http://www.ncbi.nlm.nih.gov/pubmed/20539643

16. Huang G, Pan L, Xu D, Pei J, Jia H. Holographic element for CD pickup-to-play DVD. In: Feng B, Tsunoda Y, editors. Photonics China '96. International Society for Optics and Photonics; 1996. p. 38–42.

17. Lee W-H. Holographic Optical Head For Compact Disk Applications. Opt Eng. International Society for Optics and Photonics; 1989 Jun 1;28(6):286650.

18. Kostuk RK, Castillo J, Russo JM, Rosenberg G. Spectral-shifting and holographic planar concentrators for use with photovoltaic solar cells. Proc SPIE. 2007;6649:66490I – 66490I – 8.

19. Shaji Sam TL, Vadivelan V, Ajith Kumar PT. A multi-beam holographic light concentrator for solar applications. Proc SPIE. 2007;6832(2007):68321E – 68321E – 6.

20. Ghosh A. Optimization of processing parameters of holographic concentrator for maximum efficiency operation in PV system. 2013;(1):50–3.

21. Kumar A, Deo N, Yadav H. Analysis of design parameters for wavelength selective holographic solar concentrators. Photovolt Spec …. 2008;(1):8–11.

22. Hsieh M, Lin S, Hsu KY, Burr J a, Lin S. An Efficient Solar Concentrator using Volume hologram. Conf Lasers Electro-Optics. 2011;1:4–5.

23. Mohan NK, Islam QT. Design of an off-axis HOE light concentrator to focus light from multiple directions in a plane. Opt Lasers Eng. 2006 Sep;44(9):943–53.

24. Brooks AE, Cronin AD, Russo JM, Zhang D, Vorndran S. One Year of Field Studies of Holographic Planar Concentrators At the Tucson Electric Power Solar Test Yard. Wref. 2012;1–7.

25. Sam STL, Kumar APT, Predeep P, Thakur M, Varma MKR. Design and Optimization of Photopolymer Based Holographic Solar Concentrators. 2011;248(2011):248–50.

26. Zhang D, Castro JM, Kostuk RK. One-axis tracking holographic planar concentrator systems. J Photonics Energy. 2011;1(1):015505.

27. Iurevych O, Gubin S, Dudeck M. Combined receiver of solar radiation with holographic planar concentrator. IOP Conf Ser Mater Sci Eng. 2012;29:012016.

28. Shakher C, Yadav HL. Dependence of diffraction efficiency of holographic concentrators on angle of illumination, hologram-thickness and wavelength of illuminating light. J Opt. 2000;21(6):267–72.

29. Castillo JE, Russo JM, Zhang D, Kostuk RK, Rosenberg G a. Low Holographic Concentration Effects on CIGS. Proc SPIE. 2010;7769:77690L – 77690L – 8.

30. Kostuk RK, Castro J, Myer B, Zhang D, Rosenberg G. Holographic elements in solar concentrator and collection systems. Proc SPIE. 2009;7407:74070E – 74070E – 8.

31. Castro J, Zhang D, Kostuk R. Holographic solar concentrator for residential & commercial solar power systems. Available from: http://www.physics.arizona.edu/~cronin/Solar/Talks/Presentation_2010_HSC_pepe.pdf

32. Froehlich K. Fabrication and test of a holographic concentrator for two-color PV operation. Opt Mater Technol Energy Effic Sol Energy Convers. 1994;2255:812–21.

33. Zhang YW, Ih CS, Yan HF, Chang MJ. Photovoltaic concentrator using a holographic optical element. Appl Opt. 1988;27(16):3556–60.

34. Castro JM, Zhang D, Myer B, Kostuk RK. Energy collection efficiency of holographic planar solar concentrators. Appl Opt. 2010;49(5):858–70.

35. Ghosh A, Nirala AK, Yadav HL. Dependence of wavelength selectivity of holographic PV concentrator on processing parameters. Opt - Int J Light Electron Opt. 2015 Mar;126(6):622–5.

36. Stojanoff CG. Engineering applications of HOEs manufactured with enhanced performance DCG films. Proc SPIE 6136, Pract Hologr XX Mater Appl. 2006;613601–613601 – 15.

37. Hung J, Chan PS, Sun C, Ho CW, Tam WY. Doubly slanted layer structures in holographic gelatin emulsions: solar concentrators. J Opt. 2010;12(4):045104.

38. Singh SN, Saw P, Kumar R. Techno - economic Viability of Holographic Solar Home Power Supply for Rural India Solar Energy Conversion : Solar Cells. 2012;1(1):23–8.

39. Hull JL, Lauer JP, Broadbent DC. Holographic Solar Concentrator. In: Holly S, Lampert CM, editors. 30th Annual Technical Symposium. International Society for Optics and Photonics; 1987. p. 68–74.

40. Chemisana D, Collados MV, Quintanilla M, Atencia J. Holographic lenses for building integrated concentrating photovoltaics. Appl Energy. Elsevier Ltd; 2013;110:227–35.

41. Ion Bita, Russell Wayne Gruhlke, Gang Xu MMM. Thin film holographic solar concentrator/collector. 2009.

42. Müller HFO. Application of holographic optical elements in buildings for various purposes like daylighting, solar shading and photovoltaic power generation. Renew Energy. 1994 Aug;5(5-8):935–41.

43. Naydenova I, Akbari H, Dalton C, Pang C, Wei T, Toal V. Photopolymer Holographic Optical Elements for Application in Solar Energy Concentrators. "Holography - Basic Princ Contemp Appl. 2013;

44. Toal V. Introduction to Holography. CRC Press; 2011. 502 p.

45. MEIER RW. Magnification and Third-Order Aberrations in Holography. JOSA. Optical Society of America; 1965 Aug 1;55(8):987–92.

46. CHAMPAGNE EB. Nonparaxial Imaging, Magnification, and Aberration Properties in Holography. J Opt Soc Am. Optical Society of America; 1967 Jan 1;57(1):51.

47. Kogelnik H. Coupled wave theory for thick hologram gratings. Bell Syst Tech J. 1969;48(9):2909–47.

48. Loewen EG, Nevière M, Maystre D. Grating efficiency theory as it applies to blazed and holographic gratings. Appl Opt. Optical Society of America; 1977 Oct 1;16(10):2711–21.

49. Gaylord TK, Moharam MG. Analysis and applications of optical diffraction by gratings. Proc IEEE. 1985;73(5):894–937.

50. Moharam MG, Grann EB, Pommet DA, Gaylord TK. Formulation for stable and efficient implementation of the rigorous coupled-wave analysis of binary gratings. J Opt Soc Am A. Optical Society of America; 1995 May 1;12(5):1068.

51. Lin LH, Doherty ET. Efficient and aberration-free wavefront reconstruction from holograms illuminated at wavelengths differing from the forming wavelength. Appl Opt. 1971 Jun 1;10(6):1314–8.

52. Brady DJ. Optical Imaging and Spectroscopy. John Wiley & Sons; 2009. 450 p.

53. Silvennoinen R, Jääskeläinen T. Design procedure using coupled multiwave efficiency analysis for wavelength shifted holographic optical elements. Opt Commun. 1981 Oct;39(3):123–6.

54. Herzig HP. Holographic optical elements (HOE) for semiconductor lasers. Opt Commun. 1986 Jun;58(3):144–8.

55. Awatsuji Y, Matsuura Y, Shimizu T, Kubota T. Design of the Optimum Holographic Optical Element Lens Using the Hologram Computer-Aided Design Tool. Opt Rev. 2001 Jul;8(4):249–53.

56. Shimizu T. Simulator for computer-aided design of holograms. Opt Eng. International Society for Optics and Photonics; 2001 Nov 1;40(11):2524.

57. Matsuura Y, Awatsuji Y, Kubota T. Optimum holographic optical element lens recorded by visible laser beams for an infrared two-dimensional vertical-cavity surface- emitting laser array. Opt Lett. Optical Society of America; 2003 May 15;28(10):795.

58. Ludman JE. Holographic solar concentrator. Appl Opt. Optical Society of America; 1982 Sep 1;21(17):3057–8.

59. Bloss WH, Griesinger M, Reinhardt ER. Dispersive concentrating systems based on transmission phase holograms for solar applications. Appl Opt. 1982;21(20):3739–42.

60. Macko P, Whelan MP. Fabrication of holographic diffractive optical elements for enhancing light collection from fluorescence-based biochips. Opt Lett. 2008;33(22):2614–6.

61. Kumar A, Deo N, Yadav HL. Analysis of design parameters of holographic solar concentrators for large acceptance angle. Conf Rec IEEE Photovolt Spec Conf. 2008;(11):7–10.

62. Kostuk RK, Castro J, Zhang D. Energy collection efficiency of low concentration holographic planar concentrators. In: Greene LE, Sherif RA, editors. SPIE Solar Energy + Technology. International Society for Optics and Photonics; 2010. p. 776902–776902 – 7.

63. Castro JM, Zhang D, Myer B, Kostuk RK. Energy collection efficiency of holographic planar solar concentrators. Appl Opt. Optical Society of America; 2010 Mar 10;49(5):858–70.

64. Kostuk RK, Castro J, Zhang D, Dimroth F, Kurtz S, Sala G, et al. Energy Yield Analysis of Tracking and Non-Tracking Holographic Planar Concentrators. AIP Conference Proceedings. American Institute of Physics; 2011. p. 137–40.

65. Michel C, Loicq J, Languy F, Habraken S. Optical study of a solar concentrator for space applications based on a diffractive/refractive optical combination. Sol Energy Mater Sol Cells [Internet]. 2014 Jan [cited 2015 Nov 9];120:183–90. Available from: http://www.sciencedirect.com/science/article/pii/S0927024813004509

66. Languy F. Achromatization of nonimaging Fresnel lenses for photovoltaic solar concentration using refractive and diffractive patterns. 2012 Dec 19 [cited 2015 Dec 17]; Available from: http://orbi.ulg.ac.be/handle/2268/136786

67. Altmeyer S, Hu Y, Thiée P, Matrisch J, Wallentin M, Silbermann J. Multiplexing of transmission holograms in photopolymer. 2013;3–4.

68. A. B. Sreebha, V. P. Mahadevan Pillai PTAK. Development of a Window Holographic Lens to Utilize Solar Energy, Advances in Optical Science and Engineering. Lakshminarayanan V, Bhattacharya I, editors. New Delhi: Springer India; 2015. chaper 19 p.

69. Bañares-Palacios P, Álvarez-Álvarez S, Marín-Sáez J, Collados M-V, Chemisana D, Atencia J. Broadband behavior of transmission volume holographic optical elements for solar concentration. Opt Express. Optical Society of America; 2015 Jun 1;23(11):A671–81.

70. James P a B, Bahaj a. S. Smart glazing solutions to glare and solar gain: A "sick building" case study. Energy Build. 2005;37(10):1058–67.

3 Theoretical modelling of performance of holographic optical elements

3.1 Introduction

The main purpose of the simulation work was to identify the best grating characteristics for recording devices suitable for solar collection applications. In this chapter, the numerical simulations of the variation of the diffraction efficiency with angle and wavelength are presented. The use of Kogelnik's theory [1]has been already discussed in chapter 1 and is well known for its success in predicting the behavior of volume photopolymer holograms. Therefore the theoretical modeling was carried out using Kogelnik's theory for gratings with various thicknesses at a range of spatial frequencies. In this chapter, theoretical model was then used to determine the angular FWHM of gratings at a range of spatial frequencies and thicknesses typically required to produce efficient gratings in the acrylamide based photopolymer layers. The number of gratings needed in order to collect light from an angle of ±22.5° was then calculated (based on the FWHM values).

Because the devices are expected to work in unpolarised or partially polarized light, the theoretical modeling of the performance of holographic components when probed with light of different polarization states is also presented.

3.2 Theoretical modelling of the angular selectivity of volume gratings

The most important optical characteristics of a HOE to be used in solar applications are the angular and wavelength selectivity, the diffraction efficiency and the stability of exposure to the sun. For a given material, the maximum achievable diffraction efficiency depends on the thickness of the holograms, but increasing the thickness also increases the selectivity, which restricts the range of angles of incidence for which the device will diffract light and also the wavelength range of operation.In order to optimize efficiency in these photopolymer a significant layer thickness is required. This means that there is significant angular and wavelength selectivity. Since each grating/HOE can only cover a certain range, it will be necessary to multiplex or stack a number of holograms in order to cover a larger angle and wavelength range. However, it is also known that selectivity depends on the spatial frequency of the grating. At a given thickness, a grating with a lower spatial frequency will have a much greater angular working range.

In order to explore this, the angular selectivity was modeled for a range of grating thickness between 25 μm-150 μm for six different grating spatial frequencies. In this way an optimum angular selectivity could be chosen to be tested in experimental work. This relationship can be explored using Kogelnik's theory [1] which is a widely accepted model used to relate diffraction efficiency and angular selectivity of volume gratings to the gratings' physical characteristics (thickness, spatial frequency and refractive index modulation). According to Kogelnik's theory the diffraction efficiency (η) can be calculated using equation (3.1), allowing us to model how the diffraction efficiency varies with angle of incidence, near the Bragg angle. This allows us to

observe how grating thickness and spatial frequency affect the angular selectivity of an individual grating:

$$\eta = \frac{\sin^2\sqrt{\left(\xi^2+\upsilon^2\right)}}{\left(1+\frac{\xi^2}{\upsilon^2}\right)} \quad \text{.....Equation 3.1}$$

The parameters ξ and υ are defined as:

$$\xi = \Delta\theta\frac{kd}{2} \quad \text{.....Equation 3.2}$$

$$\upsilon = \frac{\pi n_1 d}{\lambda\cos\theta} \quad \text{..... Equation 3.3}$$

Where d is the thickness of the grating, n_1 is the refractive index modulation; λ is the wavelength of the reconstructing beam; $\Delta\theta$ is the deviation from the Bragg angle and $\boldsymbol{k}$ is grating vector, normal to the fringes with a magnitude $k = 2\pi$/spatial period.

It can be seen from equation 3.2 that increasing the spatial period (reducing spatial frequency) is as effective as decreasing thickness in controlling the angular selectivity.

Figure 3.1-3.6 shows the variation of the diffraction efficiency with the incidence angle for gratings of various thicknesses at various spatial frequencies ranges between 100 lines/mm to 1000 lines/mm. It can be seen in figure 3.3 that for example at spatial frequency of 250 lines/mm, the lowest thickness of 25 μm has a wider Full Width Half Maximum (FWHM) of 7.5° and the highest thickness of 150 μm has a narrower FWHM of 1.2°. In use as a solar collector, this will mean that the thinner grating will accept light from a larger range of angles than the thicker one, reducing the number of gratings needed to cover the full angular range of the moving sun. Kogelnik's theory shows that high diffraction efficiency can be achieved by controlling the thicknesses of holographic sample, spatial frequency/fringe spacing and depth of refractive index modulation.

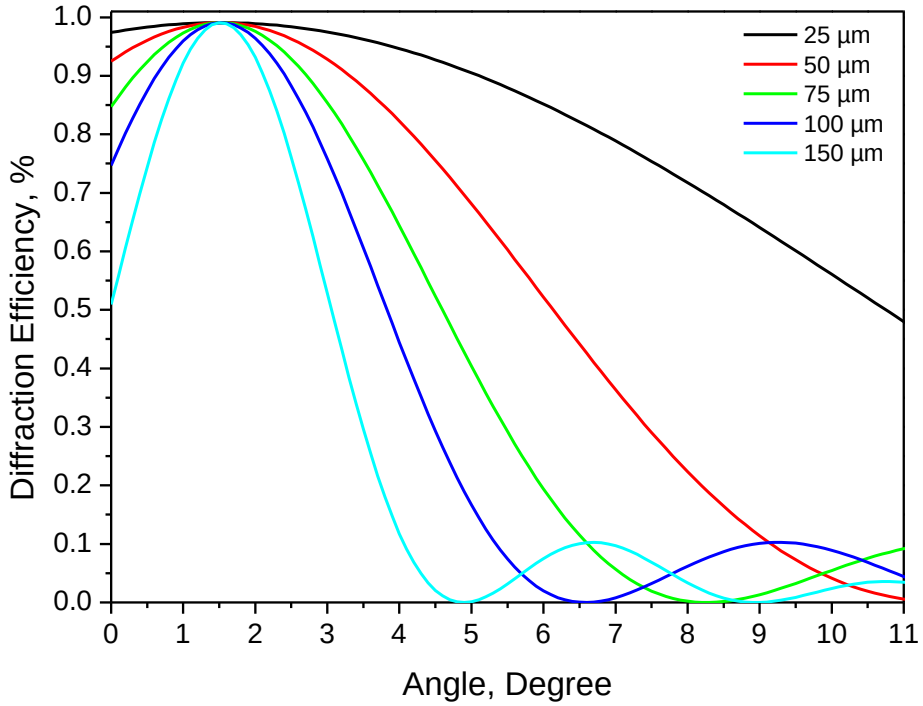

Figure 3-1 Numerical simulation of the variation of the diffraction efficiency with the incidence angle for gratings of various thicknesses, calculated for spatial frequency of 100 l/mm.

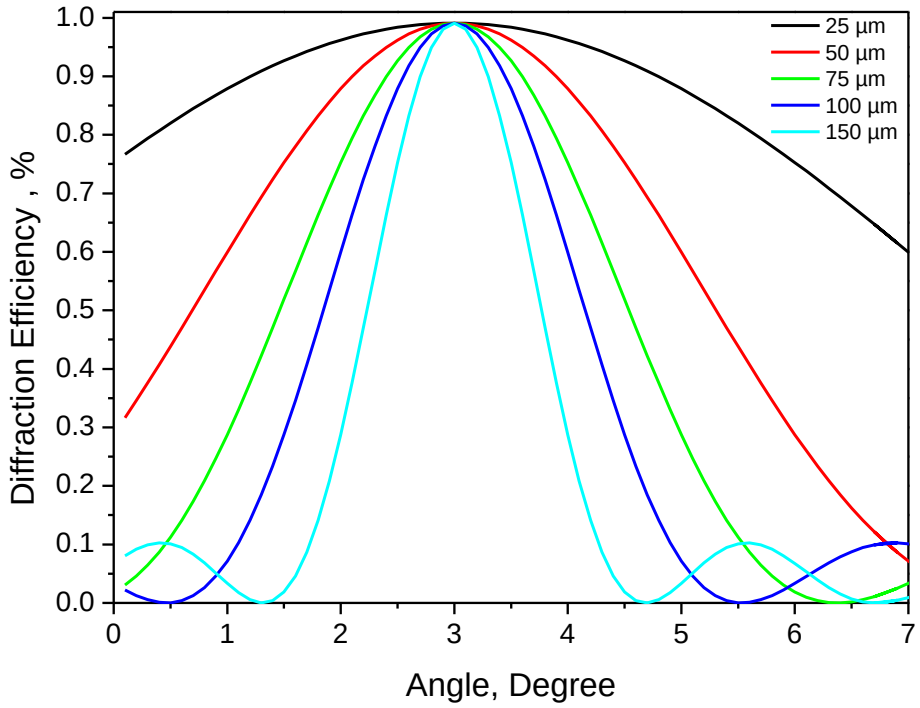

Figure 3-2 Numerical simulation of the variation of the diffraction efficiency with the incidence angle for gratings of various thicknesses, calculated for spatial frequency of 200 l/mm.

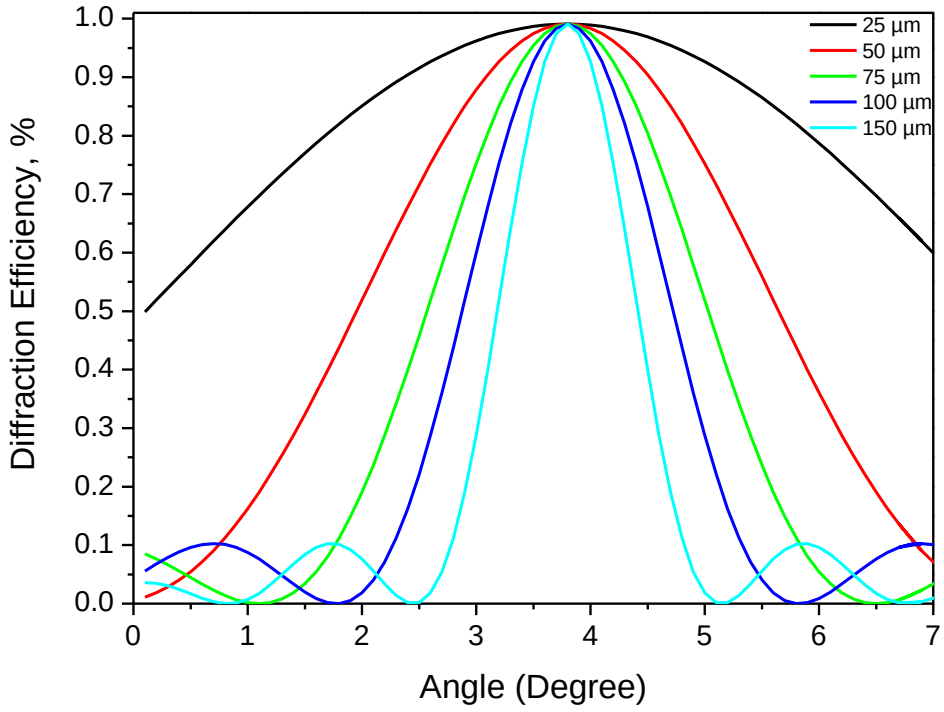

Figure 3-3 Numerical simulation of the variation of the diffraction efficiency with the incidence angle for gratings of various thicknesses, calculated for spatial frequency of 250 l/mm.

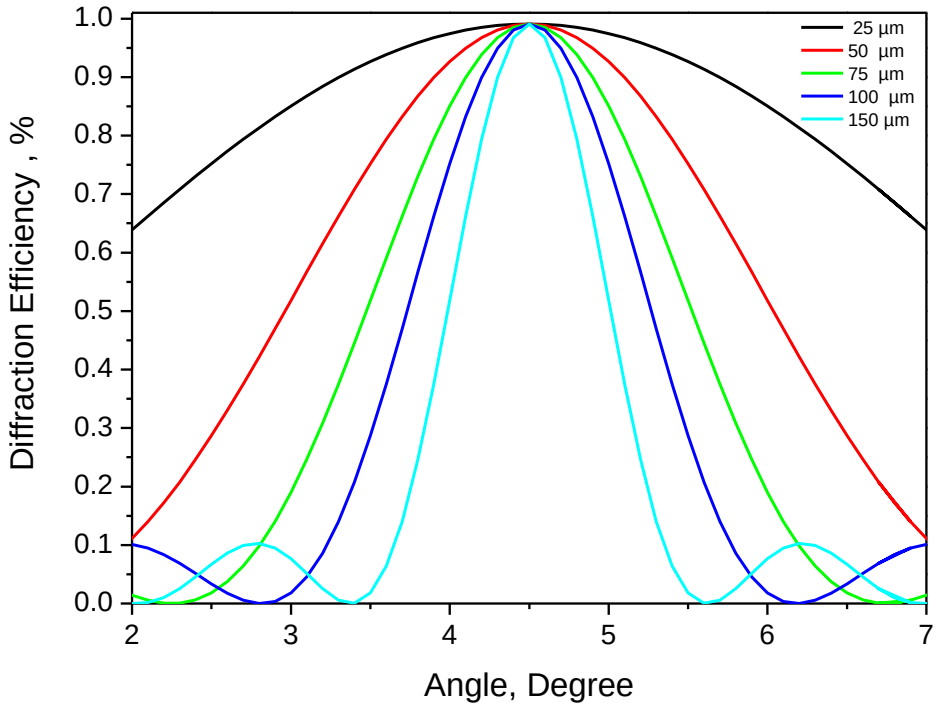

Figure 3-4 Numerical simulation of the variation of the diffraction efficiency with the incidence angle for gratings of various thicknesses, calculated for spatial frequency of 300 l/mm.

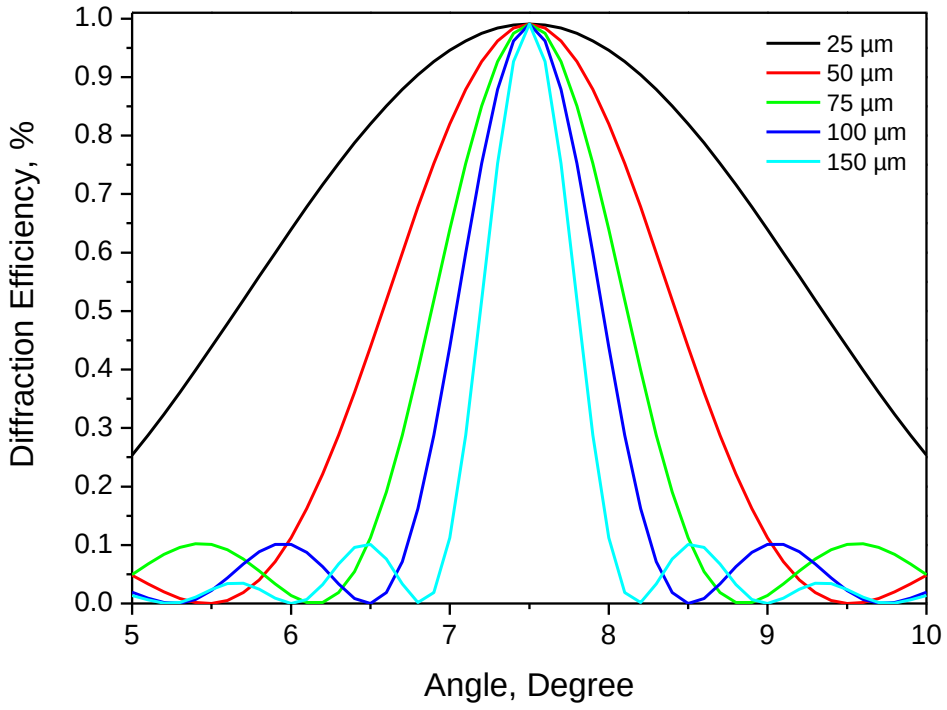

Figure 3-5 Numerical simulation of the variation of the diffraction efficiency with the incidence angle for gratings of various thicknesses, calculated for spatial frequency of 500 l/mm.

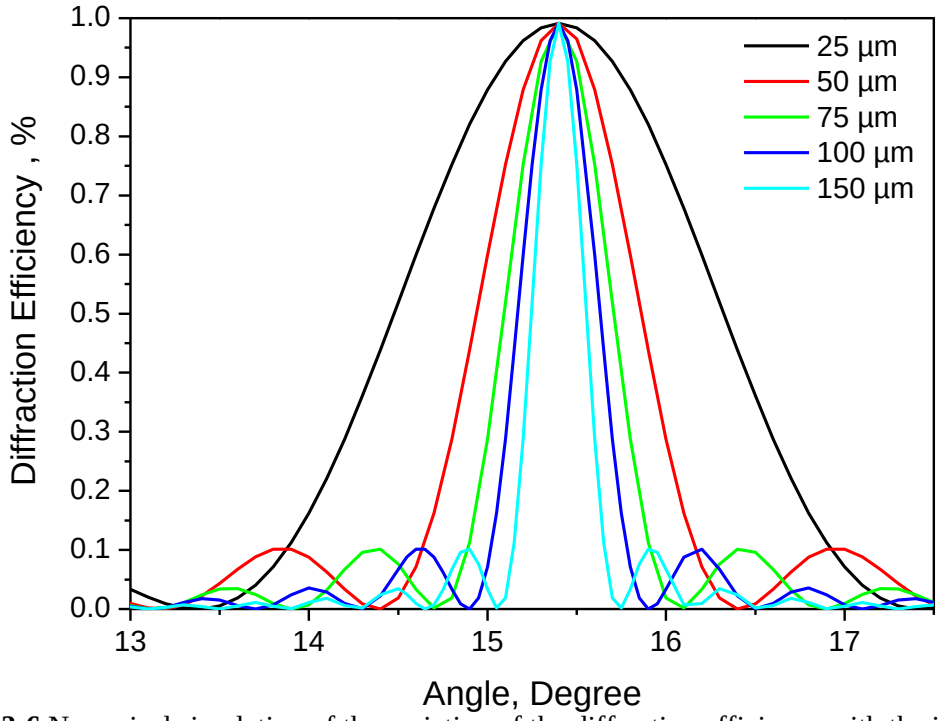

Figure 3-6 Numerical simulation of the variation of the diffraction efficiency with the incidence angle for gratings of various thicknesses, calculated for spatial frequency of 1000 l/mm.

The theoretical model was then used to determine the angular FWHM of gratings at a range of spatial frequencies and thicknesses typically required to produce efficient gratings in the acrylamide based photopolymer layers. The number of gratings needed in order to collect light from an angle of 45 ^{o} was then calculated (based on the FWHM values) and is shown in figure 3.7.

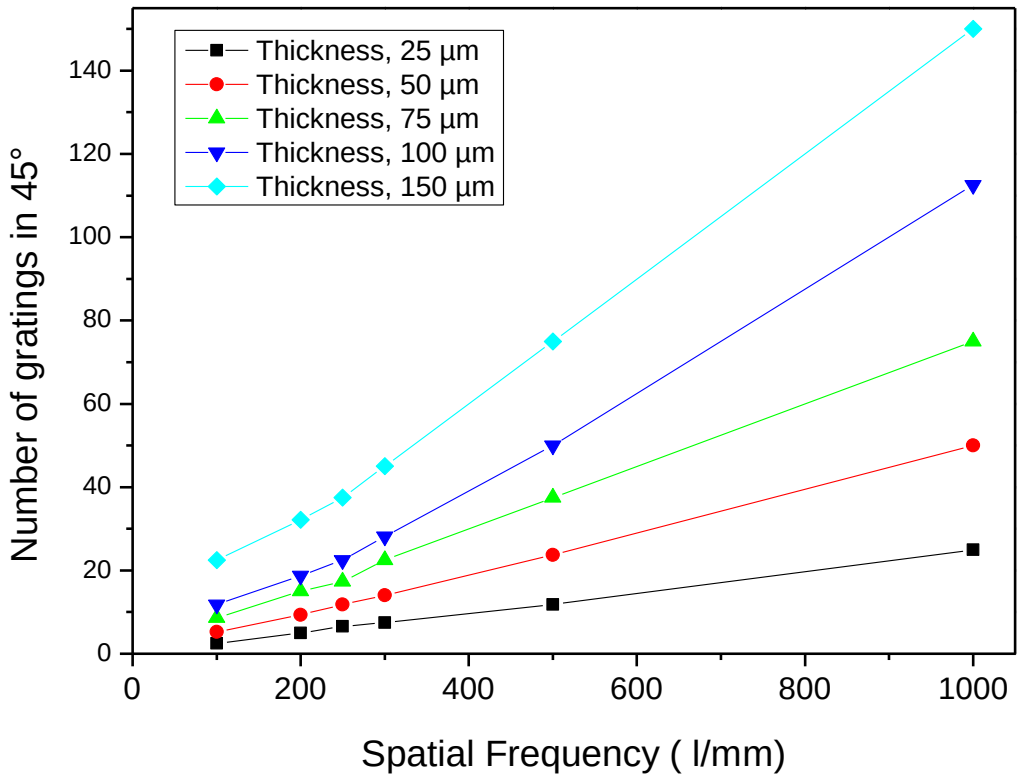

Figure 3-7 Calculation of the number of multiplexed gratings required to cover a working range of 45 degrees versus spatial frequency. Markers indicate the positions of calculated values.

From figure 3.7 one can see that collection from angles of 45^{o} is possible with a reasonably small number of gratings for spatial frequencies of 100 to 300 l/mm. however with gratings of 1000 l/mm spatial frequency over 20 gratings are required even at the lowest thickness (25 microns) in order to cover the 45° acceptance angle.

Since the lower spatial frequencies provide the most achievable numbers, holographic recording at 100, 200 and 300 l/mm was investigated experimentally.

In previous work 35 gratings with very low diffraction efficiency were multiplexed successfully in an acrylamide based photopolymer [2] for data storage applications. More recently, sets of three and five higher diffraction efficiency gratings and focusing elements have been multiplexed into a single layer of photopolymer [3], at spatial frequencies 450-1700 l/mm and thickness 100-120 microns. This demonstrated the ability to multiplex gratings but the angular range of each individual grating was small.

The challenge for solar collection is to multiplex/combine a smaller number of high diffraction efficiency, low spatial frequency gratings in order to achieve efficiency redirection of the light to the fixed detector for incident angles spanning 45°.

This chapter focuses on identifying the optimum spatial frequencies for achieving lower angular selectivity by using the well known Kogelnik theory and then the next chapter looks into the optimization of the grating recording process experimentally for these grating elements at a range of layer thicknesses.

Figure 3.8 shows the summary of the variation of the FWHM for range of spatial frequency using the theoretical simulations curves. It can clearly be observed that the FWHM is larger for the gratings recorded at lower spatial frequencies. Also indicate the dependence of the FWHM values on the thickness of the gratings. The result verifies that the lower spatial frequencies are more suitable for capturing the light from larger angle.

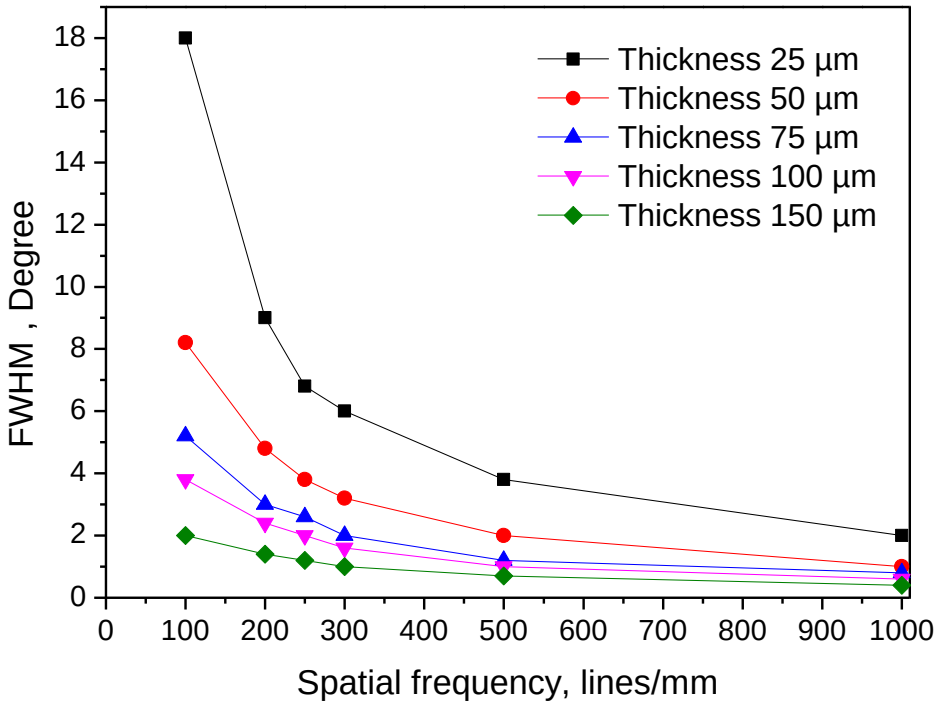

Figure 3-8 FWHM values vs spatial frequency for the range of photopolymer thicknesses

3.3 Theoretical modelling of the wavelength selectivity

The wavelength selectivity was also modelled for a range of grating thickness between 25 µm-100 µm for six different grating spatial frequencies. Knowledge of dependence of diffraction efficiency on wavelength is also of key importance for solar applications, this is influenced by hologram recording angle, thickness of the recording media and refractive index modulation. Kogelnik theory (equation 3.1) was again used [1].

This allows us to model how the diffraction efficiency varies with wavelength in visible range of spectrum. The parameter ξ is represented here in terms of wavelength:

$$\xi = \left[\frac{\Delta\lambda k^2 d}{8\pi n_0 \cos\theta_B} \right] \qquad \text{Equation 3.4}$$

Where d is the thickness of the grating, n_0 is the refractive index modulation; $\Delta\lambda$ is the deviation from the recording wavelength; θ_B is the Bragg angle and $\boldsymbol{k}$ is interference fringe vector, normal to the fringes with a magnitude $k = 2\pi$/spatial period.

Figure 3.9-3.14 shows the variation of the diffraction efficiency with the wavelength for gratings of various thicknesses at various spatial frequencies ranges between 100 lines/mm to 1000 lines/mm. The results show that the wavelength selectivity also depends on the spatial frequency and the thickness of the gratings**,** but at special frequency of lower than 500 l/mm they are not very selective over the visible wavelength range. At 250 lines/mm the FWHM for a 100 micron thick grating is more than 350 nm. The theoretical modelling result confirms that recording holographic optical elements at lower spatial frequencies are more suitable for solar applications.

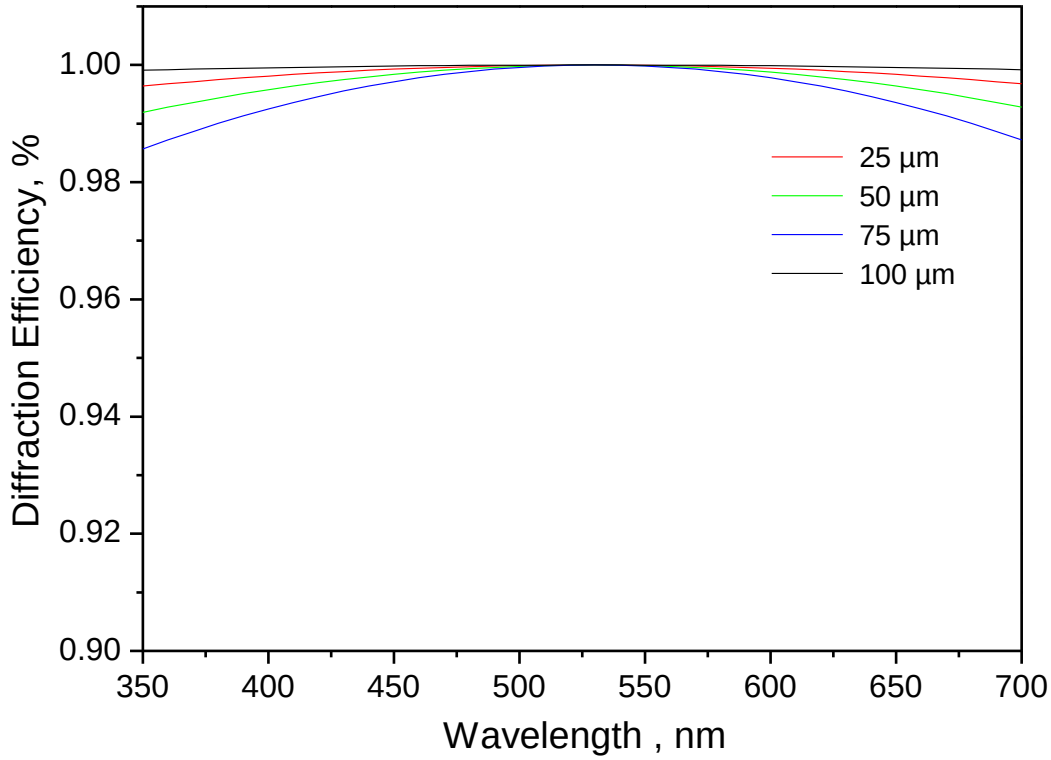

Figure 3-9 Numerical simulation of the variation of the diffraction efficiency with the wavelength selectivity of gratings of various thicknesses, calculated for spatial frequency of 100 l/mm.

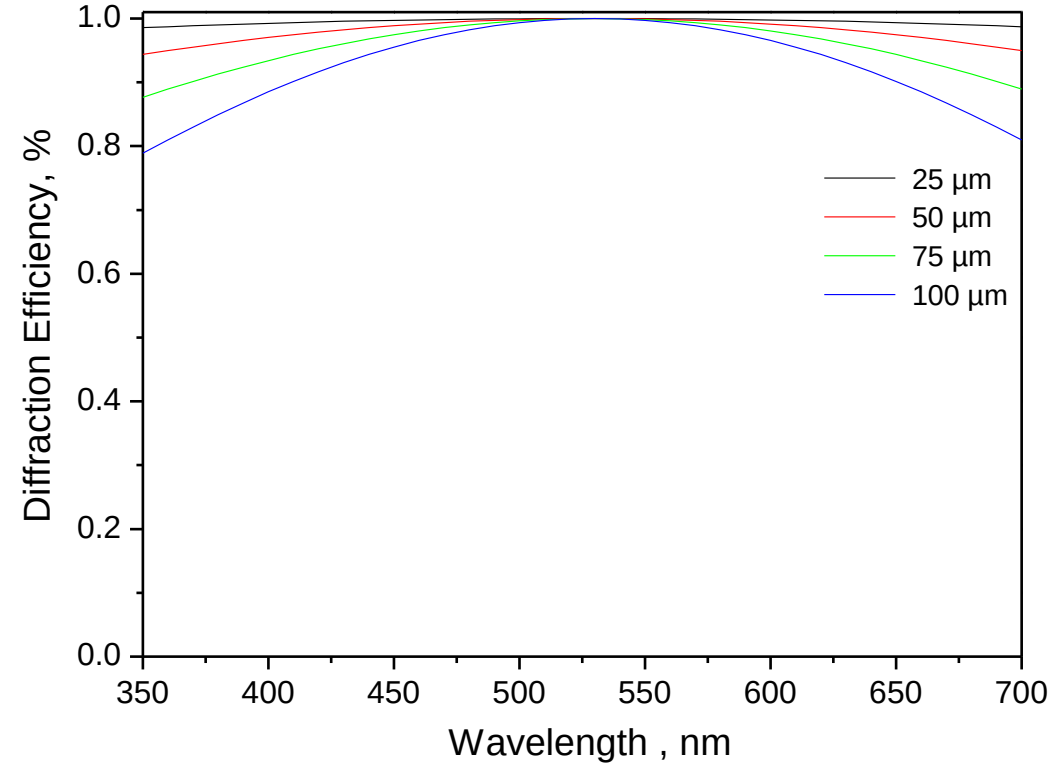

Figure 3-10 Numerical simulation of the variation of the diffraction efficiency with the wavelength selectivity of gratings of various thicknesses, calculated for spatial frequency of 200 l/mm.

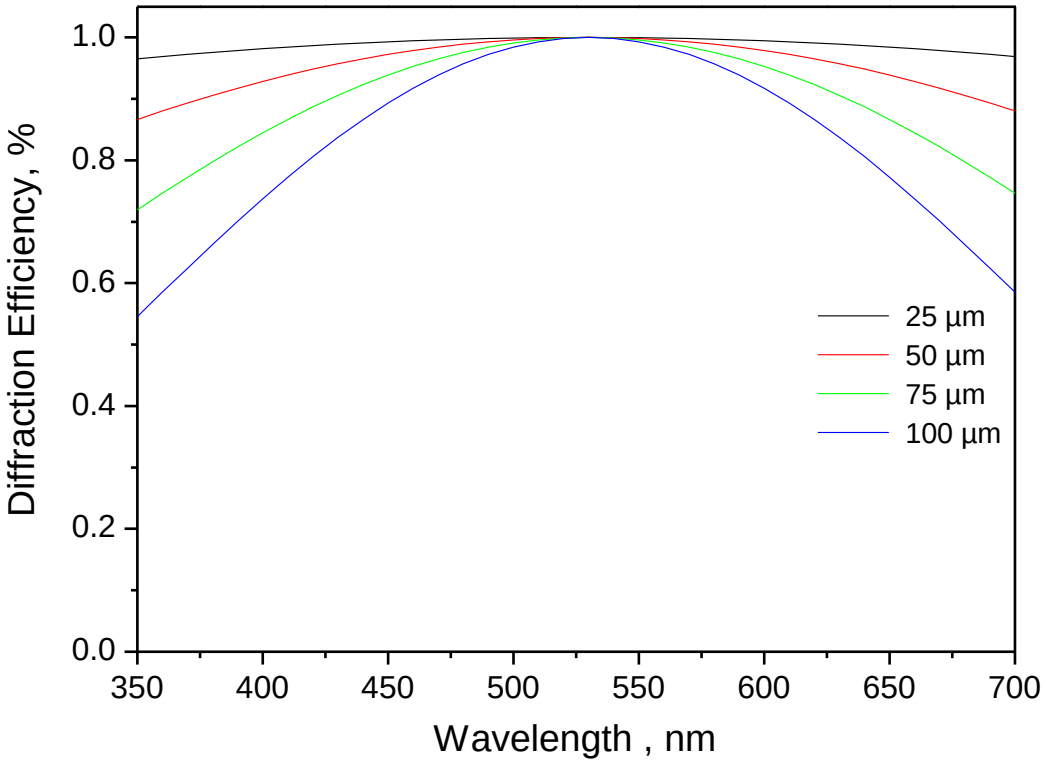

Figure 3-11 Numerical simulation of the variation of the diffraction efficiency with the wavelength selectivity of gratings of various thicknesses, calculated for spatial frequency of 250 l/mm.

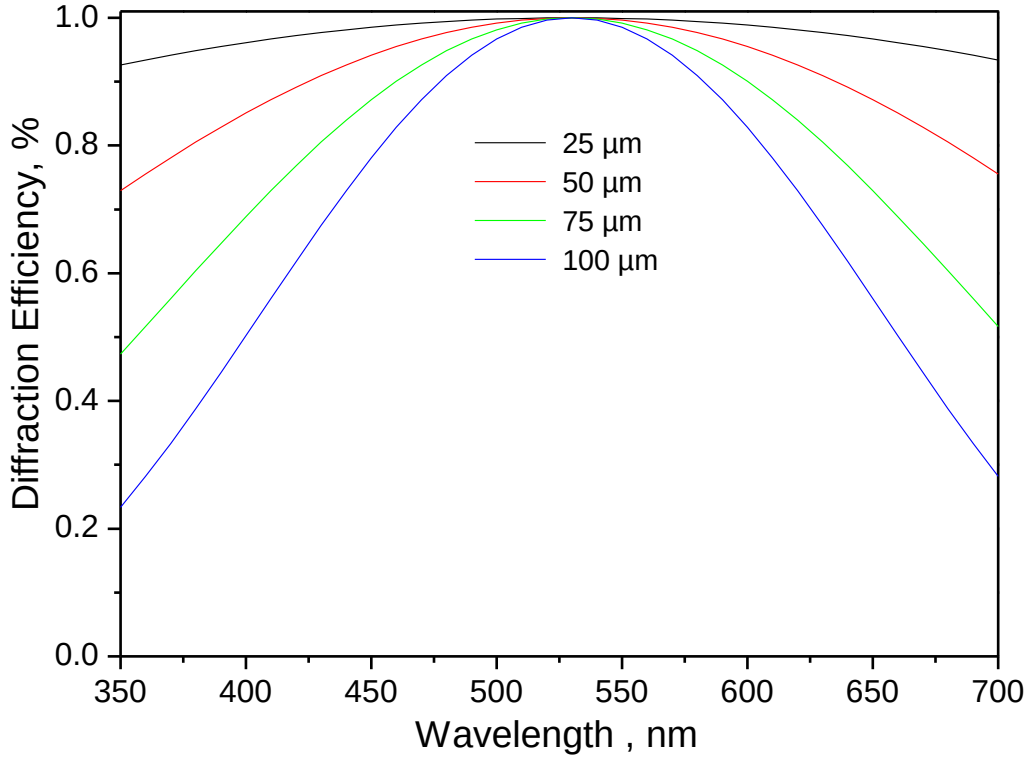

Figure 3-12 Numerical simulation of the variation of the diffraction efficiency with the wavelength selectivity of gratings of various thicknesses, calculated for spatial frequency of 300 l/mm.

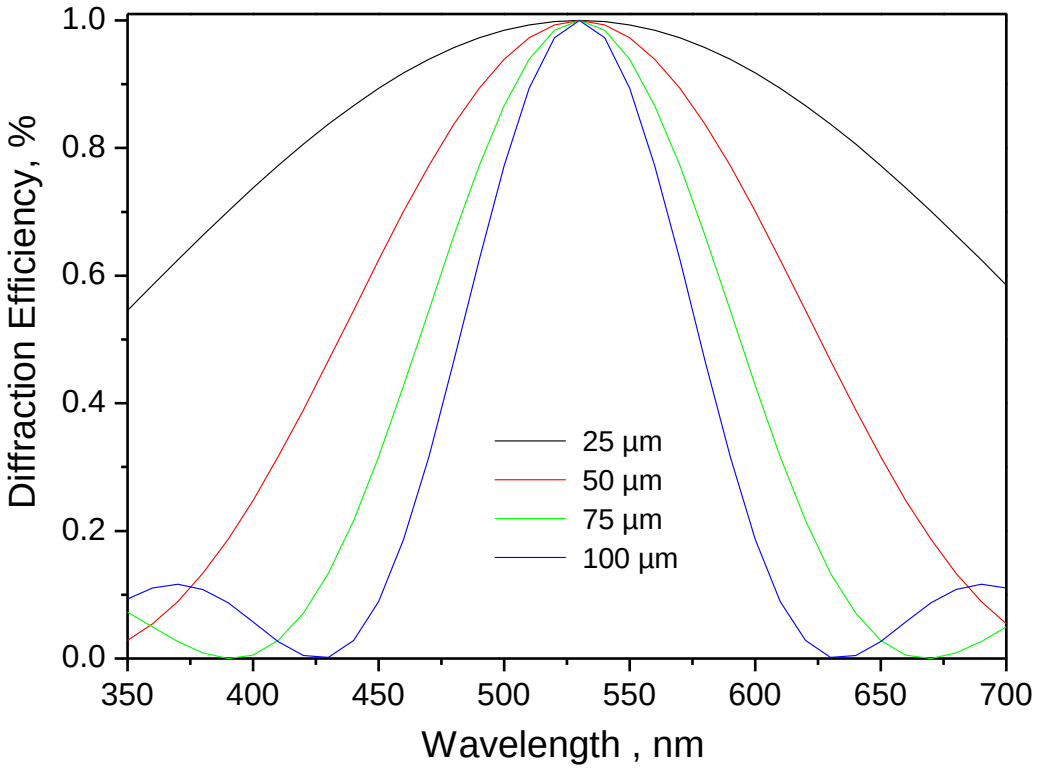

Figure 3-13 Numerical simulation of the variation of the diffraction efficiency with the wavelength selectivity of gratings of various thicknesses, calculated for spatial frequency of 500 l/mm.

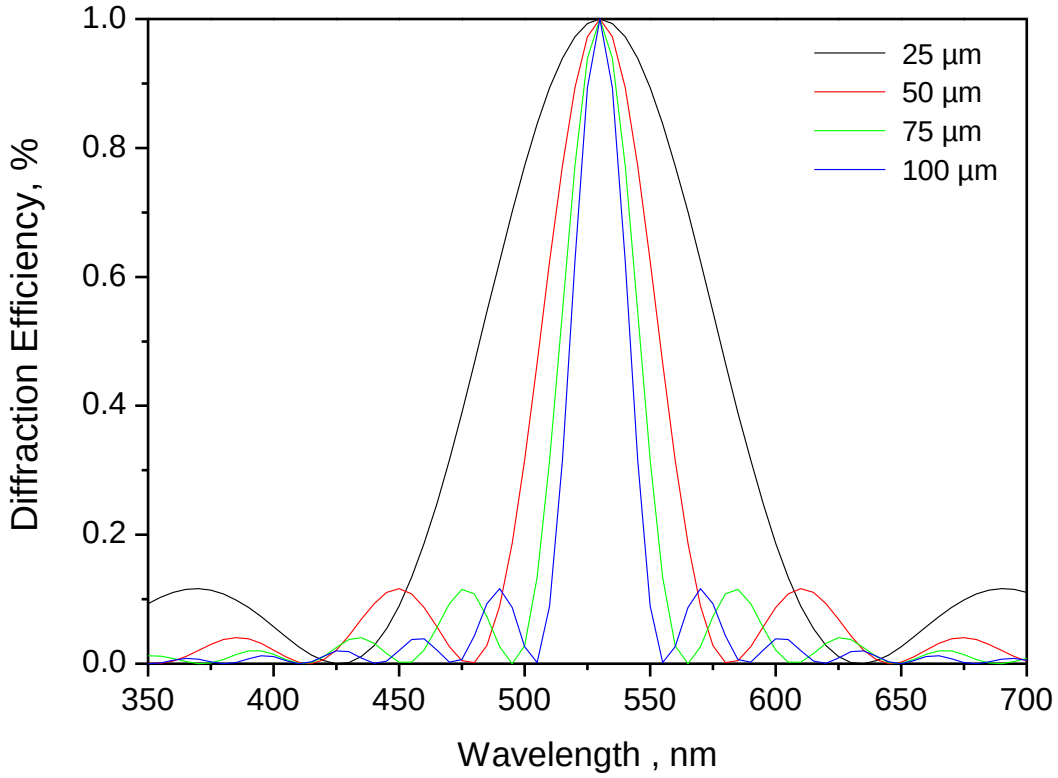

Figure 3-14 Numerical simulation of the variation of the diffraction efficiency with the wavelength selectivity of gratings of various thicknesses, calculated for spatial frequency of 1000 l/mm.

3.4 Theoretical modelling of dependence of diffraction efficiency for S and P polarization of the probe beam

The dependence of the diffraction efficiency of the gratings on S-polarization (when the electric field vector is parallel to the fringes of the grating) and P-polarization (when the electric field vector is perpendicular to the fringes) of the incoming beam at range of spatial frequencies between 100 l/mm – 2500 l/mm is investigated.

In the laboratory most gratings and HOEs are tested by illumination with laser light, however, in many real-world applications diffractive devices need to re-direct light that is not plane polarized, monochromatic, collimated laser light. Angular and wavelength changes have been discussed above, but another factor, polarization state of the incident light can also be modelled with Kogelnik's theory. As the sun produces un-polarized light, the difference in diffraction efficiency for S and P polarization of the recorded elements is of some importance.

This difference can be modelled using Kogelnik's theory and has previously been exploited in order to make specific types of holographic elements. Habraken et al reports a design for polarizing holographic optical elements. The presented theoretical and experimental results confirmed the possibility of making polarizing beam splitters by carefully controlling the relationship between the diffraction efficiency for S and P polarized light for plane diffraction gratings [4]. These were demonstrated experimentally in DCG recording material.

The polarization properties and the first order diffraction efficiency of the volume phase holographic transmission grating are also discussed by Baldry et al. The importance of considering the separate polarization states and the possibility of creating S-P-phased gratings which could achieve 100% efficiency with using unpolarized light at specific

angle has been described [5]. Also the variation of the diffraction efficiency versus Bragg angle using Kogelnik to determine the first order diffraction efficiencies at the Bragg condition was presented [1]. For unpolarized light the diffraction efficiency is given by:

$$\eta = \frac{1}{2}\sin^2\left(\frac{\pi\Delta n^2{}_1 d}{\lambda\cos\alpha}\right) + \frac{1}{2}\sin^2\left(\frac{\pi\Delta n^2{}_1 d}{\lambda\cos\alpha}\cos(2\alpha)\right) \qquad \text{Equation 3.5}$$

where the first term is for S-polarized light and the second term is for P-polarized light and Δn_1 is the refractive index modulation, d is the grating thickness and λ is the wavelength of the reconstruction beam and α is defined as the angle between the incident beam and the grating fringes.

In order to model the variation of diffraction efficiency versus grating thickness for the S and P polarization, equation 3.5 was used for the slanted grating recorded in acrylamide based photopolymer, with the fixed refractive index modulation of approximately 0.005 and fixed probe wavelength of 633 nm for a range of spatial frequency between 100 l/mm – 2500 l/mm which correspond to the fringe spacing between 10 µm – 0.4 µm. The angle α was calculated for each case inside the medium (assuming a 1.5 refractive index) depending on the geometry of reconstruction.

The results for unpolarized light, S and P states are presented in figure 3.14-3.20, which show the efficiency increasing with thickness for both polarization states and also an average of the two. The difference is of course more pronounced for greater thickness. For the graphs representing the higher spatial frequencies (> 1000 lines/mm, Λ=1 µm) there is an observable difference at the higher thickness. This confirms that the lower spatial frequencies are again better suited to these elements. The effect of polarisation on diffraction is more obvious at high spatial frequency.

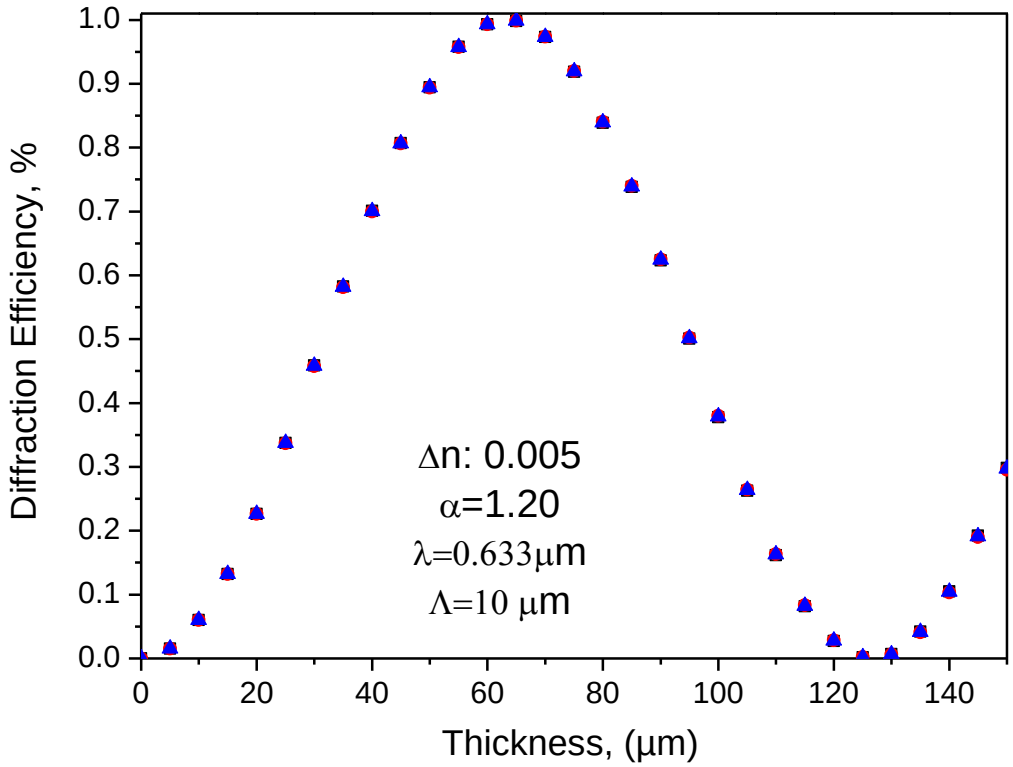

Figure 3-15 Dependence of ±1order diffraction efficiency on grating thickness for range of HOE at spatial frequency of 100 lines/mm. The theoretical results are presented for unpolarized light ▲ , S ■ and P ● polarization.

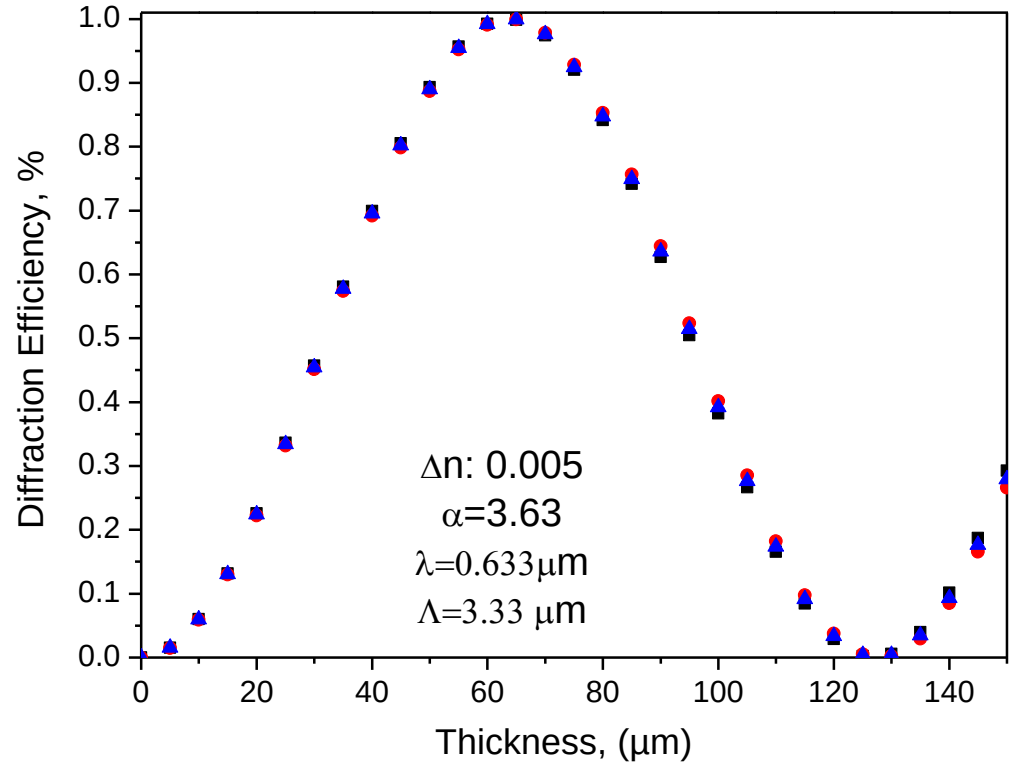

Figure 3-16 Dependence of ±1order diffraction efficiency on grating thickness for range of HOE at spatial frequency of 300 lines/mm. The theoretical results are presented for unpolarized light ▲ , S ■ and P ● polarization.

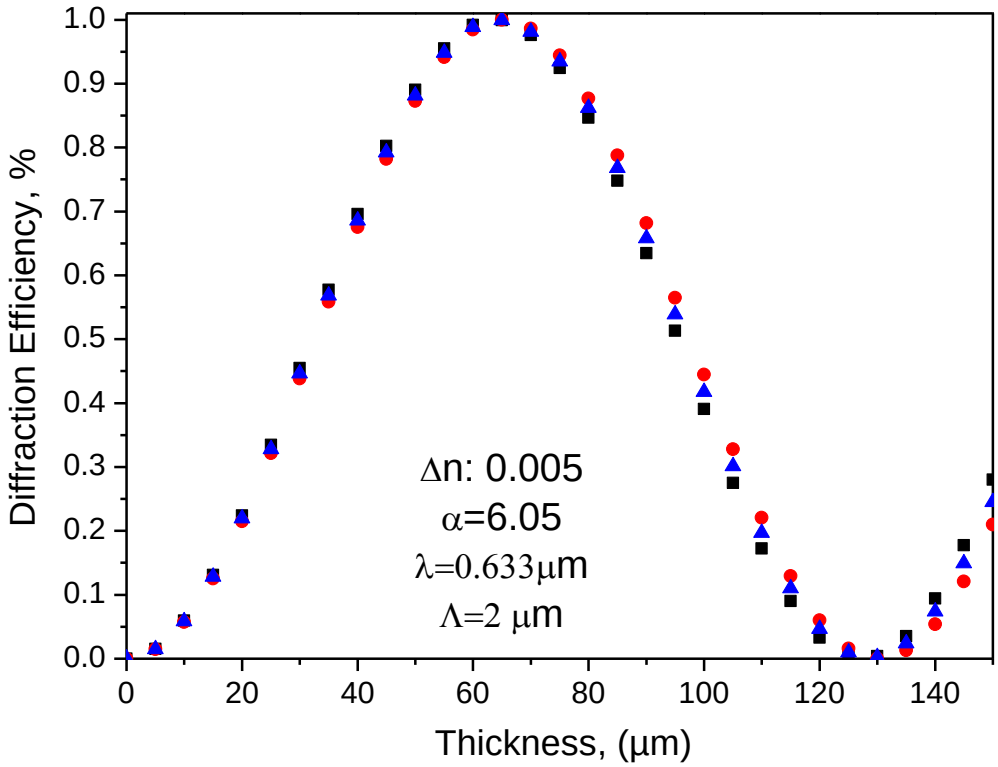

Figure 3-17 Dependence of ±1order diffraction efficiency on grating thickness for range of HOE at spatial frequency of 500 lines/mm. The theoretical results are presented for unpolarized light ▲, S ■ and P ● polarization.

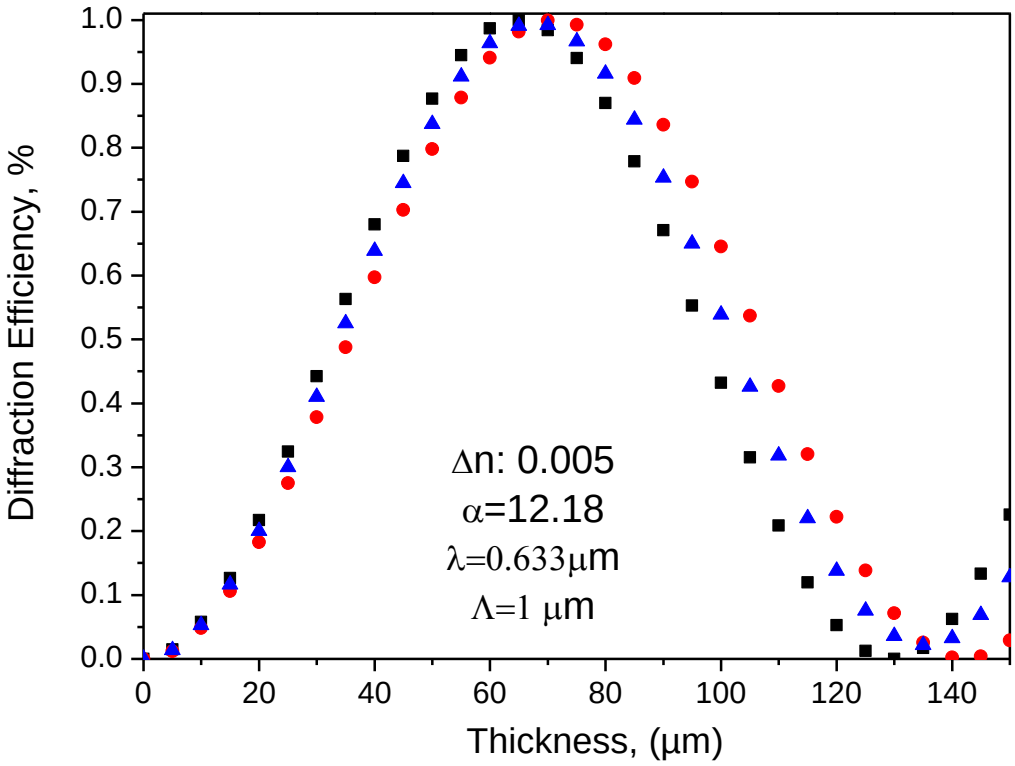

Figure 3-18 Dependence of ±1order diffraction efficiency on grating thickness for range of HOE at spatial frequency of 1000 lines/mm. The theoretical results are presented for unpolarized light ▲, S ■ and P ● polarization.

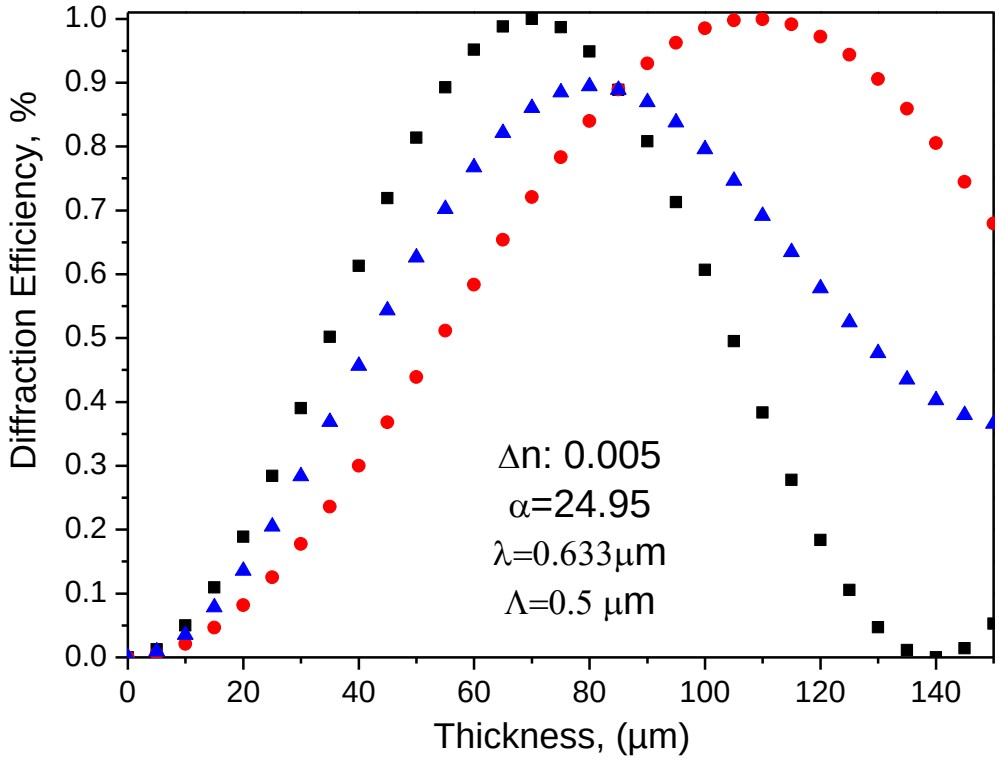

Figure 3-19 Dependence of ±1order diffraction efficiency on grating thickness for range of HOE at spatial frequency of 2000 lines/mm. The theoretical results are presented for unpolarized light ▲, S ■ and P ● polarization.

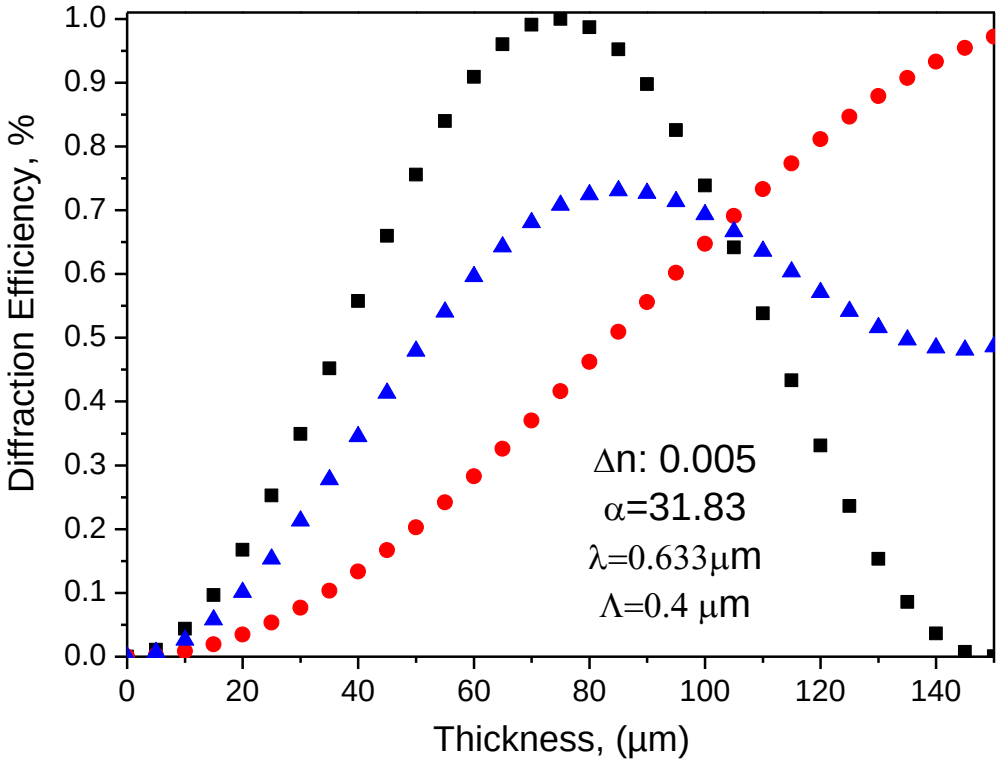

Figure 3-20 Dependence of ±1order diffraction efficiency on grating thickness for range of HOE at spatial frequency of 2500 lines/mm. The theoretical results are presented for unpolarized light ▲, S ■ and P ● polarization.

3.5 Conclusion

The materials used here perform well at low spatial frequency but need a minimum of 25-50 microns grating thickness in order to produce good diffraction efficiency gratings, for this reason reducing spatial frequency rather than thickness gives better experimental results. The results from modelling confirmed that lower spatial frequencies are more suitable for capturing light over a wide range of angles. At the thicknesses most commonly used in acrylamide based photopolymers, spatial frequencies as low as a few hundred lines per millimetre are necessary in order to keep the number of multiplexed gratings used in a solar collector low. The wavelength selectivity simulation shows that at low spatial frequency the gratings are not very selective and they can achieve high diffraction efficiency in full visible range of spectrum. Results confirmed that the difference in the diffraction efficiency for S and P polarization depends on the spatial frequency and the thickness of the layer. At higher spatial frequencies, the dependence of the diffraction efficiency on polarization state was observed to be greater compared to the lower spatial frequency. This indicates that lower spatial frequency is again preferable for use HOE in solar application, so that any fall-off in diffraction efficiency for P polarized components is minimized

The overall results indicate that the spatial frequency of below 300 l/mm is an optimum spatial frequency and will be used for further study in this application where the HOE lenses with relatively high diffraction efficiency are needed. It is necessary that the diffraction efficiency is not overly dependent on the polarization of the incident light. The next chapter investigates holographic recording in photopolymers at these low spatial frequencies in order to find the conditions for achieving devices with optimum diffraction efficiency.

Reference:

1. Kogelnik H. Coupled wave theory for thick hologram gratings. Bell Syst Tech J. 1969;48(9):2909–47.

2. Sherif H, Naydenova I, Martin S, McGinn C, Toal V. Characterization of an acrylamide-based photopolymer for data storage utilizing holographic angular multiplexing. J Opt A Pure Appl Opt. 2005;7(5):255–60.

3. Naydenova I, Akbari H, Dalton C, Pang C, Wei T, Toal V. Photopolymer Holographic Optical Elements for Application in Solar Energy Concentrators. "Holography - Basic Princ Contemp Appl. 2013;

4. Habraken S, Renotte Y, Roose S, Stijns E, Lion Y. Design for polarizing holographic optical elements. Appl Opt. OSA; 1995 Jul 1;34(19):3595–602.

5. Baldry IK, Bland Hawthorn J, Robertson JG. Volume Phase Holographic Gratings: Polarization Properties and Diffraction Efficiency. Publ Astron Soc Pacific. The University of Chicago Press; 2004 May 20;116(819):403–14.

4 Optimisation of the recording parameters for low spatial frequency photopolymer transmission gratings

4.1 Introduction

In this chapter the recording set up and the measurement techniques used to characterize the diffraction efficiency of recorded holographic gratings and holographic optical elements are explained in detail. The aim of this chapter is to record low spatial frequency gratings. The modelling carried out in the previous chapter shows that lowering spatial frequency will maximize the operational angular range of the individual elements. In this chapter we seek to record with the lowest spatial frequency possible in the photopolymer gratings without compromising the high diffraction efficiency. Optimum conditions for recording high diffraction efficiency gratings at low spatial frequencies are determined. Transmission gratings were recorded at range of three low spatial frequencies for a number of sample thicknesses and at various recording intensities. The diffraction efficiency of each recorded grating is measured in real time. The results are presented below.

Recording intensities ranging from 1 to 3 mW/cm^2 were investigated, for exposure energies of 5 to 55 mJ/cm^2. This exposure energy dependence study was carried out at three different spatial frequencies: 100, 200 and 300 l/mm and range of layer thickness 50-150 µm. The gratings were compared in terms of their maximum diffraction efficiency and the FWHM angular working range.

This chapter focusses on optimizing the diffraction efficiency and the angular selectivity, so that the individual gratings and /or focusing elements can reach the required parameters. Some of the results that are presented in this chapter have been published in [1].

4.2 EXPERIMENT

4.2.1 Sample preparation

4.2.1.1 Stock solution of polyvinyl alcohol (PVA)

9% polyvinyl alcohol (PVA) was prepared by adding 10 grams of polyvinyl alcohol with specified molecular weight into 100 ml of deionized water which was slowly heated up to temperature of about 80°C; The component were stirred until completely dissolved by using an electrical stirring plate.

4.2.1.2 Stock solution of dye

The 0.11% wt/v of dye solution was prepared by dissolving 0.11 grams of erythrosine B in 100 ml of deionized water. The solution was stirred until all the dye was dissolved. The solution was always kept in the dark.

4.2.1.3 Acrylamide-based photopolymer stock solution

The material used in this research is a self-developing acrylamide-based water-soluble photopolymer as previously described[2]. The composition of this material is acrylamide and methylenebisacrylamide monomers, triethanolamine as an initiator, and a polyvinyl alcohol binder. The components shown in table 4.1 were mixed well in a dark room by using a magnetic stirrer. The average refractive index of the fabricated photopolymer layer was measured by an Abbe refractometer and it was found that it is n_0 =1.50 +/- 0.005 [3].

Table 4.1: Concentrations of the photopolymer composition

Components	*Amount*
Acrylamide	11 mmol
Methylenebisacrylamide	1.3 mmol
Polyvinyl alcohol (10% wt/v stock)	17.5 ml
Triethanolamine	15 mmol
Erythrosine B dye(0.11% wt/v)	5 µmol

4.2.2 Layer Preparation

A specific volume of photopolymer solution is spread evenly on a 26 x 76 mm^2 glass plate placed on a levelled surface and allowed to dry. The thickness of the sample is controlled by the amount of the solution. The samples were left in dark room to dry for usually about 18–24 hours at temperature ranging between 20 - 23 degrees and relative humidity ranging 30-40 %.

4.2.3 Experimental set up

A two-beam holographic optical setup as shown in figure 4.1 was used to record un-slanted transmission gratings using a S-polarised Nd:YVO4 laser (532 nm). The spatial frequency was altered by changing the angle between the beams used to record the gratings. Equation 4.1 was used to calculate the required angle between the two interfering beams:

$$\sin\theta = \frac{\lambda}{2\Lambda} \qquad \text{Equation 4.1}$$

where λ is recording wavelength, Λ is fringe spacing; θ is half of the angle between the two interfering beams.

During the recording the vibration was minimized by using a Newport optical table with pneumatic isolation. Newport magnetic stands were used in order to hold the optical equipment. The intensity of the recording beams was controlled using a neutral density

filter. The absorption of the photopolymer sensitized with Erythrosin B dye is negligible at 633 nm, Therefore a He-Ne laser (633 nm) was used as a probe beam. The probe beam was arranged at the appropriate Bragg angle in order to monitor the diffraction efficiency of the grating, during exposure, in real time.

In order to characterize the diffracted intensity dependence on the incident angle of the probe beam (angular selectivity), the grating was placed on a rotational stage (Newport, ESP 300) and an optical power meter (Newport 1830-C) was used to record the intensity of the diffracted beam as the sample was rotated. The data was recorded by a data acquisition card and LabVIEW program. The rotational stage has accuracy of 1×10^{-3} deg.

The diffraction efficiency, η of the gratings is defined in equation 4.2 as the ratio of the intensity in the first diffraction order I_d and the incident intensity I_{in} of the probe beam:

$$\eta = \frac{I_d}{I_{in}} \times 100 \qquad \text{Equation 4.2}$$

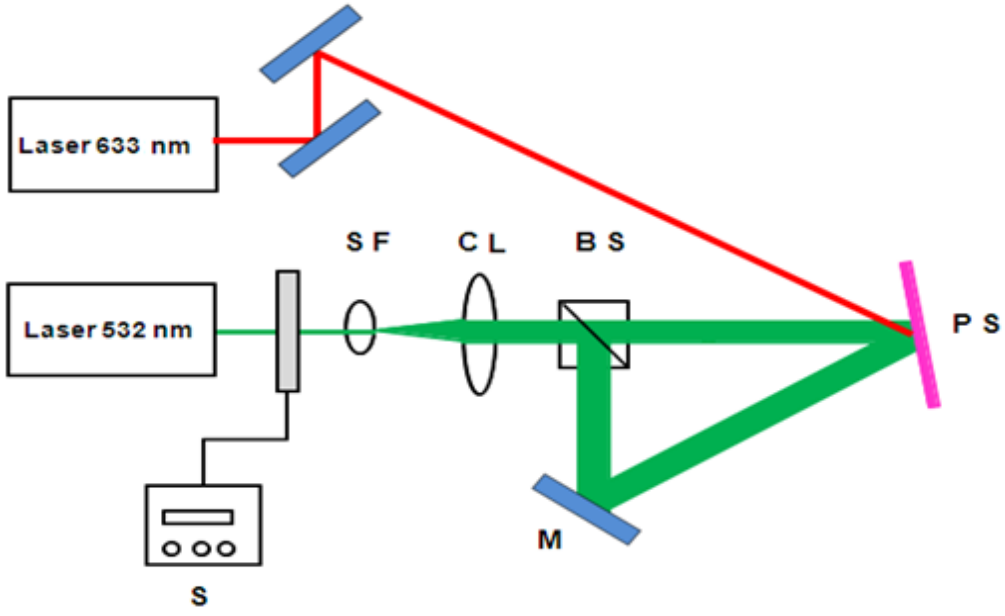

Figure 4-1 Experimental set up: S: shutter, CL: collimating lens, BS: beam splitter, SF: spatial filter, M: mirror, PS: photopolymer sample.

4.3 Results and discussion

4.3.1 Comparison of the diffraction efficiency of transmission gratings recorded at different spatial frequencies and recording intensities for a range of layer thicknesses

The diffraction efficiency of gratings were measured during holographic recording and compared for polymer layers of thicknesses ranging from 50 µm to 150 µm at spatial frequency 300 l/mm, 200 l/mm and 100 l/mm. Exposure intensity was varied between ranges of 1 mW/cm^2- 3 mW/cm^2. The results for all three spatial frequencies with the exposure intensity of ranges between 1 mW/cm^2 – 3 mW/cm^2 are presented in the next few pages. High efficiency achieved at low thickness and low spatial frequency is of most interest as these are the gratings that will have the maximum working range.

The maximum diffraction efficiency observed here was 80% and this was achieved at spatial frequencies of 200 and 300 l/mm for layer thicknesses 75 µm and above. Samples with thickness 50 µm achieved 75% efficiency at a spatial frequency of 300 l/mm. For layers of thickness of 150, 100 µm and even 75 µm over-modulation was observed at longer exposures.

Over-modulation indicates that the refractive index modulation is greater than the value needed for maximum diffraction efficiency for that holographic recording. As can be seen from equation 1.3 the diffraction efficiency will initially increase as the refractive index modulation increases. However if the refractive index modulation increases beyond the point where the phase difference introduced by the diffraction grating is 180^o, the diffraction efficiency will decrease. This is referred to as over-modulation.

From these results we observe that the grating recorded at very low spatial frequency of 100 l/mm does not achieve high diffraction efficiency, but 200 and 300 l/mm perform well. It was also observed that layers of thickness as low as 50 µm can achieve high efficiency at spatial frequency of 300 l/mm. The low diffraction efficiencies observed at 100 l/mm are due to a combination of reduced diffusion and loss of light into higher orders because the grating is now behaving less like a thick grating. For ease of comparison the y-axis on each of the three graphs in figure 4.2- 4.4 are given the same scale and range.

4.3.1.1 Low recording intensity (1mW/cm²)

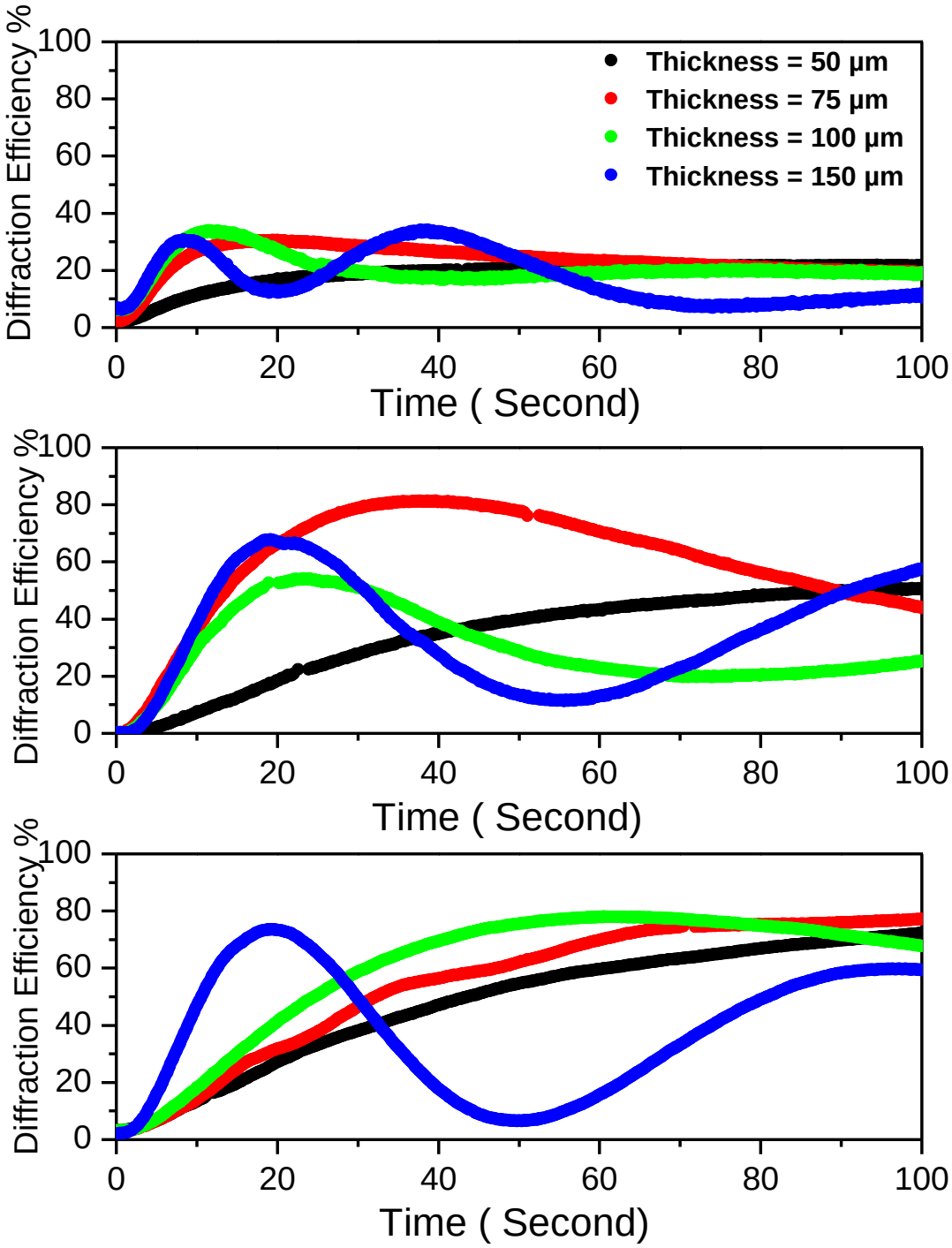

Figure 4-2 Real time measurements of the diffraction efficiency of gratings recorded in polymer layers of various thicknesses; recording intensity is 1 mW/cm^2 and the spatial frequency is a) 100 l/mm, b) 200 l/mm, c) 300 l/mm.

4.3.1.2 Moderate recording intensity (2 mW/cm²)

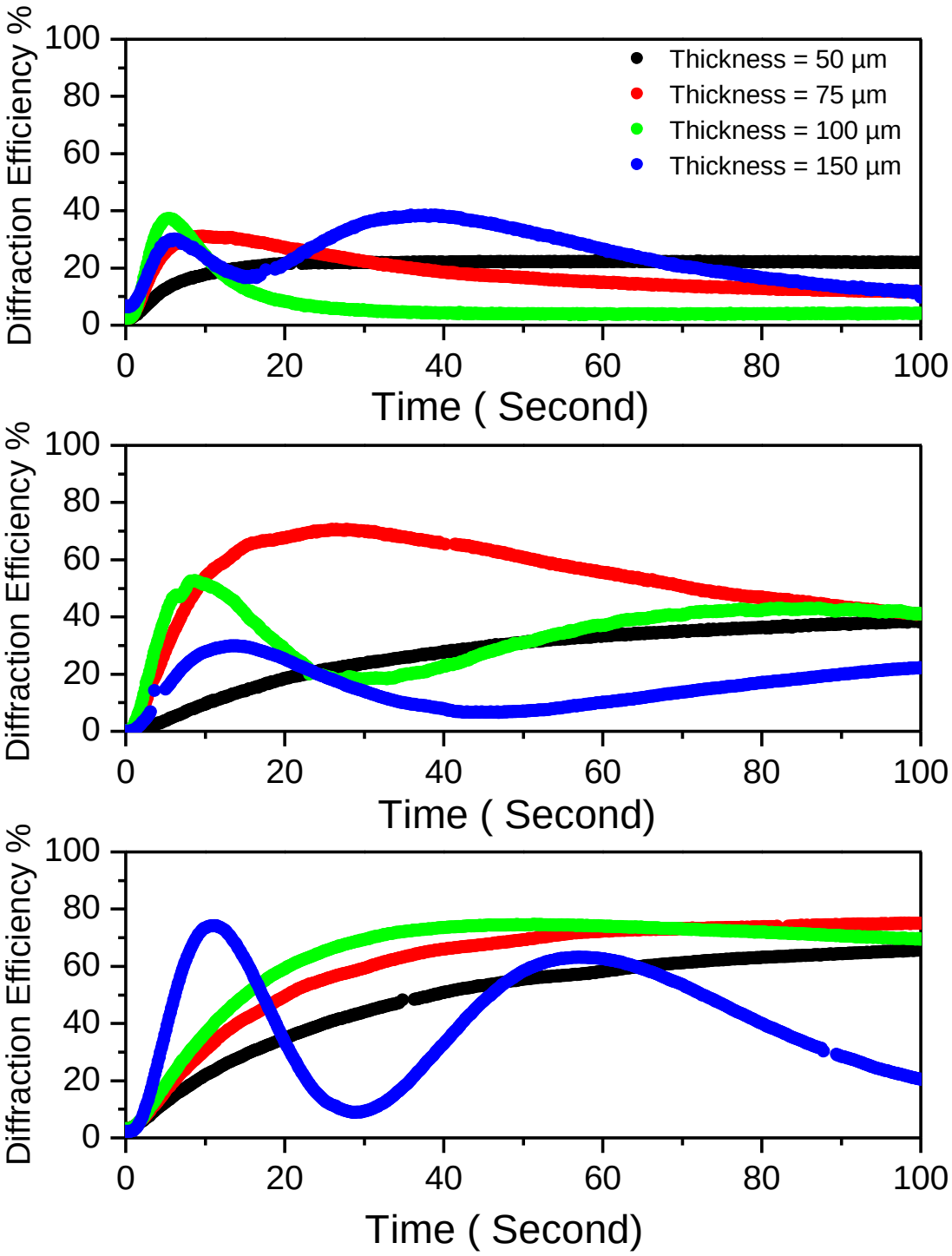

Figure 4-3 Real time measurements of the diffraction efficiency of gratings recorded in polymer layers of various thicknesses; recording intensity is 2 mW/cm^2 and the spatial frequency is a) 100 l/mm, b) 200 l/mm, c) 300 l/mm.

4.3.1.3 Higher recording intensity (3mW/cm²)

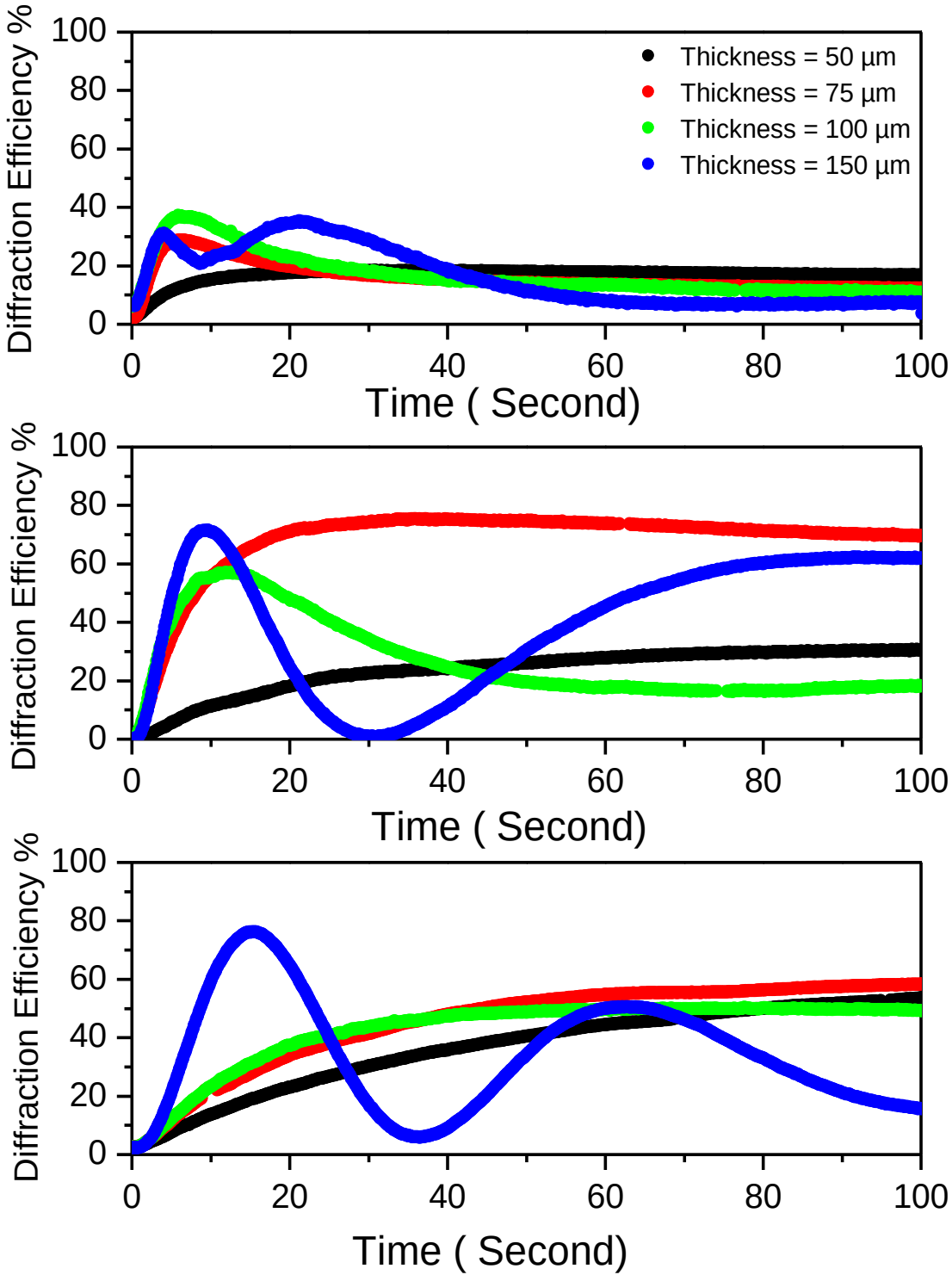

Figure 4-4 Real time measurements of the diffraction efficiency of gratings recorded in polymer layers of various thicknesses; recording intensity is 3 mW/cm^2 and the spatial frequency is a) 100 l/mm, b) 200 l/mm, c) 300 l/mm.

The next study examined how the diffraction efficiency evolution during recording depends on the recording intensity. The purpose of this study was to identify the maximum diffraction efficiency achievable at each spatial frequency by optimizing the recording conditions. The summery of the results are presented in table 4.2.

Table 4.2: Concentrations of the photopolymer composition

Spatial Frequency	Thickness of layer	Exposure energy	Maximum DE
100 lines/mm	50 µm	55 mJ/cm^2	18 %
	75 µm	20 mJ/cm^2	30 %
	100 µm	10 mJ/cm^2	25 %
	150 µm	55 mJ/cm^2	22 %
200 lines/mm	50 µm	55 mJ/cm^2	40 %
	75 µm	30 mJ/cm^2	80 %
	100 µm	30 mJ/cm^2	60 %
	150 µm	25 mJ/cm^2	70%
300 lines/mm	50 µm	55 mJ/cm^2	60 %
	75 µm	55 mJ/cm^2	63 %
	100 µm	55 mJ/cm^2	79 %
	150 µm	20 mJ/cm^2	75 %

4.3.2 Dependence of diffraction efficiency on recording intensity at spatial frequency of 300 l/mm

In order to determine the optimum recording intensity at each spatial frequency, results for exposure at different intensities was compared for each spatial frequency and thickness tested.

The results presented in figure 4.5-4.8 show the relationship between first order diffraction efficiency of the transmission gratings and recording intensity, for a spatial frequency of 300 l/mm, in layers of thicknesses with the range between 50µm -150µm.

From the results, it can be observed that the maximum diffraction efficiency is achieved at lower recording intensities. A clear dependence of diffraction efficiency on recording intensity was observed in both layers of 50 and 75 µm thickness. Recording at lower intensity leads to higher diffraction efficiency. At lower intensity the polymerisation process is slower and thus the monomer molecules have enough time to diffuse from dark to bright regions and contribute to the final refractive index modulation.

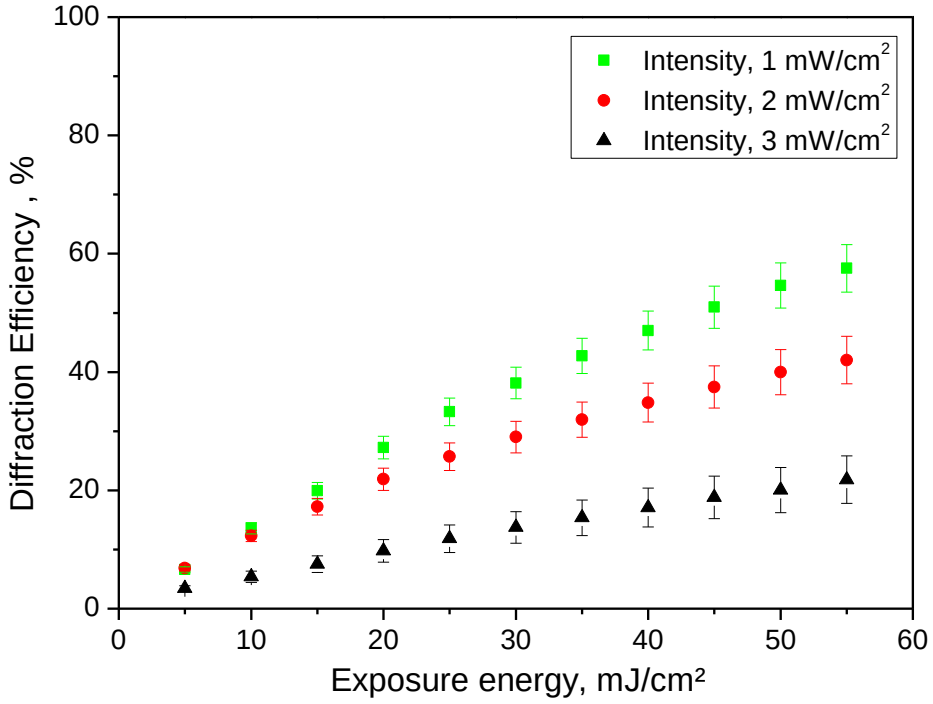

Figure 4-5 Measured diffraction efficiency vs. Exposure energy for the transmission gratings with various intensities between 1-3 mW/cm^2 at spatial frequency of 300 l/mm was investigated for sample thicknesses of 50 µm.

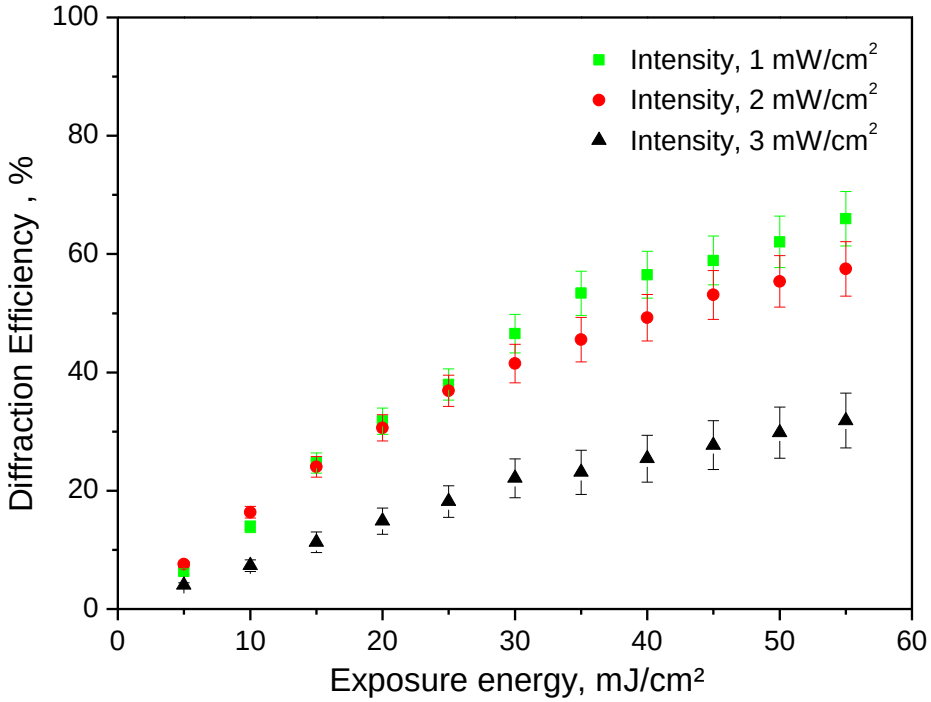

Figure 4-6 Measured diffraction efficiency vs. Exposure energy for the transmission gratings

with various intensities between 1-3 mW/cm^2 at spatial frequency of 300 l/mm was investigated for sample thicknesses of 75 µm.

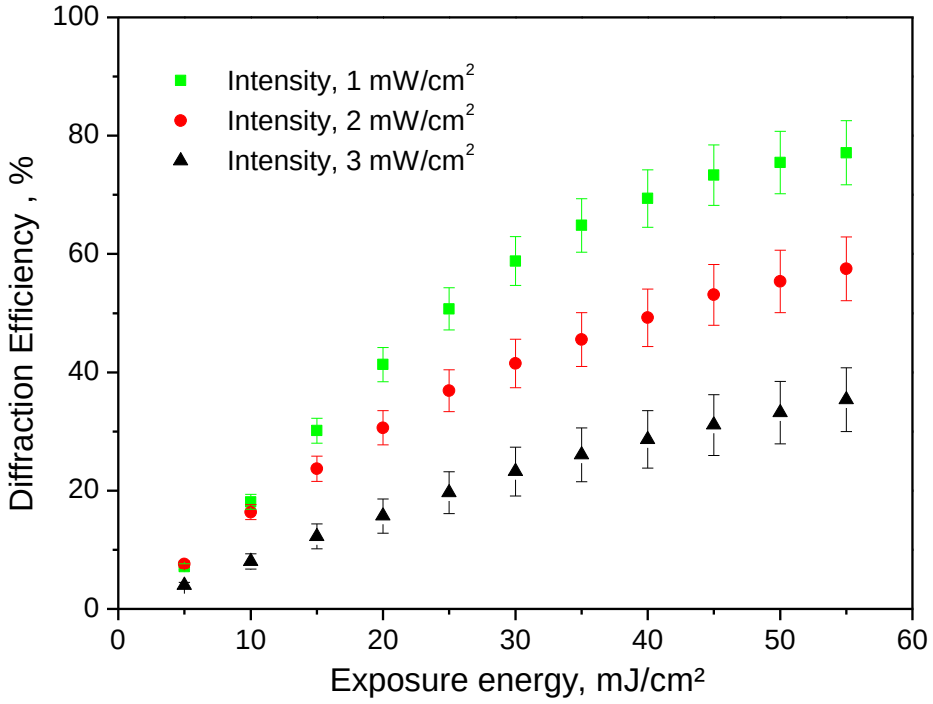

Figure 4-7 Measured diffraction efficiency vs. Exposure energy for the transmission gratings with various intensities between 1-3 mW/cm^2 at spatial frequency of 300 l/mm was investigated for sample thicknesses of 100 µm.

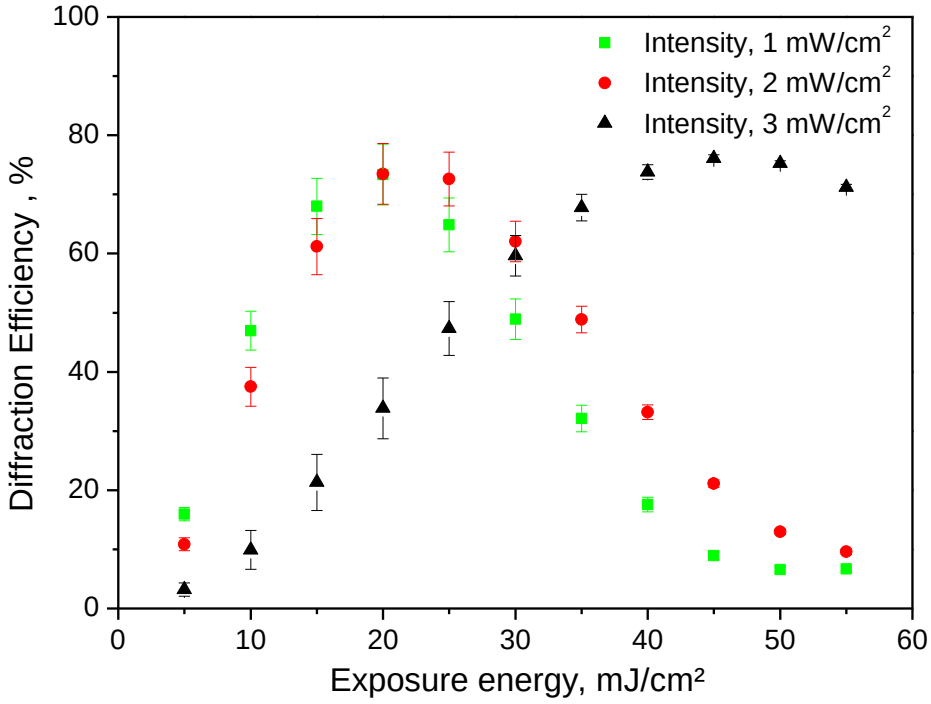

Figure 4-8 Measured diffraction efficiency vs. Exposure energy for the transmission gratings

with various intensities between 1-3 mW/cm^2 at spatial frequency of 300 l/mm was investigated for sample thicknesses of 150 µm.

4.3.3 Dependence of diffraction efficiency on recording intensity at spatial frequency of 200 l/mm

The same comparison was made for each thickness used a 200 l/mm. At this spatial frequency, the maximum diffraction efficiency obtained was about 80% for the sample with the thickness of 75 µm. This was obtained at a recording intensity of 1 mW/cm^2.

The results reveal that there is intensity dependence at this spatial frequency. As has been observed in previous work [4], that delivery of the same energy over a longer time period allows longer polymer chains to be formed and increases the diffraction efficiency achieved. This is because diffusion rate is high relative to the rate of polymerization. This is easier to observe at higher spatial frequency because the smaller fringe spacing allows easy diffusion of monomer into the bright fringe regions from the dark fringe regions. Figure 4.9-4.12 presents the diffraction efficiency dependence on intensity at spatial frequency of 200 l/mm for the range of sample thicknesses between 50 µm - 150 µm.

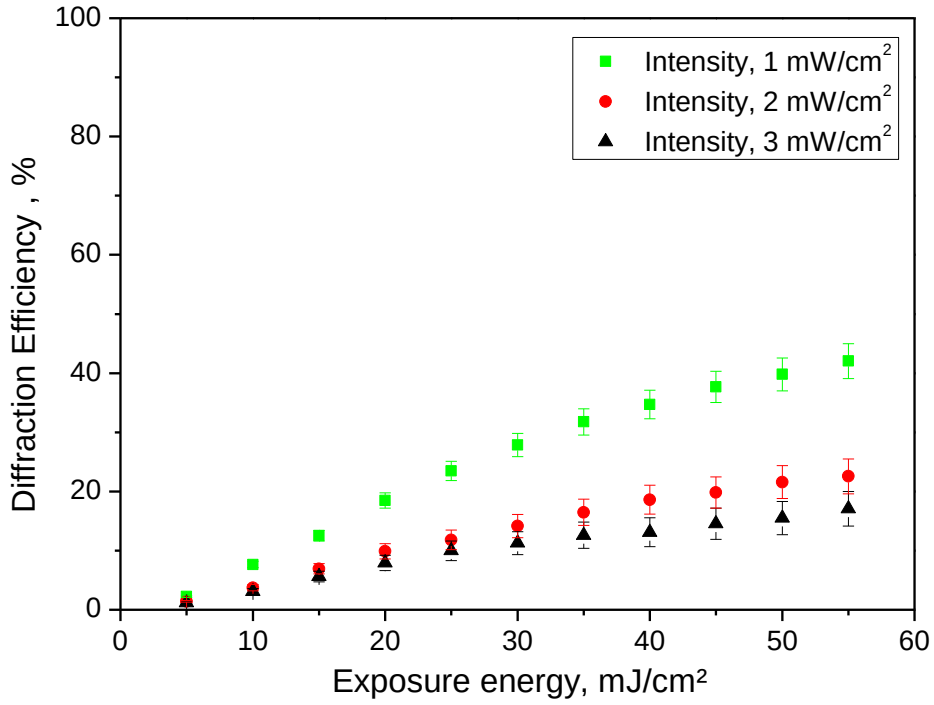

Figure 4-9 Measured diffraction efficiency vs. Exposure energy for transmission gratings recorded with intensity between 1-3 mW/cm^2 at spatial frequency of 200 l/mm was investigated for sample thicknesses of 50 µm.

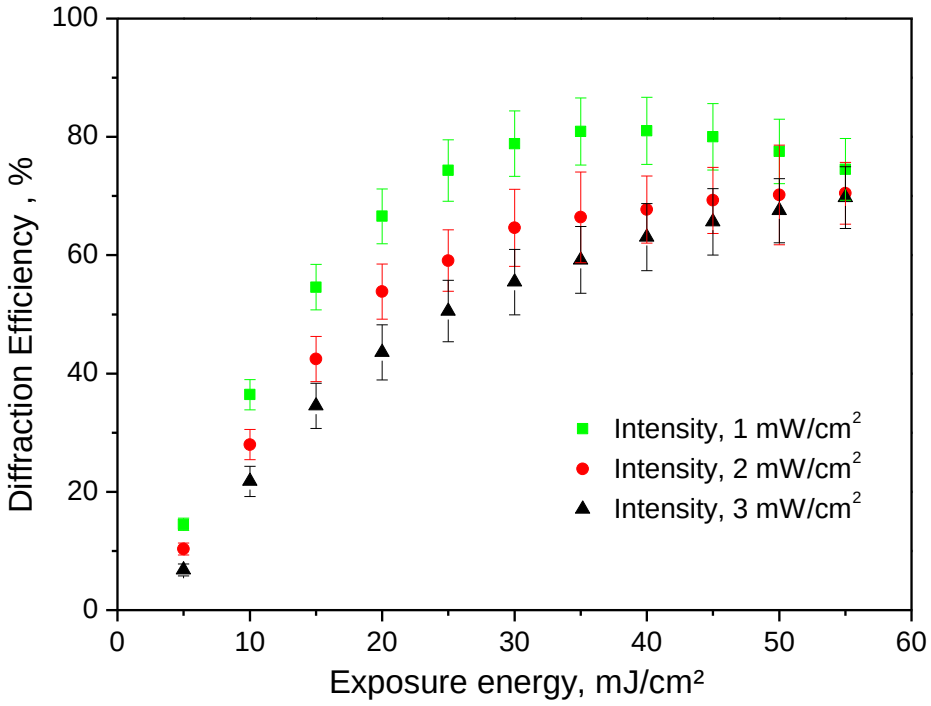

Figure 4-10 Measured diffraction efficiency vs. Exposure energy for transmission gratings recorded with intensity between 1-3 mW/cm^2 at spatial frequency of 200 l/mm was investigated for sample thicknesses of 75 µm.

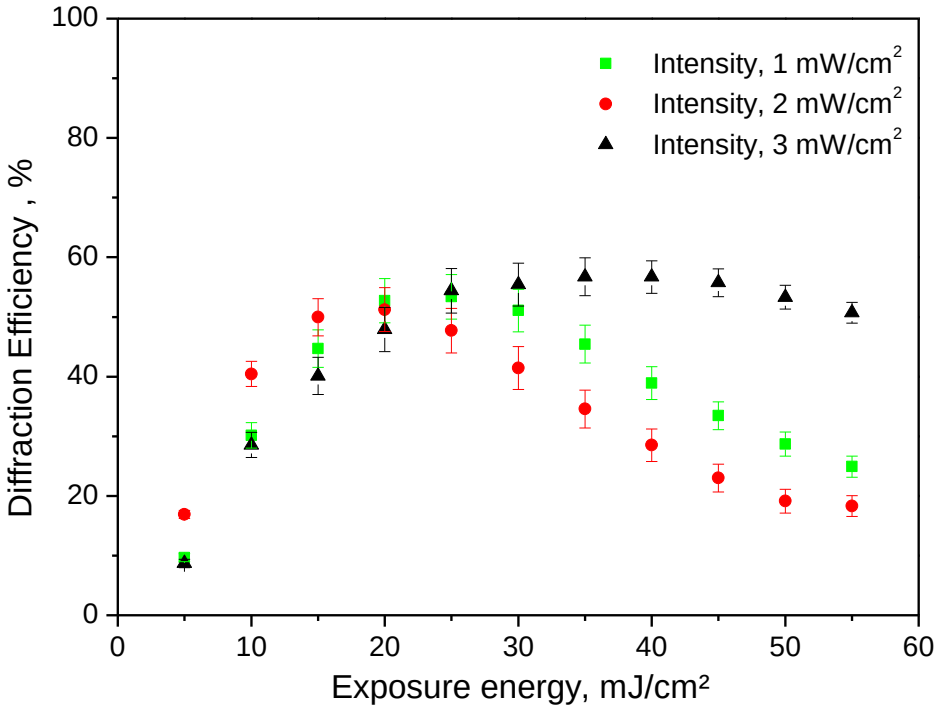

Figure 4-11 Measured diffraction efficiency vs. Exposure energy for transmission gratings recorded with intensity between 1-3 mW/cm^2 at spatial frequency of 200 l/mm was investigated for sample thicknesses of 100 µm.

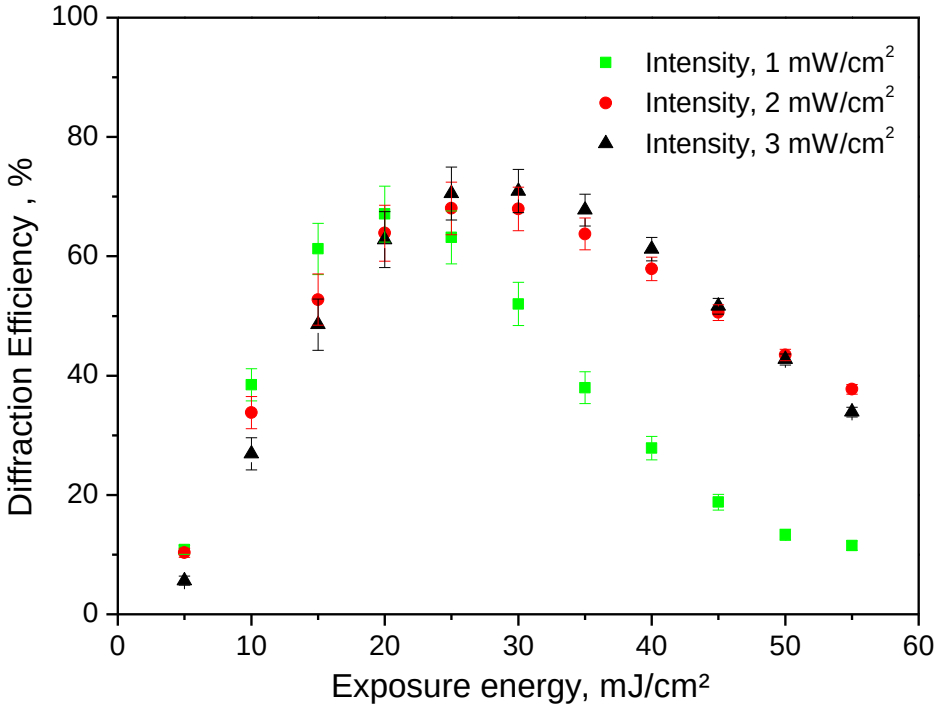

Figure 4-12 Measured diffraction efficiency vs. Exposure energy for transmission gratings recorded with intensity between 1-3 mW/cm^2 at spatial frequency of 200 l/mm was investigated for sample thicknesses of 150 µm.

4.3.4 Dependence of diffraction efficiency on recording intensity at spatial frequency of 100 l/mm

The experiment was repeated for spatial frequency of 100 l/mm. The results presented in figure 4.13-4.16 show the relationship between first order diffraction efficiency of the transmission gratings and recording intensity, for a spatial frequency of 100 l/mm, in layers of thicknesses with the range between 50 µm -150 µm. From the graphs it can be clearly seen that the diffraction efficiency achieved at each exposure is not highly dependent on recording intensity (in the studied intensity range) at this particular spatial frequency.

This observation could be explained by the large fringe spacing, 10 µm. Both 1 mW/cm^2 and 2 mW/cm^2 lead to similar values of the maximum achievable diffraction efficiency. Recording with $3mW/cm^2$ intensity leads to a slight decrease in the diffraction efficiency. The maximum diffraction efficiency achieved at spatial frequency of 100 l/mm was about 35%.

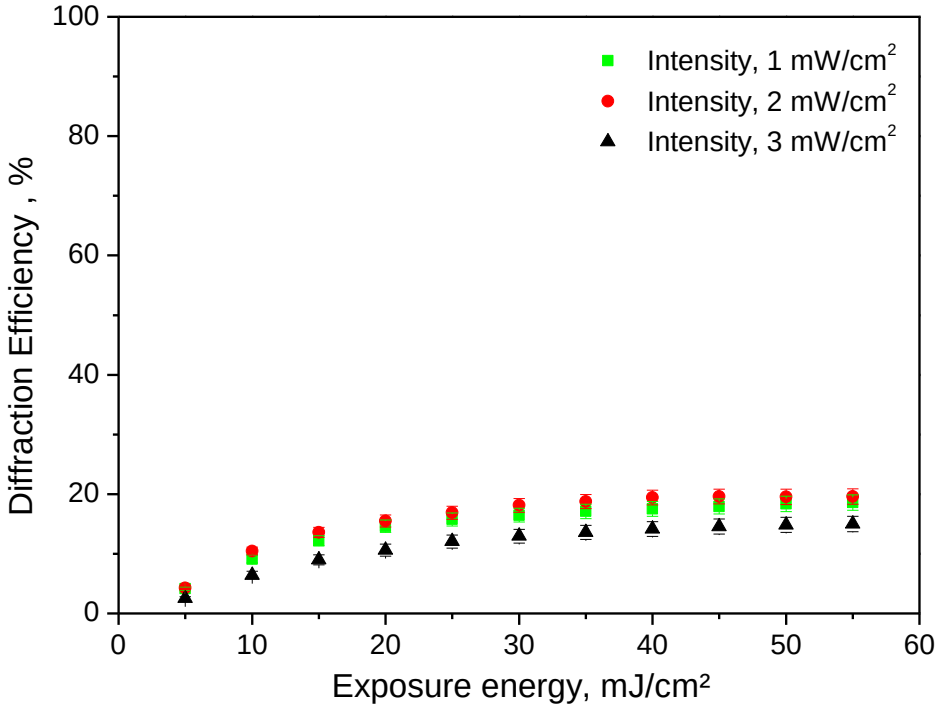

Figure 4-13 Measured diffraction efficiency vs. Exposure energy for transmission gratings with intensity from 1-3 mW/cm^2 at spatial frequency of 100 l/mm investigated for sample thicknesses of a) 50 µm.

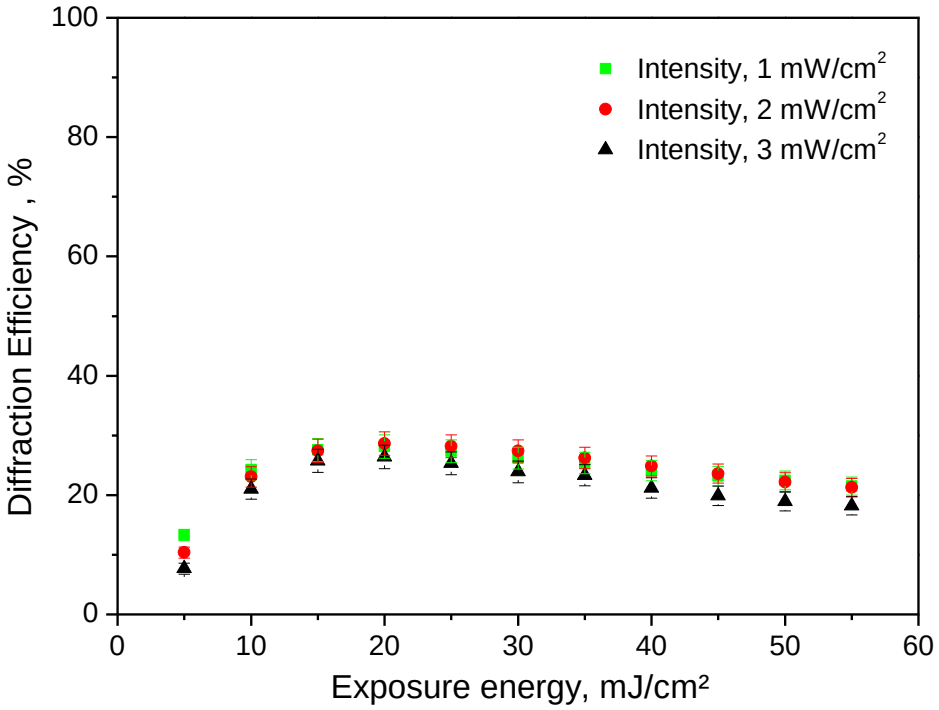

.

Figure 4-14 Measured diffraction efficiency vs. Exposure energy for transmission gratings with intensity from 1-3 mW/cm^2 at spatial frequency of 100 l/mm investigated for sample thicknesses of a) 75 µm.

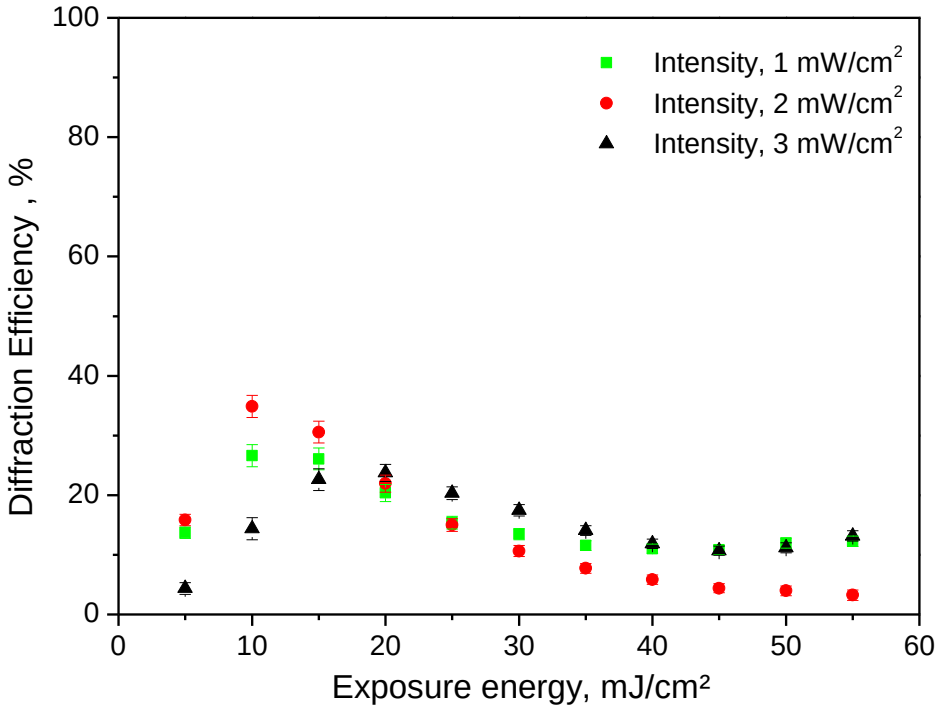

Figure 4-15 Measured diffraction efficiency vs. Exposure energy for transmission gratings with intensity from 1-3 mW/cm^2 at spatial frequency of 100 l/mm investigated for sample thicknesses of a) 100 µm.

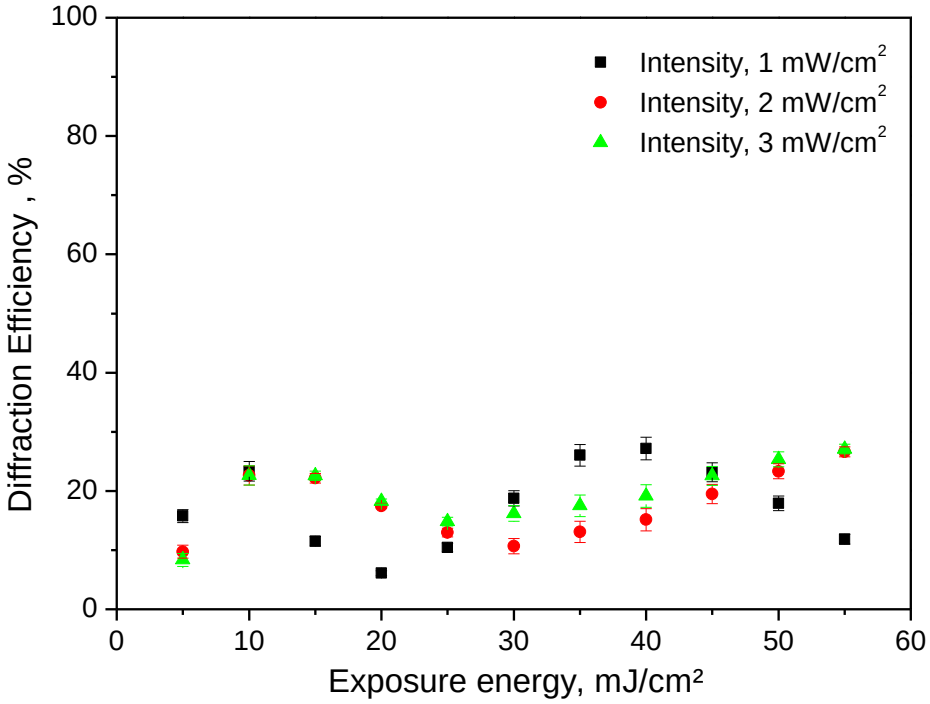

Figure 4-16 Measured diffraction efficiency vs. Exposure energy for transmission gratings with intensity from 1-3 mW/cm^2 at spatial frequency of 100 l/mm investigated for sample thicknesses of a) 150 µm.

4.3.5 Bragg selectivity of the transmission gratings

A set of transmission grating was recorded using the optimum recording parameters and the FWHM of each grating were measured. The variation of diffraction efficiency with angle of incidence for a grating recorded with various spatial frequencies is shown in Figure 4.17-4.19. The thickness of the samples was 75 microns. The solid line shows the theoretical relationship predicted using the equations in section 3.2. The experimental data matches closely with the theoretical results. From the graph, it can be observed that the FWHM of the recorded grating is 3.4 ± 0.1 degrees, 2.0 ± 0.1 degree and 0.8 ± 0.1 degree at spatial frequency of 100 lines/mm, 300 line/mm and 1000 line/mm respectively.

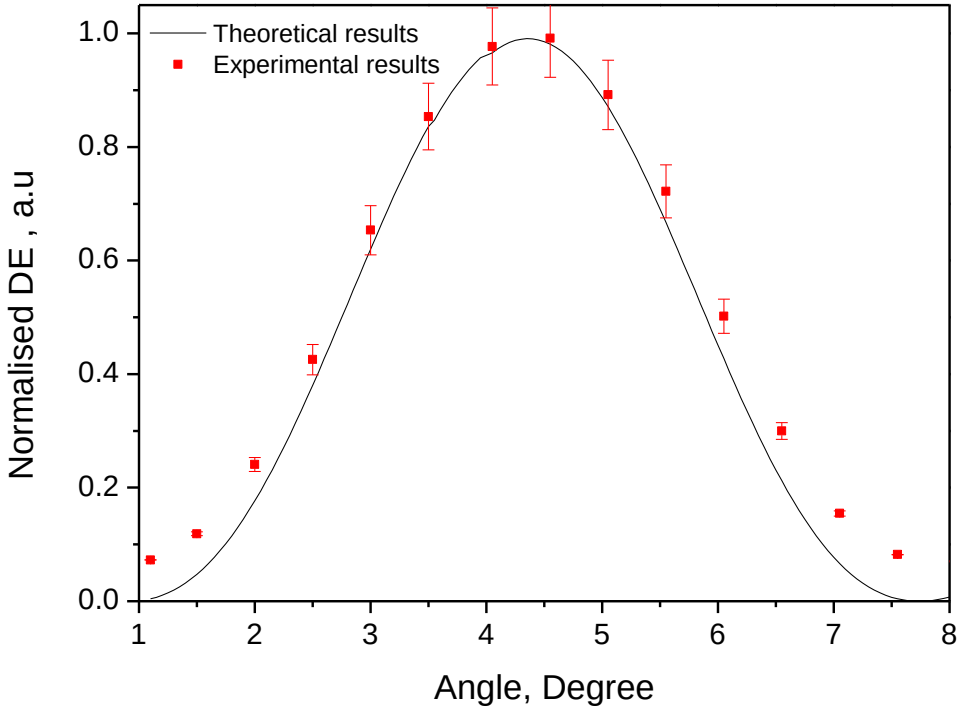

Figure 4-17 Experimental and theoretical angular selectivity curves for a grating recorded at spatial frequency of 100 l/mm with thickness of 75 µm.

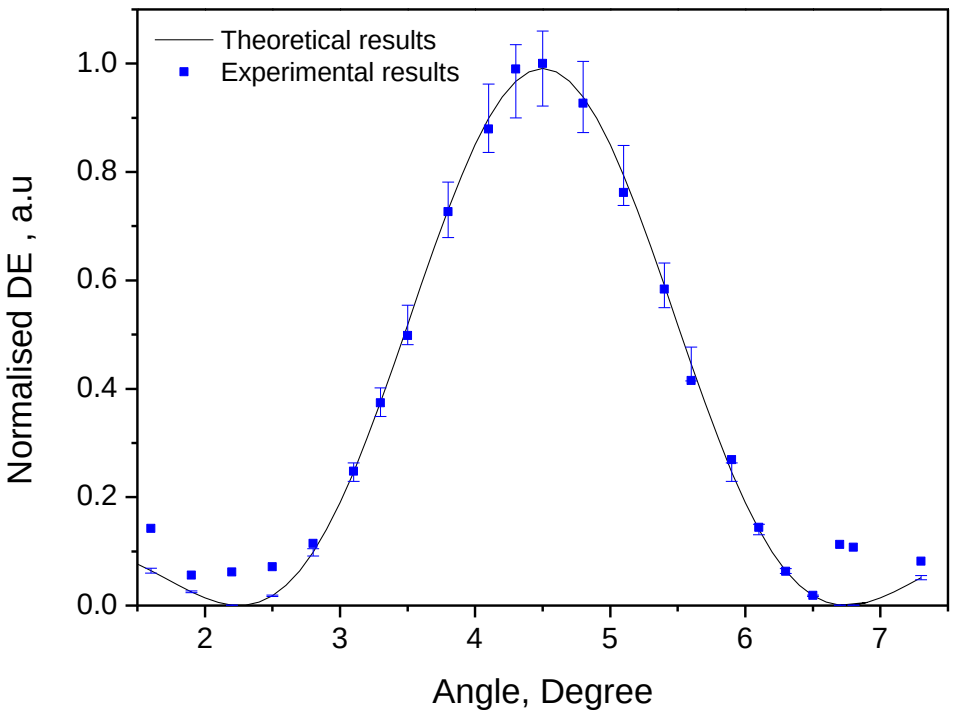

Figure 4-18 Experimental and theoretical angular selectivity curves for a grating recorded at spatial frequency of 300 l/mm with thickness of 75 µm.

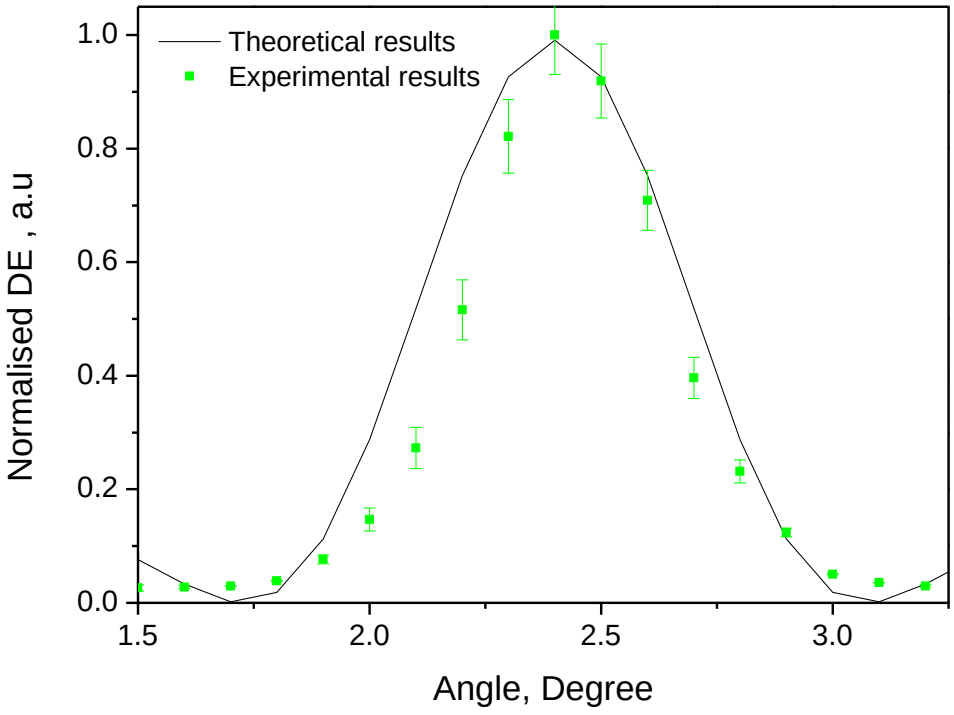

Figure 4-19 Experimental and theoretical angular selectivity curves for a grating recorded at spatial frequency of 1000 l/mm with thickness of 75 µm.

4.3.6 Initial Life time study

An investigation into the stability of the diffraction efficiency of an acrylamide-based photopolymer HOEs in different environmental conditions was carried out and laminating method was improved. So far, an improvement has been observed in the life time of fabricated HOEs by laminating the samples before recording. This allows for control over humidity changes in the samples, which can be detrimental to stability. This characterisation needs to be continued in much more detail for different environmental conditions. This work involves development of a protocol for sealing photopolymer gratings, and a study of the lifetime of sealed gratings in a range of environmental conditions such as at room temperature, below room temperature and open to atmosphere changes. Their diffraction efficiency was monitored at appropriate intervals over 15 months.

Some primarily results are shown in figure 4.20. In this study first set of samples were recorded on plastic substrate while the samples were laminated using the hot plate before recording. A range of slanted and unslanted holographic gratings at low spatial frequency were recorded on plastic substrates. Three samples from each set were placed in three different environmental conditions, at room temperature, laboratory cooling fridge and outdoor. In order to characterise the performance of each sample after time under each conditions, the diffraction efficiency of each sample was measured every week for the first two months and then it was monitored only every few months. Due to poor lamination, the samples which were left in outdoor were damaged after three months. This can be explaining by dropping the temperature in winter time so that the plastic substrate was cracked and the samples were damaged by absorption of water from the rain.

It can be observed that the diffraction efficiency of the grating remains constant after 4 months; however in some of the sample about 10% decrease in diffraction was observed. This can be explained by the weather exposure. The primarily results confirm that the gratings recorded in photopolymer material have a relatively long shelf and the maximum diffraction efficiency over 85% was achieved after 15 months.

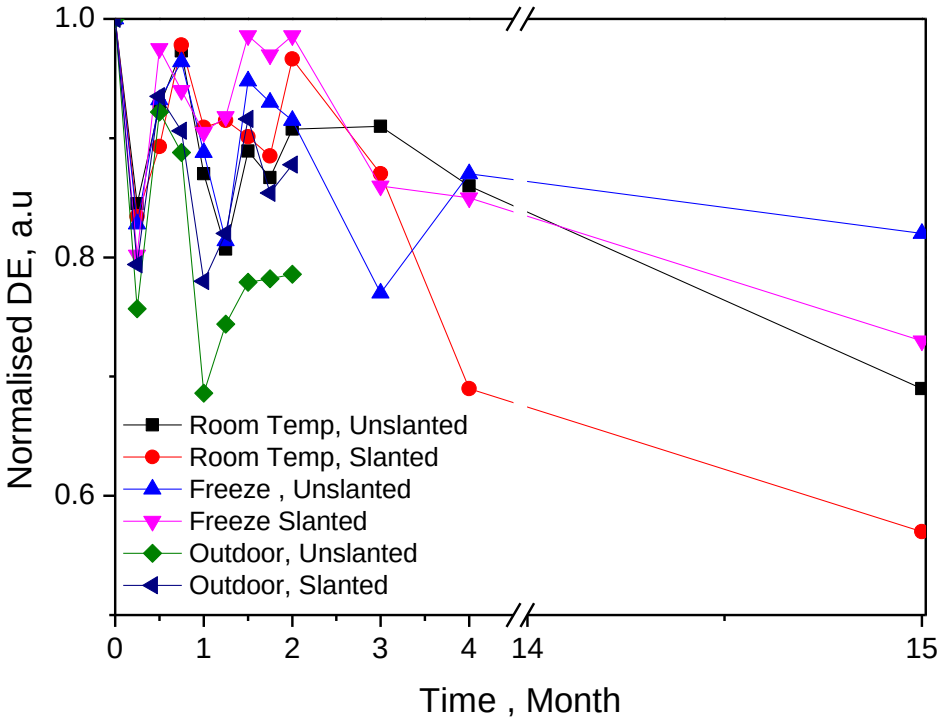

Figure 4-20 Life time study of laminated holographic grating

4.4 Conclusions

The holographic recording capability of the acrylamide based photopolymer in transmission mode of recording has been characterised for low spatial frequency gratings 100-300 lines/mm. The purpose was to determine how low the spatial frequency could be lowered without compromising the diffraction efficiency.

The intensity dependence of the growth of low spatial frequency gratings was also measured in order to maximize the recorded diffraction efficiency. This showed that low intensity of the recording beams produces higher efficiency gratings. Maximum diffraction efficiencies of 75% and 80% were observed in photopolymer layers of 50 µm and 75 µm thickness at these spatial frequencies. This means that 80% of the incident light was measured in the diffracted beam with no correction for reflection, absorption or other losses.

The FWHM of the grating recorded at range of spatial frequencies was also compared with the theoretical results and it was in good agreement. The advantage of using thinner layers and lower spatial frequency of recording in this application is the larger angular range of the optical component. Figure 4.21, shows the photograph of gratings recorded with optimum recording parameters under diffuse light.

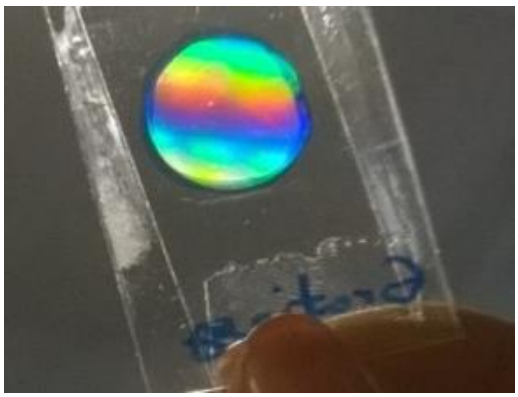

Figure 4-21 Photograph of holographic grating recorded on photopolymer at spatial frequency of 300 l/mm.

Reference:

1. Akbari H, Naydenova I, Martin S. Using acrylamide-based photopolymers for fabrication of holographic optical elements in solar energy applications. Appl Opt. OSA; 2014;53(7):1343–53.

2. Martin S, Feely CA, Toal V. Holographic recording characteristics of an acrylamide-based photopolymer. Appl Opt. 1997;36(23):5757–68.

3. Cody D, Mihaylova E, O'Neill L, Babeva T, Awala H, Retoux R, et al. Effect of zeolite nanoparticles on the optical properties of diacetone acrylamide-based photopolymer. Opt Mater (Amst). Elsevier B.V.; 2014;37:181–7.

4. Naydenova I, Jallapuram R, Howard R, Martin S, Toal V. Investigation of the diffusion processes in a self-processing acrylamide-based photopolymer system. Appl Opt. 2004;43(14):2900–5.

5 Fabrication and testing of low spatial frequency off-axis focussing HOEs

5.1 Introduction

In agreement with volume holographic grating theory [1], the theoretical work in chapter 3 showed that HOEs recorded on thinner layers at low spatial frequencies have a much greater acceptance angle [2]. Chapter 4 showed through experimental investigation that in this photopolymer 50 and 75 micron layers could produce highly efficiency HOEs even at spatial frequencies as low as 200 and 300 lines/mm. This chapter presents the results for experimental recording and characterisation of off axis lens elements based on the optimal parameters determined by the preceding chapters.

The photopolymer material responds by producing a local variation in refractive index that records the interference fringe planes. In order to produce a focussing diffractive element, the object beam is formed as a spherical or cylindrical wave, which can interfere with the reference wave. This produces an interference pattern that will cause diffraction of light incident at the appropriate angle, to achieve the desired focussing effect (more detailed explanation of how HOEs work is presented in Chapter 2.) Controlling the interference pattern allows control of the diffraction properties of the element recorded. The fact that the photopolymer records a thick phase grating allows for high transparency and efficiency in the device.

In this chapter, a range of high diffraction efficiency HOEs (spherical/cylindrical) are recorded and their performance is characterised in terms of diffraction efficiency and angular and/or wavelength selectivity. The optical recording processes are described and the results are discussed.

5.2 Experiment

5.2.1 Materials

The photopolymer used for the preparation of samples is water-soluble and consists of acrylamide (monomer), N, N' - methylenebisacrylamide (cross linking monomer), triethanolamine (electron donor), polyvinylalcohol (binder) and Erythrosine B (photosensitizer). The photosensitive layer was prepared with the composition described in the previous chapter. Briefly, the monomers, 0.6 g acrylamide and 0.2 g of N,N' Methylene-bisacrylamide and 2 ml of triethanolamine was added to 17.5 ml stock solution of polyvinyl alcohol (PVA) (10% w/w), the components were mixed well by using a magnetic stirrer and 4 ml of Erythrosin B dye was added finally to sensitise at 532 nm. Specific volumes of photopolymer solution were spread evenly on a 26 x 76 mm^2 glass plate placed on a levelled surface and dried for 18-24 hours at temperature ranging between 20 -23 degrees and relative humidity ranging 30-40 %.

5.2.2 Methods

A 532 nm Nd:YVO4 laser was used in a holographic optical setup shown in Figure 5.1 to record off-axis lenses. The angle between two recording beams was set as 9.14^o (ratio of the two beam was 1:1) in order to obtain a central spatial frequency of about 300 l/mm. The exposure time was kept constant at 60s, thus exposure energy of 60 mJ/cm^2 in a layer of thickness 50 ± 5µm was achieved. Optical lenses with a range of focal lengths (3-10 cm) were placed in the object beam, (see Figure 5.1). In order to maximize the aperture of recorded HOE, it was essential that the object beam and the reference beam fully overlapped at the photosensitive layer.

In order to maximize this overlap, it is typical to focus a large collimated beam into a smaller diameter at the photosensitive layer, however, this requires large collimating optics in one of the recording beams; this was not feasible due to the small angle between the two beams. The same aperture of HOE was fabricated without the need for large optics by using a diverging beam; the HOE element can then be used to focus the light by reversing the recorded HOE. The distance from the photopolymer sample to the focus point of lens, defines the focal length of the recorded HOE at the recording wavelength. The distance between optical lens and photopolymer layer was adjusted depending on the focal length of optical lens in order to record all spherical/cylindrical HOEs with a same focal length of 5 cm.

The recording intensity was controlled by a variable neutral density filter. In order to measure the diffraction efficiency of the recorded HOEs, the focusing beam was blocked and the collimated beam was used to probe the HOE. The intensity of the 1st order diffracted beam was measured near the focus point of HOE using an optical power meter (Newport 1830-C) to determine the diffraction efficiency of the recorded lenses.

A vertically polarized Helium-Neon laser (He-Ne) at 633 nm was used as a probe beam at the Bragg angle in order to measure the angular selectivity of the HOE lenses. The probe beam was at the centre of the HOE unless otherwise noted. When the incident beam is probing the HOE lenses at the Bragg angle the diffraction efficiency is at its maximum.

After recording, the thickness of the layers was measured using a white-light surface profiler (Micro XAM S/N 8038), and was found to be 50 ± 5 μm.

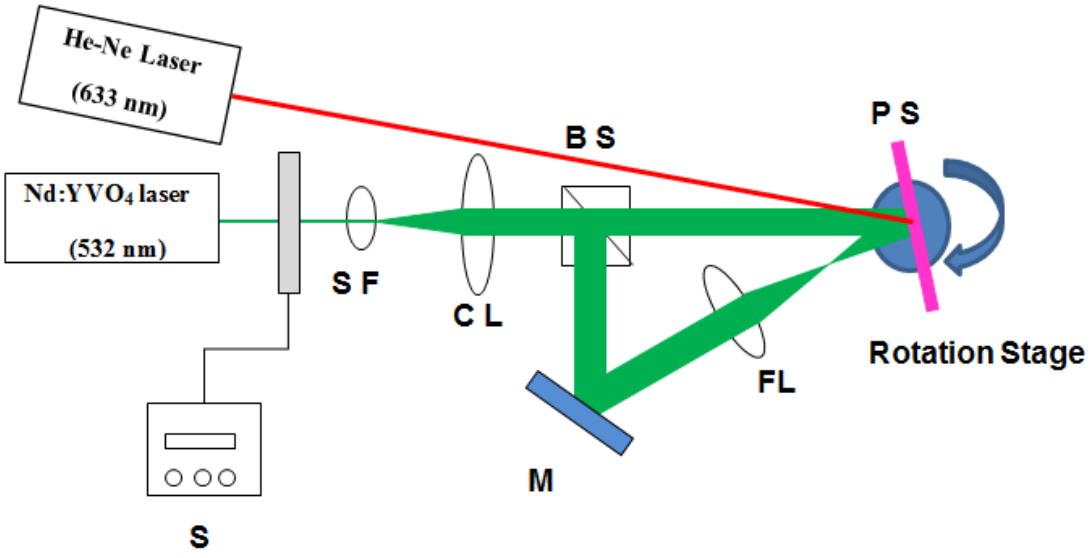

Figure 5-1 Experimental setup for recording off-axis focussing HOEs: S: shutter, CL: collimating lens, BS: beam splitter, SF: spatial filter, M: mirror, FL: focusing lens, PS: photopolymer sample.

5.2.3 Theoretical calculation of Minimum and Maximum spatial frequency of the fringes produced by the experimental set up

The illustration of the experimental arrangement used in this work is shown in figure 5.2. Using simple geometry it is possible to calculate the range of spatial frequencies expected in a HOE for various recording parameters such as lens focal length and position, diameter of the recording beam and the angle between the recording beams. The HOE is a complex diffractive element which can be thought of as a series of slanted gratings that re-direct the incident light towards the focal point and the spatial frequency and slant angle of the grating planes vary across the HOEs. It is helpful to estimate the expected spatial frequency range and slant angles produced during recording in order to better interpret the HOEs influence on the diffracted beam produced during 'reconstruction' or use as an optical device.

In this research, the experimental set-up was assembled as shown and typical values for the dimensions would be: d_1= 0.7 cm, d_2= 4.9 cm, d_3= 6 cm and d_4= 37.3 cm. Where d_1 is the half of the diameter of the recording beam; d_2 is the focal length of lens used in the set-up; d_3 is the distance between the centre of recording beam and the mirror and d_4 is the distance between the mirror and the sample holder. It is essential to find the angle between each recording beam in order to calculate the minimum and maximum spatial frequency of holographic set up. The angle of θ and γ were calculated to be 8° and 81° respectively, therefore the angles of α and β can be calculated by inserting the corresponding values into equations (5.1) and (5.2):

$$\alpha = 90 - \gamma + \theta \qquad \text{Equation 5.1}$$

$$\beta = 90 - \gamma - \theta \qquad \text{Equation 5.2}$$

Finally the values of α = 17° and β=1° were used in equation (5.3) and (5.4), in order to find the minimum and maximum spatial frequency of the recorded HOEs.

$$2\Lambda_{\text{Max}}.\text{Sin}\,\frac{\alpha}{2} = \lambda \qquad \text{Equation 5.3}$$

$$2\Lambda_{\text{Min}}.\text{Sin}\,\frac{\beta}{2} = \lambda \qquad \text{Equation 5.4}$$

It was found that the spatial frequency of HOEs (f_{HOE}= 5cm) recorded with an intended central spatial frequency of 300 lines/mm varies in the range from 38 line/mm to 559 line/mm.

Table 5.1 show the range of spatial frequencies that can be achieved within the HOE for various focal lengths and diameters of HOEs. As expected, it can be seen that the variation in range of spatial frequency is much narrower for the HOEs with smaller diameter.

Table 5.1: Variation of spatial frequency within the recorded HOEs

HOE focal length	Recording lens focal length	HOE diameter	Minimum/maximum spatial frequency
f_{HOE}= 5 cm	f= 25mm	d_{HOE}=1.4cm	38 l/mm< 300 l/mm < 559 l/mm
f_{HOE}= 5 cm	f= 50mm	d_{HOE}=1.0cm	112 l/mm< 300 l/mm < 485 l/mm
f_{HOE}= 5 cm	f= 80mm	d_{HOE}=0.8 m	150 l/mm< 300 l/mm < 450 l/mm

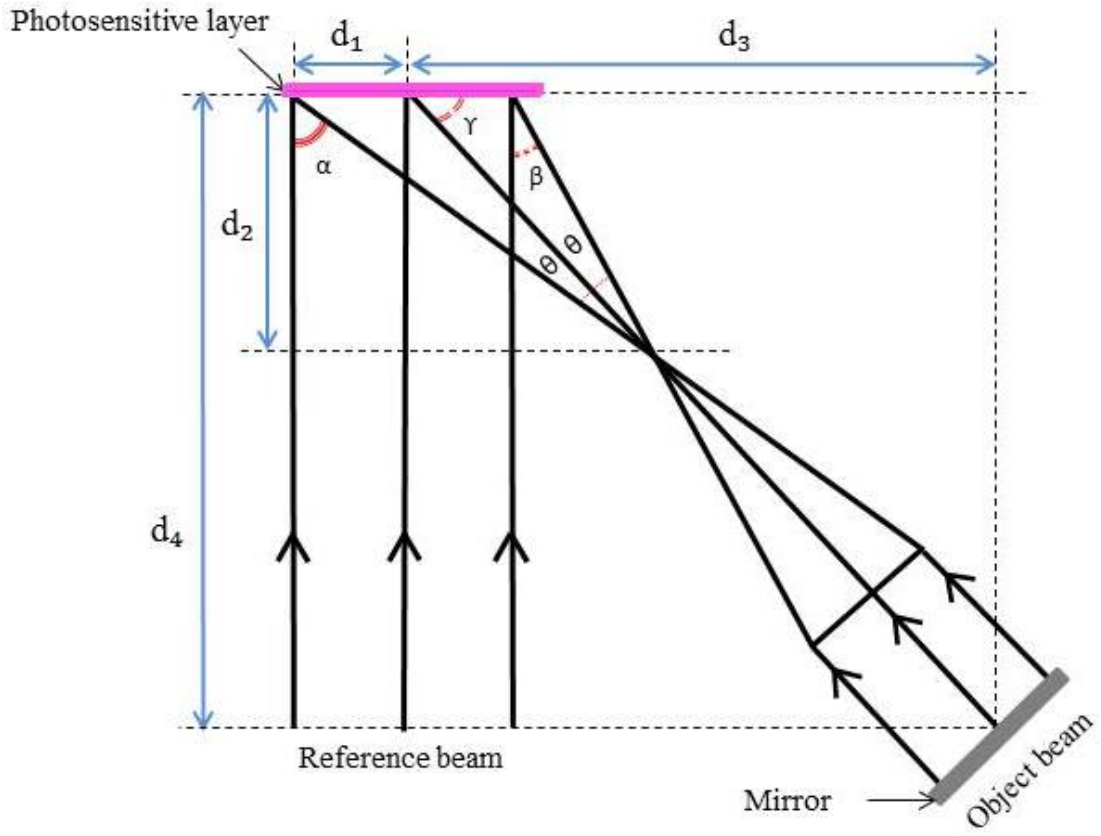

Figure 5-2 Illustration of experimental set up, used for estimation of the minimum and maximum spatial frequency recorded in a focusing element.

5.3 Results and discussion

5.3.1 Spherical HOEs

5.3.1.1 Characterisation of the diffraction efficiency of HOEs recorded at a range of exposure intensities

In order to investigate the high diffraction efficiency focussing elements, a range of holographic lenses with an off-axis focusing effect were recorded at a range of intensities. The recorded HOEs have a central spatial frequency of 300 l/mm. The focal length of the recorded spherical/cylindrical lens element was 5 cm and the element diameter was approximately 1.4 cm. The diffraction efficiency of each HOE was determined using equation 5.5, by measuring the diffracted beam's intensity close to the focal point.

$$\eta = \frac{I_d}{I_0} \times 100 \qquad \text{Equation 5.5}$$

Where I_d is the diffracted beam intensity, I_0 is the transmitted beam intensity and η is the diffraction efficiency of the grating.

As real-time monitoring of the diffraction efficiency was not possible in this instance, the diffraction efficiency was determined for a series of HOEs made using different exposure energy. The results are shown in figure 5.3 for the sample recorded in layers of 50 µm thickness; it is observed that the diffraction efficiency reaches a maximum of about 75% with the exposure energy of about 80 mJ/cm^2. The results are with good agreement with the optimization of the grating which have been demonstrated in the previous chapter. Also comparison with the real-time measurements for gratings of similar thickness and spatial frequency shows that recording is very similar for gratings and focusing elements.

The results in figure 5.3 show that the same trend as seen in the gratings (chapter 4) was observed throughout the experiments. The HOEs recorded with the lower intensities achieved higher diffraction efficiency. The diffraction efficiency of over 75% was achieved for the sample with thickness of 60 ±5 µmat the exposure energy of about 80 mJ/cm^2 and higher.

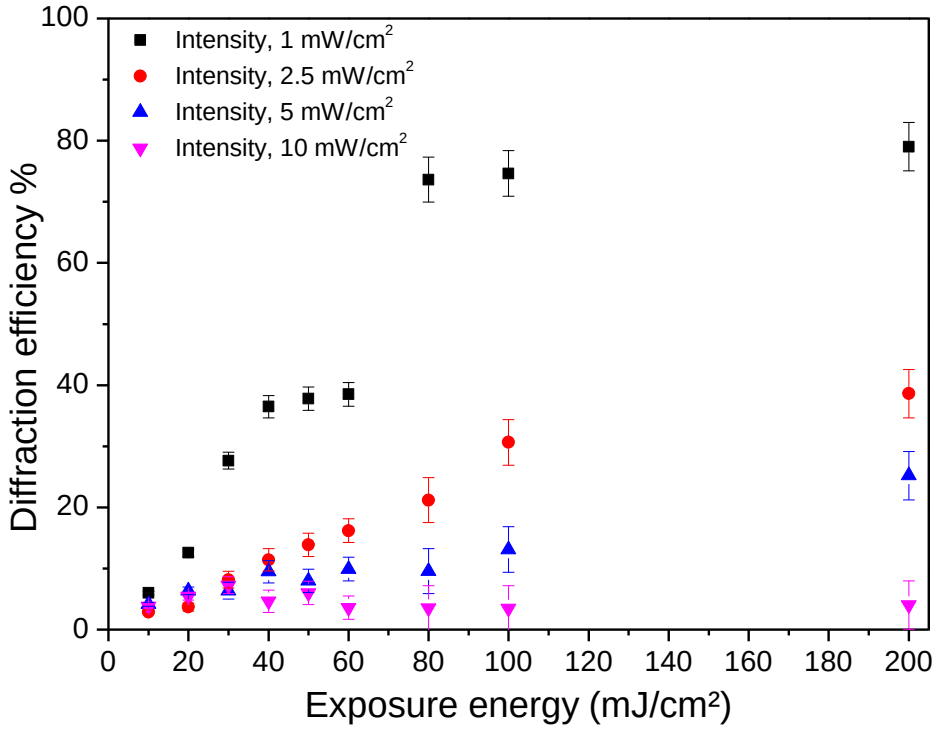

Figure 5-3 Diffraction efficiency vs. Exposure energy for range HOE lenses recorded with various intensity between 1 mW/cm^2 – 10 mW/cm^2 at the spatial frequency of 300 l/mm was investigated for sample thickness of 50 ±5 µm.

5.3.1.2 Dependence of the diffraction efficiency of the HOEs on diameter of the probe beam

The experiment was carried out in order to characterise the dependence of the diffraction efficiency of the recorded HOEs on the diameter of probe beam. As explained in section 5.2.3, the spatial frequency and slant angle of the grating planes vary across the HOE. For example, the spatial frequency of the grating at point A in the figure 5.4 will be much greater than the spatial frequency at point B, but the slant angle of the grating planes will be greater at B than A. The material used must be capable of recording the desired range of spatial frequencies.

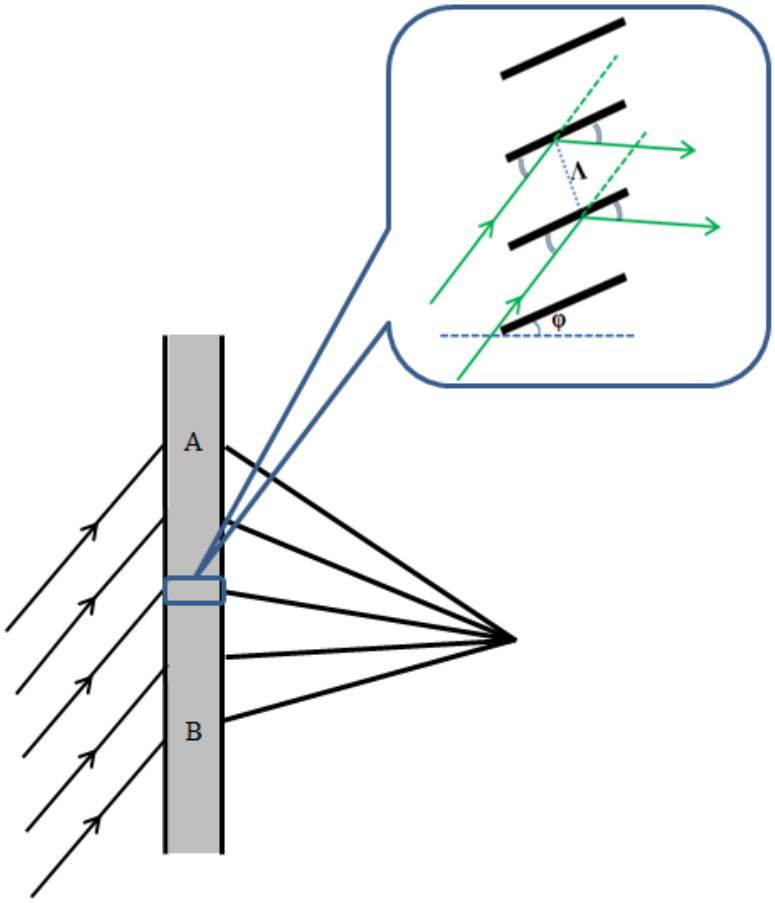

Figure 5-4 Schematic of the Holographic Optical Elements (HOEs) which redirects the incident light to an off axis focus point, with inset showing typical fringe structure. Where Λ is the fringe spacing and φ is the angle between the fringes and the normal to the plane.

The variation of the diffraction efficiency of the recorded HOE with the diameter of the probe beam was investigated. Numbers of the HOEs with the focal length of 5 cm were recorded using the exposure energy of about 1 mW/cm^2 on the layer with the thickness of 50 µm. The results shown in figure 5.5 indicate that there is about 15% decrease in diffraction efficiency as the diameter of the probe beam was increased due to the range of spatial frequency within HOE and the Gaussian intensity profile of the recording beams. Results can be improved by using a non-gaussian exposing beam.

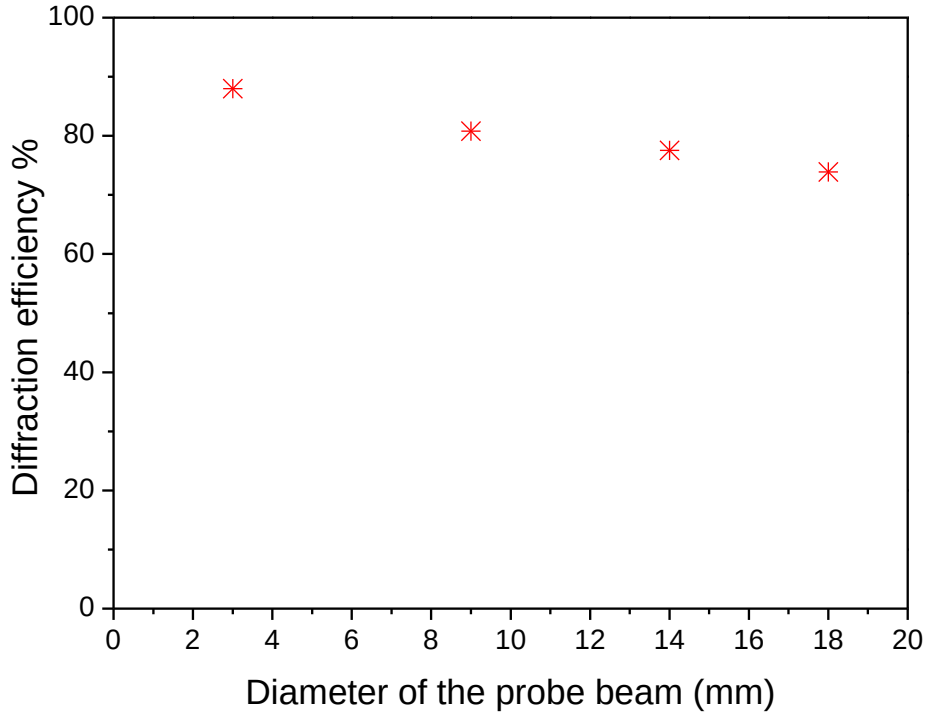

Figure 5-5 Diffraction efficiency vs. diameter of the probe beam for the HOE lenses recorded with exposure intensity of 1 mW/cm^2 at spatial frequency of 300 l/mm for the layer with the thickness of 50 µm.

The results showed that diffraction efficiency of HOEs varies depending on the probe beam diameter. For the comparison of the performance of the device in the real application, the experiment was carried out and the FWHM of the focusing elements was measured. The results will be discussed in the next section.

5.3.1.3 Dependence of the diffraction efficiency and FWHM of the HOEs on position of probe beam at the sample

The diffraction efficiency of the HOE was measured when the unexpanded probe beam was exposed to the same grating at various lateral positions. The probe beam was placed at the centre of the gratings and then was shifted 4 mm to the left and/or right side of the grating from centre to edge.

The efficiency and angular selectivity of the diffractive lenses was measured for the same sample but the probe position was varied cross the sample. Results for the range of probe position are shown in figure 5.6. In this study, the diameter of the probe beam was kept constant at 3 mm. Therefore in this set of data only position varies cross the HOE.

The result in figure 5.6 indicates that due to the variation in spatial frequency across HOE, the diffraction efficiency and the FWHM can be vary depending on the position of the probe the HOE. In this set of data, approximately 10 % decrease in diffraction efficiency and about 0.5±0.1 degree change in FWHM was observed. The change in diffraction efficiency can be explain due to the Gaussian beam profile during recording and the variation in beam ratio due to the focused beam. Where the variation in FWHM values is due to the change of slant angle and spatial frequency. This is simply due to the fact that there is a range of spatial frequency, slant angle across each recorded elements.

For simple comparisons during the research presented in this thesis, the probe beam is routinely placed at the centre of the diffractive lenses. However, for testing the device for real applications, in the next section the performance of the holographic device is characterised using an expanded beam which fills the entire HOE.

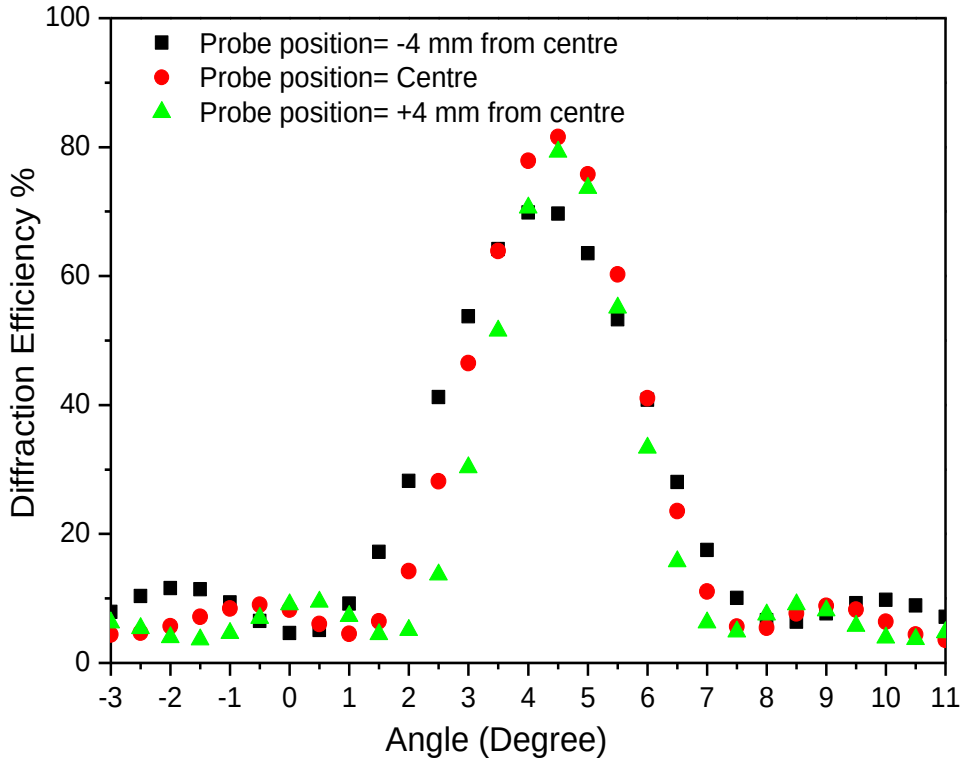

Figure 5-6 Angular selectivity curves for a spherical diffractive lenses recorded at spatial frequency of 300 l/mm in layers with thickness of 50 µm at various probe position. Focal length of HOE was 5 cm.

5.3.2 Cylindrical HOEs

5.3.2.1 Dependence of the angular selectivity of the HOEs on numerical aperture of the lens

The overall aim of this set of experiments is to compare the characteristics of holographic lenses recorded using three cylindrical lenses with different focal lengths to focus the object beam.

Cylindrical lens elements are of interest because they focus light in one plane only, forming a line at the focus rather than a spot. Although the concentration factor may be lower than for spherical lenses, because the light is concentrated along one axis only, the linear shape of the focussed light is compatible with certain solar conversion systems, particularly thermal systems. Holographic techniques can be used to make thin lightweight cylindrical HOEs which will re-direct and focus incoming light to the desired 'line' for conversion.

The first step was to record and compare a range of holographic lenses with the same focal length, but different numerical apertures. Standard refractive cylindrical lens with focal lengths of 25 mm, 50 mm, 80 mm were placed in the object beam of the recording set up. As shown in figure 5.7 the distance from the cylindrical lens to the photopolymer layer was varied in order to record holographic elements with approximately the same focal length. This allows us to investigate how the HOE performance is affected by increasing the numerical aperture without changing the focal length. The performance of three HOEs was compared in terms of diffraction efficiency and the angular selectivity.

The focal length of the HOE that has been recorded using the lens with focal length of 25 mm and the optical set up with the centre spatial frequency300 lines/mm is about 5 cm. The minimum focal length HOE possible in the current setup is about 5 cm in order to avoid the lens impinging on the reference beam, the HOEs focal length was kept constant at 5 cm throughout this research. The HOE with much shorter focal length at low spatial frequency can be achieved by recording on-axis focusing elements. The HOEs with the focal length of 5 cm was successfully recorded using all three cylindrical lenses.

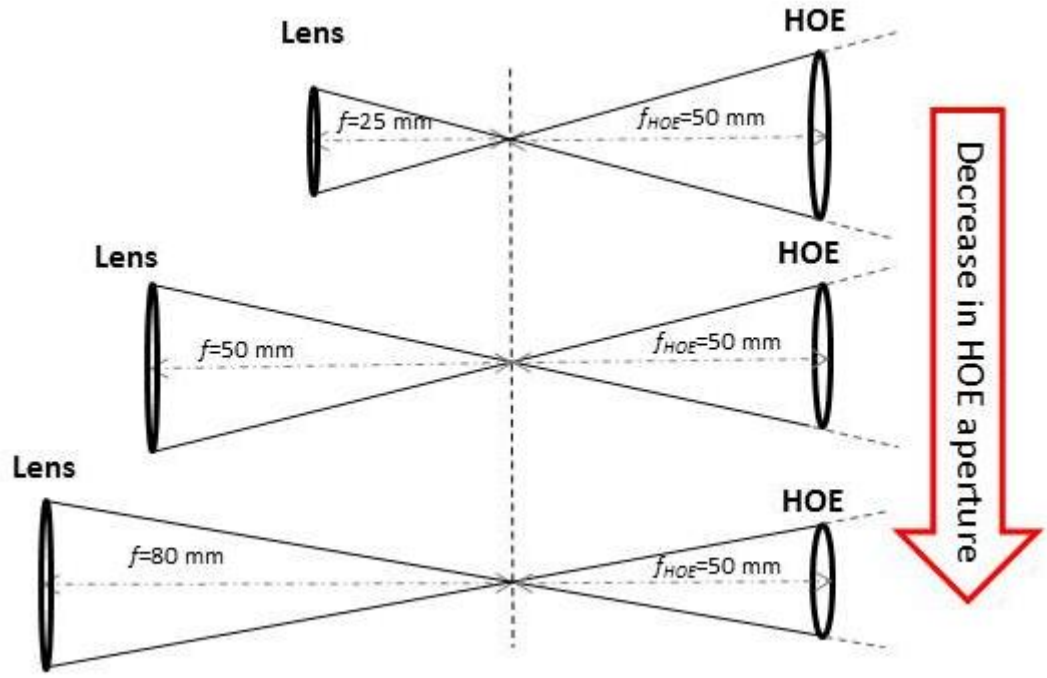

Figure 5-7schematic diagram showing the various focal lengths of the optical lenses and aperture of HOEs.

Then the angular FWHM of each recorded elements was characterised. The angular selectivity of the recorded HOEs with focal length of 5 cm recorded with various lenses in the object beam is shown in figure 5.8. The probe beam was positioned approximately 1 mm away from the edge of the HOEs while the size of the probe beam

was kept constant at 3 mm. It can be observed that the FWHM of the HOE lenses recorded with the lens with the shorter focal length is larger compare to HOE lenses with the longer focal length as it was discussed in section 5.2.3. The FWHM of the grating recorded with 25 mm, 50 mm and 80 mm focal length lenses (but the arranged to give the same focal length HOE) are respectively about 4.4°, 4.1°, and 2.2°.This is because of the more highly convergent/divergent object beam, which gives rise to a greater range of spatial frequencies in the HOE. Using the lens with longer focal length can achieve the HOEs with the focal length of only few millimetres, although this does reduce the aperture of HOE significantly.

The third step was to probe the gratings at three different positions. This study further illustrates how the spatial frequency, FWHM and diffraction efficiency varies across the HOE.

The results in figure 5.8, demonstrate that range of spatial frequency increase through HOE from right to left of the gratings. It can be clearly seen that the FWHM of recorded HOEs was increased left to right toward to the lower range of spatial frequency.

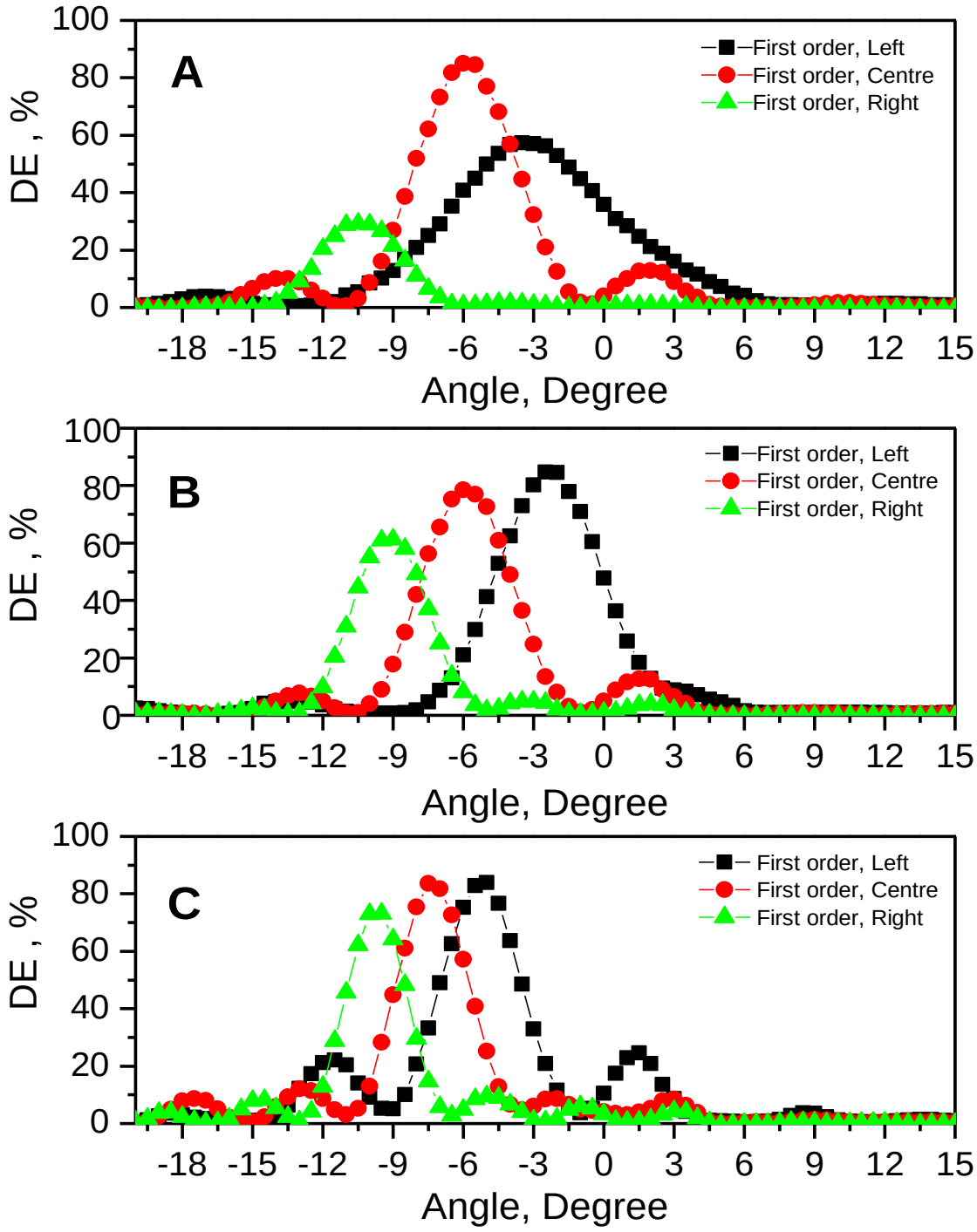

Figure 5-8 The angular selectivity of the HOEs recorded on the layer with the thickness of 60 ±5 μm with the range of cylindrical lens with focal lengths (a) 25 mm, (b) 50 mm and (c) 80 mm.

In the next section, the angular selectivity of the cylindrical HOEs using the expanded beam will be presented.

5.3.2.2 Angular selectivity of HOE using expanded beam

Results from the previous section confirm that HOEs are complex devices and consist of a range of spatial frequencies. Figure 5.9 shows that HOEs recorded using the lens with shorter focal length can achieve wider FWHM, as the diameter of the recorded HOE is greater and the range of spatial frequencies is greater. In order to use our device with solar cells (silicon cells, dye cells) we would prefer the HOEs with the short focal length (one millimetre would be the ideal).

In order to characterise the total efficiency and the acceptance angle of the device for solar application, the probe beam was expanded to the same size of the grating by using additional two lenses in the probe set up. Then the total intensity of the incident beam for the first order of each grating was measured at the range of angles. From the results we can conclude that there is clear dependence of the numerical aperture of the recording beam which can be customized by using the lens with various focal lengths.

Dependence of FWHM on the focal length of the lens that has been used during recording was measured using an expanded beam is shown in figure 5.9. The FWHM of the grating recorded at 25 mm, 50 mm and 80 mm are respectively about 5.7 ± 0.1 degree, 5.5 ± 0.1degree and 5.1 ± 0.1degree. It can be observed that the FWHM of the grating recorded with shorter focal length is relatively wider.

From the results achieved with the an expanded beam, the optimum focal length of the lens to be used in this study is 25 mm and 50 mm, since they would have wider acceptance angle.

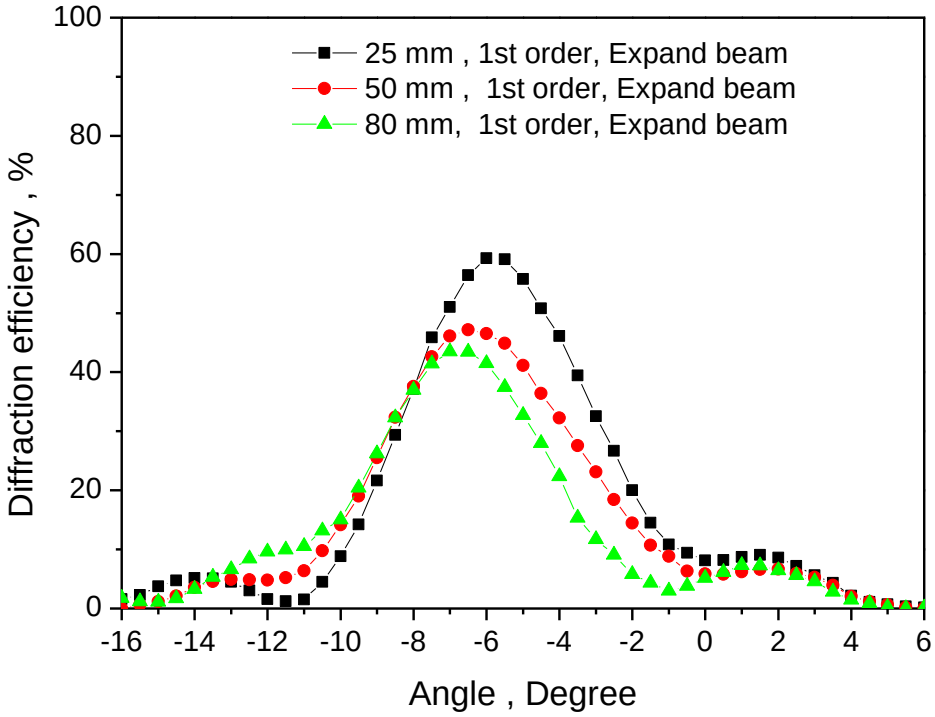

Figure 5-9 The angular selectivity of the HOEs recorded with the range of cylindrical lens with focal lengths (a) 25 mm, (b) 50 mm and (c) 80 mm using expanded probe beam.

The optical lens with the focal length of 50 mm was used in future studies as it will give more flexibility in the experimental set up to record the HOEs with shorter focal length. This lens achieved the FWHM of 4.1° and 5.5° for unexpanded and expanded beam respectively.

A number of holographic focusing elements were recorded with the focal length of 5 cm using the lens with the numerical aperture of 50 mm. Their angular and wavelength selectivity will be compared in the next section.

5.3.3 Investigation of the variation of angular selectivity of both spherical and cylindrical HOEs using unexpanded beam

Spherical/cylindrical HOE lenses were recorded at the central spatial frequency of 300 l/mm. Plots of diffraction efficiency as a function of the deviation from the Bragg angle demonstrate the angular selectivity of the recorded elements.

Figure 5.10 A, shows the variation of diffraction efficiency with angle of incidence for number of the spherical HOEs while figure 5.10 B shows for number of the cylindrical HOEs. The results are compared with the theoretical result which is presented in solid line. For accurate comparison, the probe beam was placed in the centre of the gratings throughout the measurements. The variation in FWHM can be explained due to inaccuracy of the position of the probe beam at the sample and thickness variation. The FWHM of the lens varies between 3.0 ± 0.1 degrees to 4.0 ± 0.1 degrees for each sample.

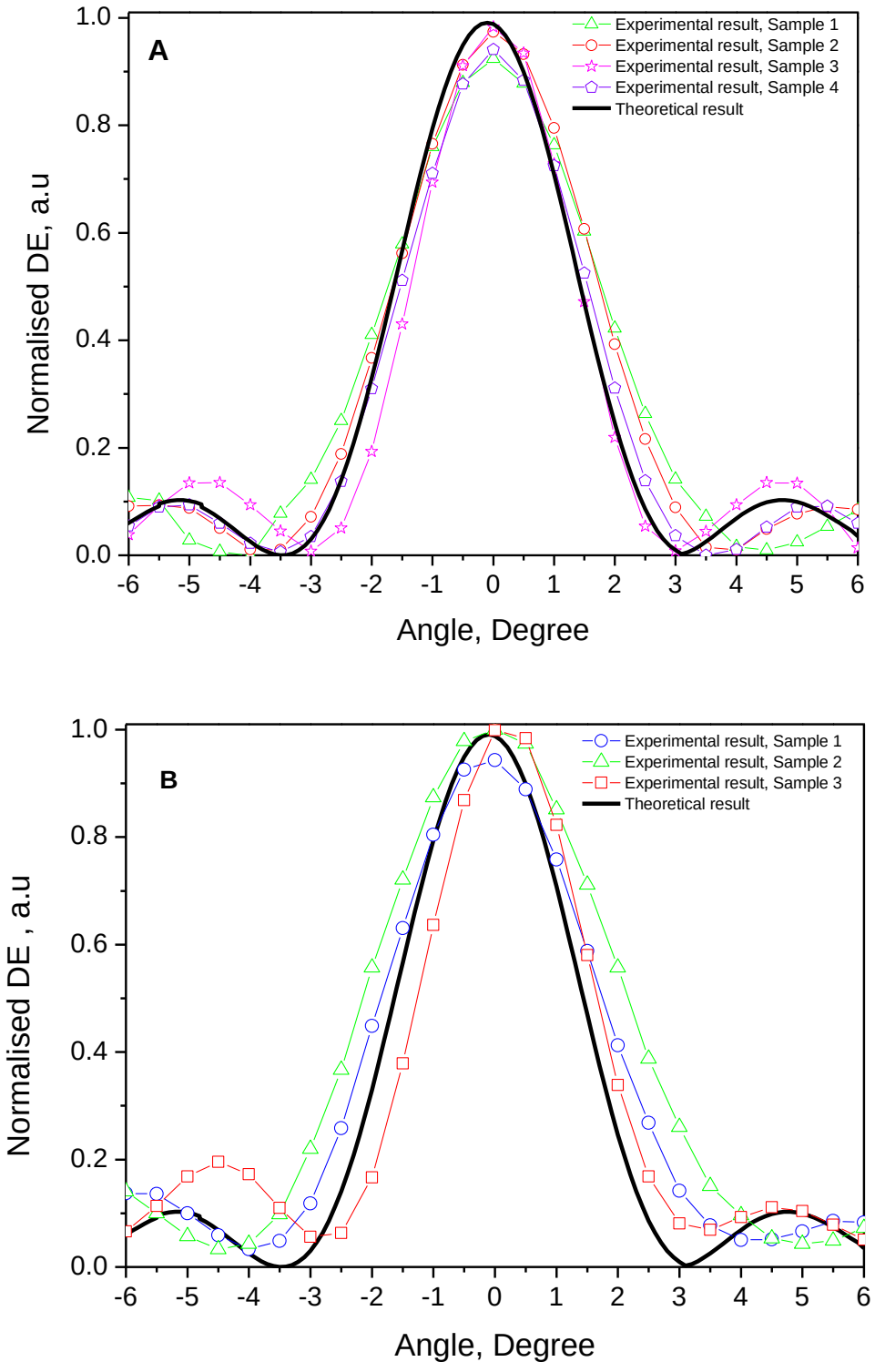

Figure 5-10 Diffraction efficiency vs. angle for HOEs at spatial frequency of 300 l/mm and recording intensity of 1 mW/cm^2 was investigated for A) spherical HOE, B) cylindrical HOE with sample thickness of 50 ± 5 µm.

5.3.4 Wavelength selectivity of both spherical and cylindrical HOEs using unexpanded beam

The wavelength selectivity of the grating can be observed if the wavelength of the probe beam is varied while the incident angle is constant. Volume transmission gratings are generally much less selective to variations in wavelength over the visible range than in angle. However, in order to confirm that there is a reasonable working range for these devices the wavelength selectivity of recorded HOEs was determined using probe beams of different wavelengths.

A range of cylindrical/spherical HOEs was recorded using 532 nm lasers at spatial frequency of 300 l/mm with the total exposure energy of 60 mJ/cm^2. The thicknesses of the recorded HOEs were about 50 ± 5 µm. The results are shown in figure 5.11 and figure 5.12. The diffraction efficiency of the HOEs was recorded using the laser source with the range of three different wavelengths (473 nm, 532 nm and 633 nm).

Results in figure 5.11 A and 5.12 A, show the normalised diffraction efficiency vs. wavelength and compare the theoretical and experimental results. While figures 5.12 B and 5.13 B show the angular selectivity curves of the HOEs at each wavelength. It can be seen that the spherical HOEs achieved a maximum diffraction efficiency of about 90% at wavelength of 473 nm, over 75% at wavelength of 540 nm and about 60% was achieved at wavelength of 633 nm. The cylindrical HOEs achieved a maximum diffraction efficiency of about 98% at wavelength of 473 nm, 93% at wavelength of 532nm and 75% at wavelength of 633 nm.

Results for off-axis HOEs confirm that the working range covers a significant portion of the visible spectrum for these gratings and the results are in good agreement with the theoretical results.

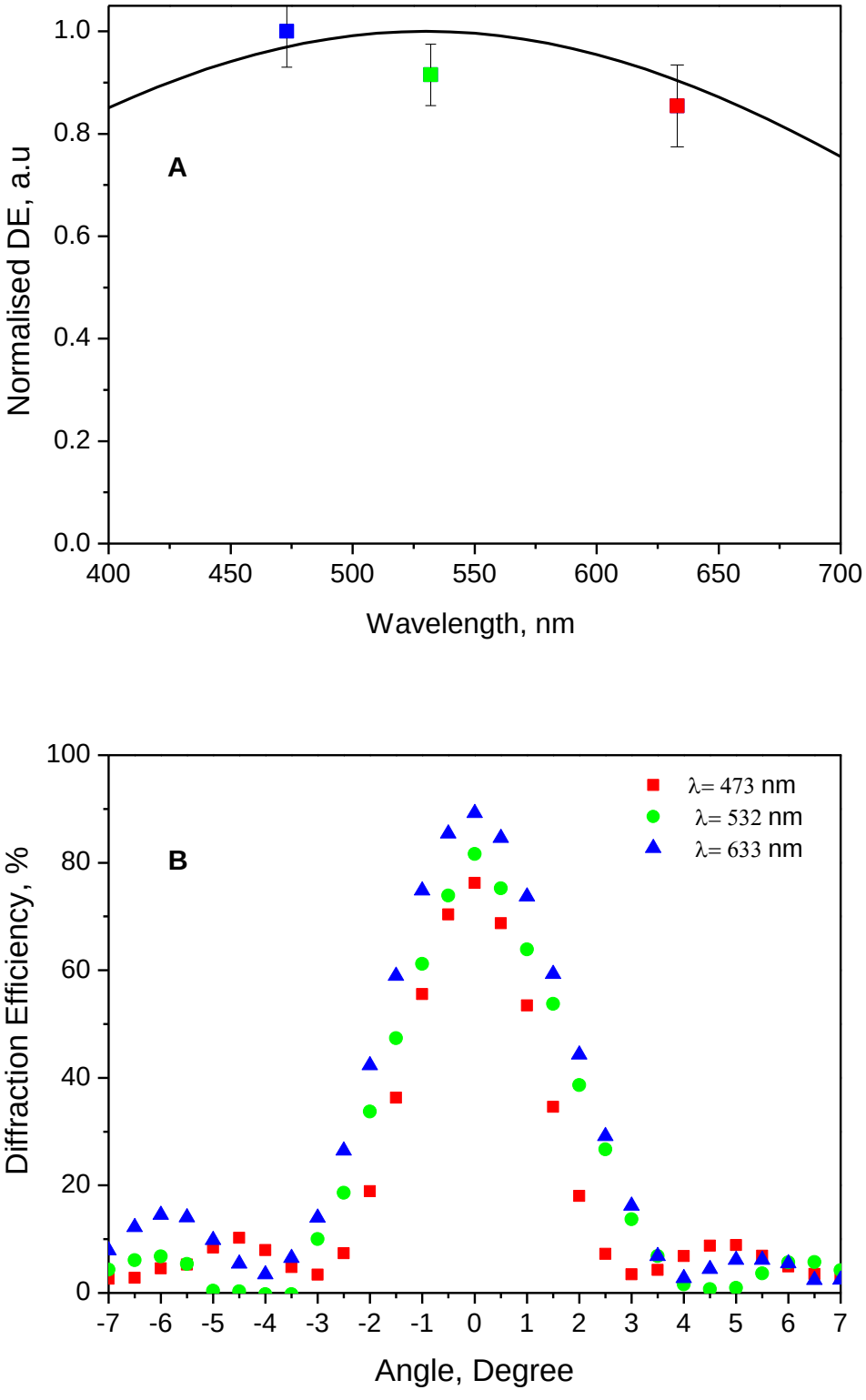

Figure 5-11 Wavelength selectivity of the spherical HOE at various wavelengths of 473 nm, 532 nm, 633 nm with the sample with thickness of 50 ± 5μm.

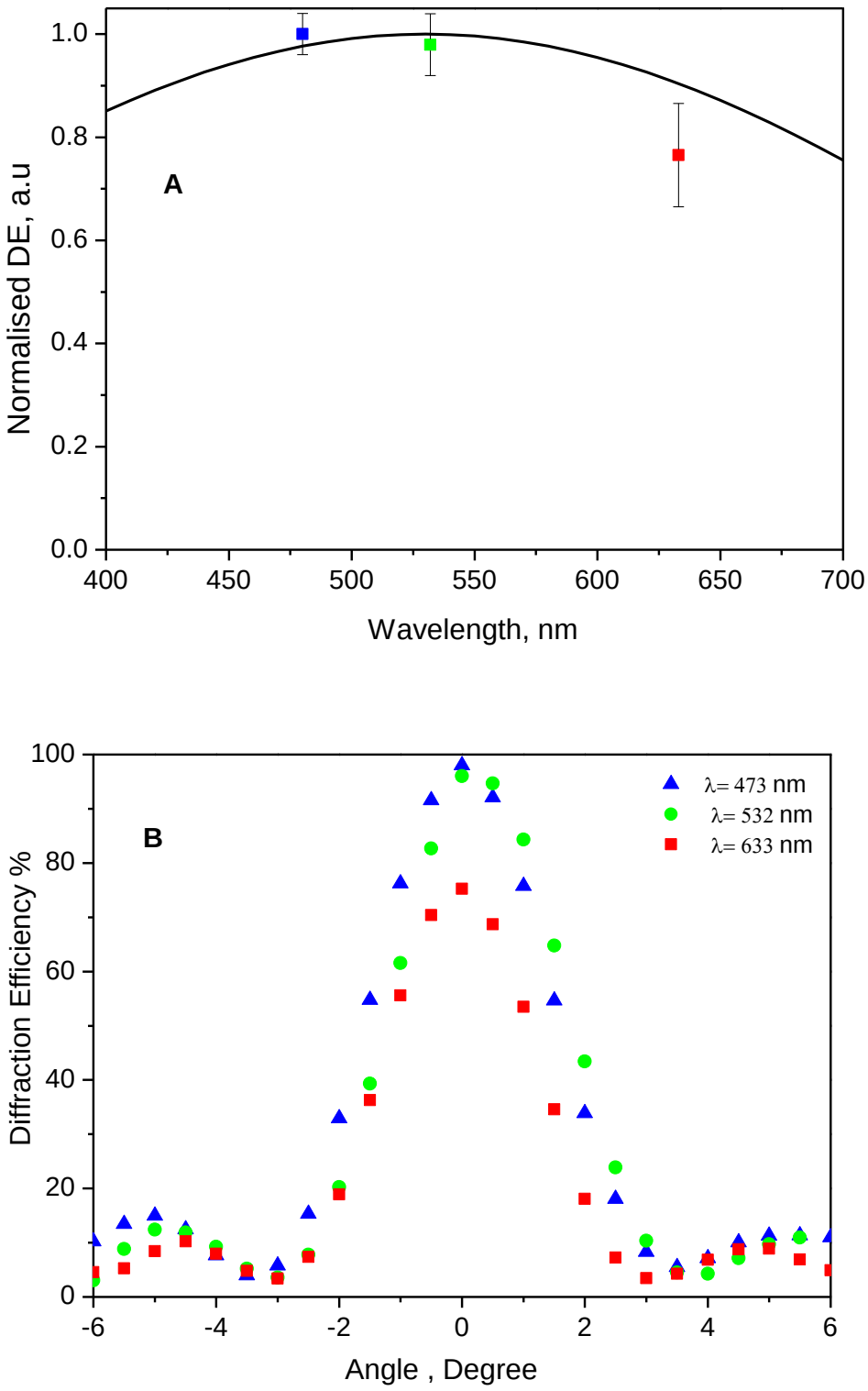

Figure 5-12 Wavelength selectivity of the cylindrical HOE at various wavelengths of 473 nm, 532 nm, 633 nm with the sample with thickness of 50 ± 5μm.

5.3.5 Wavelength selectivity of off-axis HOEs using an expanded beam

The aim of this study is to optimize the device for use in solar applications, it was important to characterise the angular and wavelength selectivity of the HOEs using an expanded diverging white light source. In order to monitor the maximum diffraction efficiency of the HOEs at each wavelength, blue, green and red filter was placed in front of the light source. The maximum diffraction efficiency was achieved when the HOEs were exposed to the light at the Bragg angle. In this study, the recording set up was re-arranged in order to make sure that the Bragg angle was equal to the angle of incidence. The results are presented in figure 5.13.Maximum diffraction efficacy of over 85% was achieved at wavelength of 480 nm and 633 nm. The maximum diffraction efficiency of about 70% was achieved at 540 nm. The change in diffraction efficiency at each wavelength using the laser source and white light source can be easily be observed. This can be explained by analysing the spectrum of the white light source (Chapter 7).

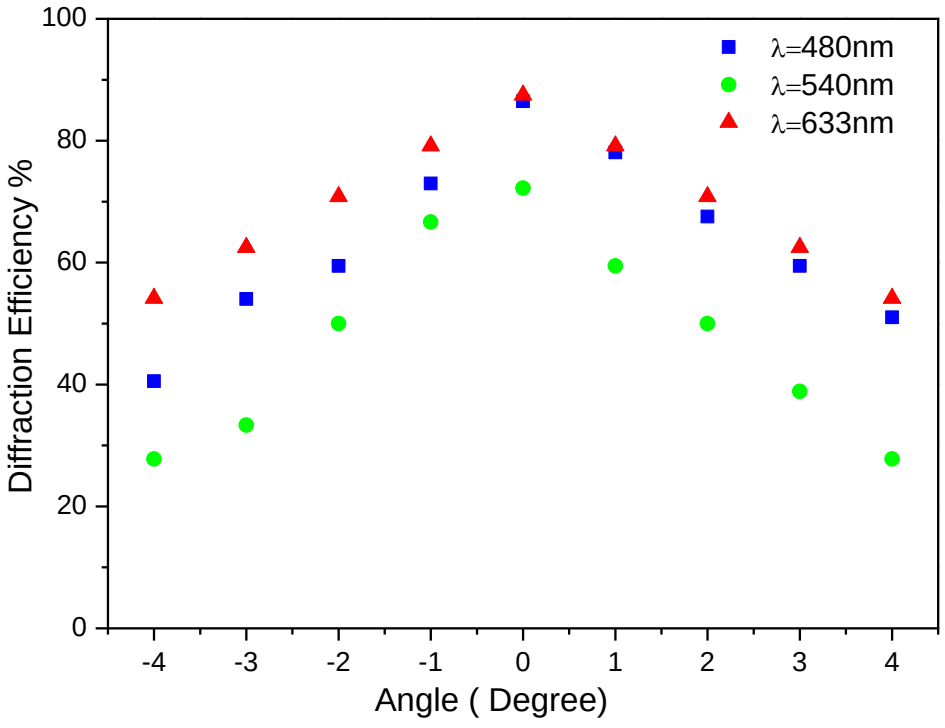

Figure 5-13 Diffraction efficiency vs. angle using expanded diverging beam for the HOEs recorded at spatial frequency of 300 l/mm with recording intensity of 1 mW/cm^2.

5.3.6 Recording high efficiency Diffractive Optical Elements on flexible glasses substrate

This section describes an exploratory study demonstrating successful holographic recording of focusing elements with low spatial frequency and broad working range on flexible glass (Corning® Willow® Glass)[3]. This novel glass is beneficial for our purpose as it provides better transparency as well as other advantages. The flexible glass substrate is dimensionally stable to enable required layer-to-layer alignment, while also displaying low scattering, haze, and absorption. The flexible glass substrate has been demonstrated to be compatible with roll-to-roll and sheet-level coating, lamination, printing processes, as well as stacked multi-layer devices with low parallax [4,5].

A spherical holographic lens with an off-axis focusing effect was recorded on Willow® Glass of size 26 x 76 mm^2 and 50 ± 5 µm thicknesses. The layer preparation conditions were identical to the conditions used for other substrate. The diffractive lens element was recorded with the slant angle of 10.5° outside the medium in order to compare the functionality and the performance of the lens element with that recorded on a glass or plastic substrate. Figure 5.14 shows the angular response of the 1^{st} diffraction order of the number of recorded lens element. For the accurate comparison, the Bragg curves of the number of recorded HOEs with the same thickness were compared. The focal length of the recorded lens element was 5 cm with diameter of 0.9 cm. It can be observed that a maximum diffraction efficiency of over 90% was achieved, where the FWHM was approximately 3.5°. These very promising results demonstrate that flexible glass is a suitable and stable substrate for holographic recording, while achieving high diffraction efficiency with similar working ranges to the lens elements recorded on plastic and glass substrates. Also indicate the repeatability of the fabricated devices.

The high optical quality of flexible glass (low scattering, birefringence and absorption) will enable the fabrication of improved devices in any application where device thickness/weight is an issue and where optical losses should be minimized. In addition, the conformable nature of holographic photopolymer devices made on optical glass will enable new device configurations including laminated stacked holographic devices, deformable holographic devices and combinations of holographic and optoelectronic devices.

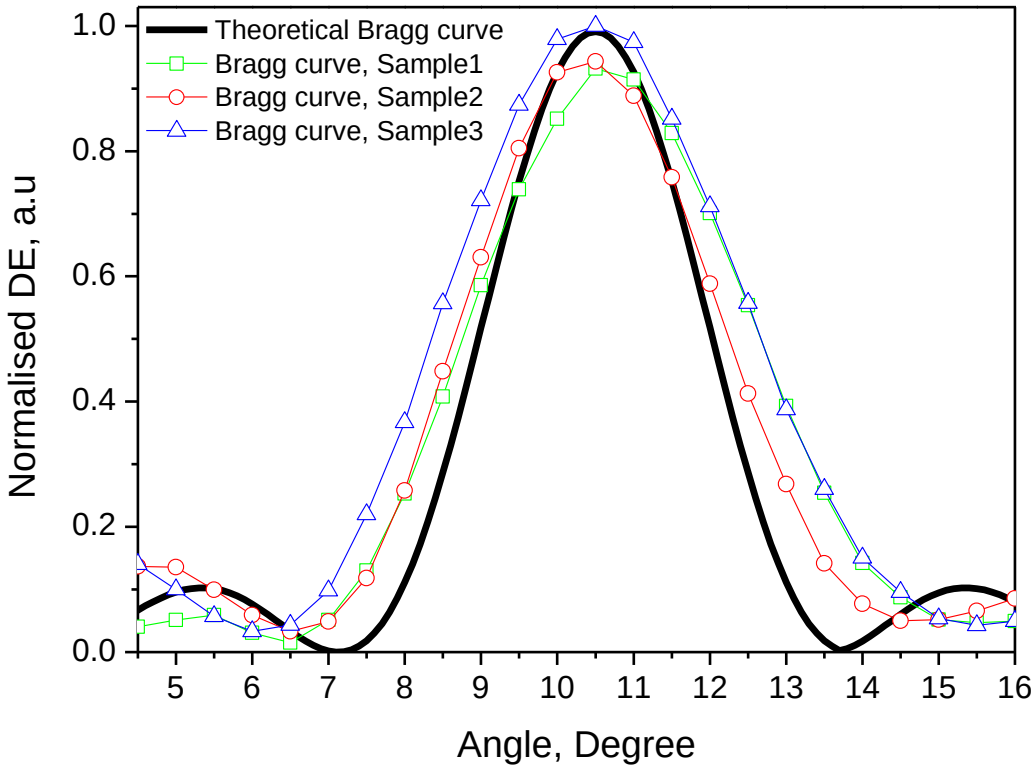

Figure 5-14 Angular selectivity curves for number of lens elements recorded at slant angle of 10.5°on flexible glass substrate with the exposure energy of 60 mJ/cm^2 at spatial frequency of 300 l/mm and sample thickness of 50 ± 5 µm.

The photograph of one of the photopolymer focusing elements recorded as described above is shown in figure 5.15. The photopolymer is sandwiched between two protective plastic layers and a single off-axis focusing element is visible towards the centre of the layer.

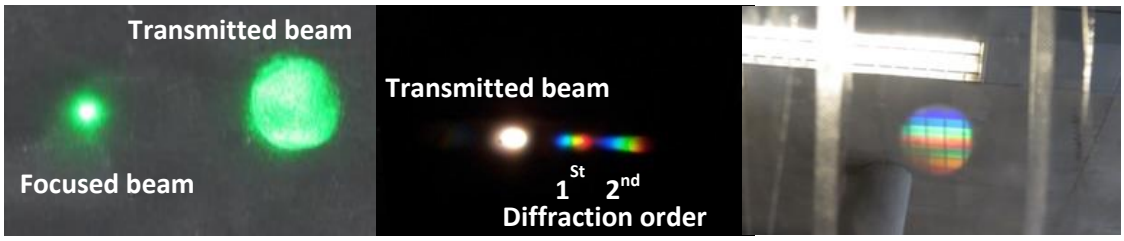

(a) **(b)** **(c)**

Figure 5-15 Photo taken through holographic lenses recorded in acrylamide photopolymer reconstructed with, a) Unexpanded laser beam, b) White light beam, c) Diffuse beam.

5.4 Conclusions

A range of on and off-axis focusing HOEs with the diffraction efficiency over 85% and large angular selectivity have been recorded successfully in acrylamide-based photopolymer. The results demonstrate that the FWHM of the recorded elements was varied depending the numerical aperture and the position of the probe beam.

The lens with the focal length of 50 mm achieved the FWHM of approximately 4.1 ± 0.1 degree and 5.5 ± 0.1 using unexpanded and expanded beam respectively. The thickness of the layers was around 50 ± 5 µm.

Recalling the results of the theoretical simulation of the HOEs are presented in chapter 3, the gratings recorded at relatively low spatial frequency are not very selective. Recorded focusing elements achieved maximum diffraction efficacy of over 85% at wavelength of 480 nm and 633 nm and about 70% at 540 nm. The results confirmed that HOEs recorded at optimum recording parameters are not very selective. Therefore they are expected to performance well in solar applications.

In addition a single lens element also successfully demonstrated on a flexible glass substrate (Corning® Willow® Glass) for the first time. The diffraction efficiency of over 90% with FWHM of around 5 degree was achieved for the later with the thickness of 40 ± 5 µm.

Reference:

1. Kogelnik H. Coupled wave theory for thick hologram gratings. Bell Syst Tech J. 1969;48(9):2909–47.

2. Akbari H, Naydenova I, Martin S. Using acrylamide-based photopolymers for fabrication of holographic optical elements in solar energy applications. Appl Opt. OSA; 2014;53(7):1343–53.

3. Garner S, Glaesemann S, Li X. Ultra-slim flexible glass for roll-to-roll electronic device fabrication. Appl Phys A. 2014;116(2):403–7.

4. Garner, S., Merz, G., Tosch, J., Chang, C., Lin, J., Kuo, C., Tseng, J., Chang, M., Lewis, S., Kohler, R., Tian, L., Simpson, L., Owens, M.,. Li, X., Huang, S., Shih, J., Wei, A., Lin, M.C., Huang, C.S., Lin, H.T., Lin, C.L., Chang, S.Y., Wang, C.T. S. Ultra-Slim Flexible Glass for Electronic Application. MRS Fall Meeting, Boston, Nov 28. 2012.

5. Garner SM, He M, Lo PY, Sung CF, Liu CW, Hsieh YM, et al. Electrophoretic displays fabricated on ultra-slim flexible glass substrates. IEEE/OSA J Disp Technol. 2012;8(10):590–5.

6 Development of light collecting devices using multiple HOEs

6.1 Introduction

The purpose of the diffractive solar collector is to gather sunlight form a large area and direct it onto a smaller area, where it can be converted to electric or thermal energy by, for example, using PV cells or thermal conversion. The advantage of using a collector is that the light can be harvested cheaply from a larger area and the energy per unit area on the converter can be increased. As mentioned in previous chapters, diffraction gratings can be used to change the direction of a light beam very efficiently but they are only efficient over a small range of angles close to the Bragg angle, so they need to be used in combination with number of different gratings if they are to be useful in collecting sunlight over most of the day.

The aim of this work is to multiplex/combine a small number of high diffraction efficiency gratings with larger angular working range so that efficient redirection of the incoming light is achieved for incident angles spanning a larger angle and light from the full range of angles falls on a single location.

An important factor is the design of the component devices or multiplexed holograms. In our earlier chapters and publications we modeled the number of gratings needed to span a wide angular range by simply adding the FWHM values. Other researchers have demonstrated the potential of multiplexed HOE devices [1],with the same approach, by recording identical gratings with up to 60% efficiency in the same layer through angular multiplexing. Here we demonstrate up to 80% efficiency in stacked gratings recorded with a range of slant angles.

We also address the issue of collection onto a single detector/convertor in a static/passive collection device. Stacked or multiplexed gratings do indeed diffract with high efficiency at a range of angles of incidence, but for each combined grating the output appears at a different output angle. In a passive collector device, directing all beam to the same location is as important as high efficiency, otherwise the energy will not be converted. In the work presented here the individual elements are designed so that they independently diffract light from a range of angles to the same location, which requires control of the slant angles for each recorded grating and careful overlap of the grating areas.

The first part of this chapter will investigate the fabrication of holographic concentrator devices by stacking a number of holographic gratings to redirect the incoming beam with larger angular working range. A preliminary design for a device for solar collection is presented, based on stacked low spatial frequency gratings/HOEs. The strengths and weaknesses of this approach are then discussed. The second part of this chapter, will demonstrate the fabrication of arrays of high efficiency holographic lenses, while making sure that the relative position, focal length and Bragg angle are appropriate to the direction of light into one location (the position of a static solar cell). It was important to design the final device to focus the incoming beam in order to improve the concentration factor.

In this chapter, the dependence of the diffraction efficiency of the HOEs recorded at spatial frequency of 300 lines/mm and 1000 lines/mm on the polarization state of the source is investigated. This study will help us to optimize the efficiency of the holographic device when used with an unpolarized light source such as the sun. The two linear polarization states are compared; S-polarization (when the electric field vibration is perpendicular to the plane of incidence and parallel to the fringes in a typical

transmission grating) and P-polarization (when the electric vector is parallel to the plane of incidence of the incoming beams).

Throughout this study, the same photopolymer composition was used with optimum recording parameters and geometry as explained in chapters 5.

6.2 Stacking methodology

The aim of this study is to increase the angular working range of the diffractive lens by stacking three layers of high efficiency optical elements on top of each other so that light is collected (and focused) from a broader range of angles. The angular range of each individual lens element is important, and work has already been done in an acrylamide-based photosensitive polymer to broaden the angular range of individual elements using holographic recording at a low spatial frequency.

The design concept for this diffractive solar collector is a combination of several low spatial frequency photopolymer gratings laminated or stacked together so that light is collected from a broad range of angles. The gratings will form a flat array that will not need to move in order to track the sun's motion across the sky. The low spatial frequency ensures that the angular selectivity of each individual grating is low so that the range of angles accepted by each individual grating is maximized and the number of gratings needed in the combined device in minimized.

Figure 6.1 shows the basic concept of the device. Here, for simplicity, the concept is illustrated for three gratings each having a working range of 6^{o} and a lens/focusing element also having a working range of 6^{o} degrees. In practice, a larger number of gratings will be needed if the working range for individual gratings is smaller and/or the

desired working range is larger. In the schematic in figure 6.1 each element is shown separately, but in the practice the gratings will be laminated together without any air gap in order to reduce reflections.

In this example the three gratings are combined to make a device that has a working range of 24 degrees (-3^o to $+21^o$). If light is incident along or near the normal (0^o angular deviation – shown in figure 6.1 (a)) it will pass through the three gratings A, B, C and be focused by the focusing element D. This element will efficiently focus light over a 6^o range or 3^o either side of normal incidence.

For light that is incident at angles between 3^o and 9^o deviation from normal, the light will be transmitted by A and B but will be on-Bragg for grating C, which will then bend the light though 6^o ensuring its correct alignment for focusing by D (as shown in Figure 6.1 (b)).

For light incident with a deviation of $9\text{-}15^o$ from normal, the direction is corrected by B and then by C before being focused by D. Similarly for light incident at $15\text{-}21^o$ all three gratings will correct the path of the incident light in sequence before it is focused by D. Gratings A,B and C are all identical in terms of grating spatial frequency and efficiency but the grating slant angle increases moving towards the top of the stack.

Examples of stacked displays on flexible glass substrates have previously been demonstrated [2]. Use of flexible substrates also enable high-volume continuous manufacturing methods such as roll-to-roll device fabrication [3].

As can be seen below, angular range of each individual lens element is important as it will determine the overall range and/or number of stacking layers needed. The following experimental work is aimed at testing this concept by stacking three layers of grating on top of each other. The key challenge is to control the working ranges of the

individual holographic elements so that when laminated together the Bragg selectivity curves overlap sufficiently with expected working range. For this study, three gratings /off axis focusing elements are then stacked together, each designed for a different angle of incidence, so that when combined, the stack is capable of focusing light incident from a broader range of angles.

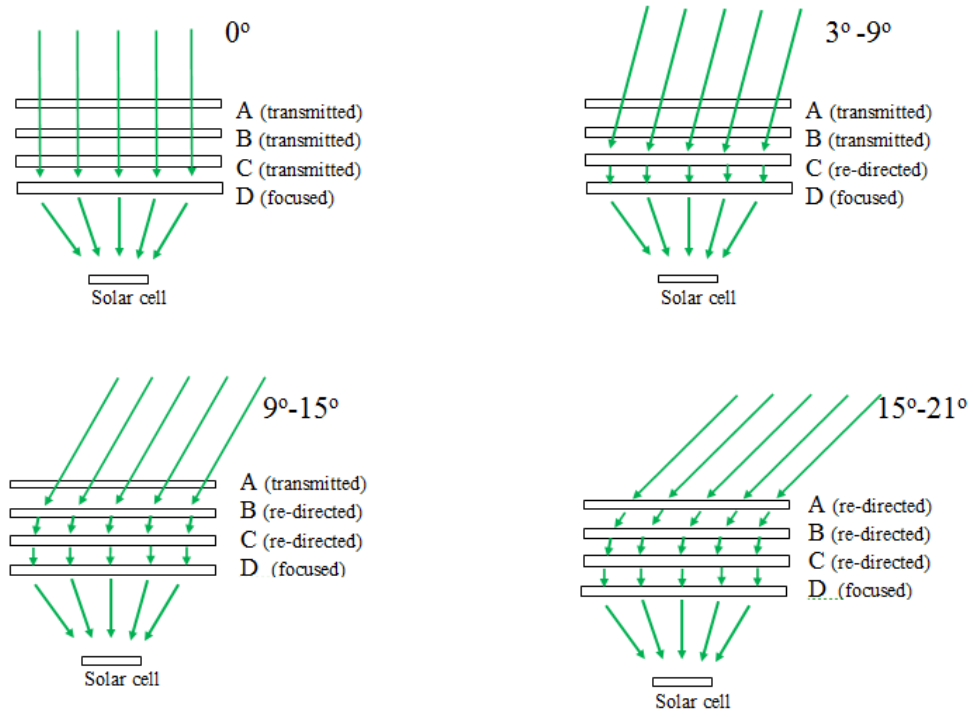

Figure 6-1 Schematic of the combined diffractive device showing the path of light incident from a range of angles.

6.2.1 Experimental study of the acceptance angle of holographic gratings before and after stacking

The first step of this study was to record range of slanted gratings with a central spatial frequency of 300 l/mm using exposure energy of 60 mJ/cm^{2}and recording intensity of 1mW/cm^2. A rotation stage (Newport, ESP 300) was used to record range of slanted gratings. Figure 6.2 shows the ray diagram for a) recording b) reconstruction beam angles of slanted gratings/HOEs. The absorption of the photopolymer layer at 633 nm is negligible even before exposure; therefore a 633 nm He-Ne laser was used as a probe beam at the Bragg angle to be enabled to characterize the diffracted intensity dependence on the incident angle of the probe beam. An optical power meter (Newport 1830-C) recorded the intensity of the diffracted beam and the data was transferred to a computer via a data acquisition card. A LabVIEW program was used to control the experiment and to record the data.

In figure 6.2, θ_1 and θ_2 are the angles of incidence of the two recording beams where θ_1' and θ_2' are the refraction angles inside photosensitive material according to Snell's law. Angle θ_B is Bragg angle which is defined as the angle between the incident beam and the grating fringes and the fringe spacing, angle φ is the angle between grating fringes and the normal, Λ is the grating period.

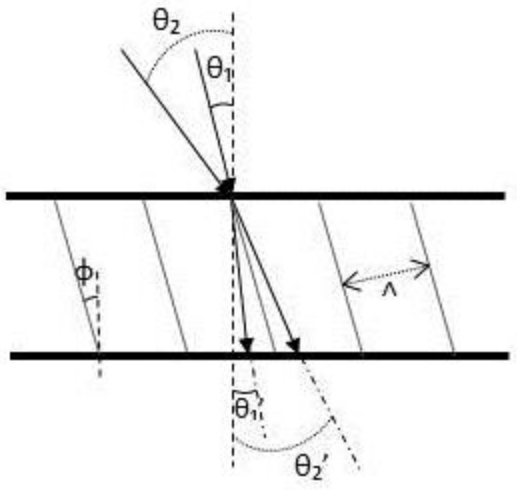

(a)

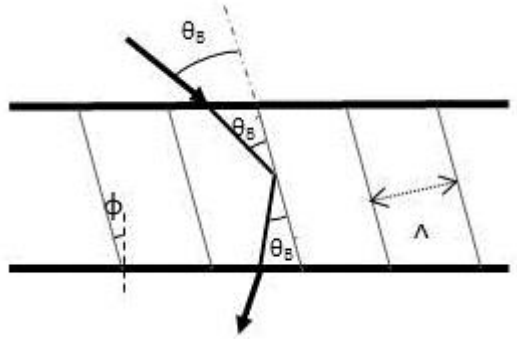

(b)

Figure 6-2 Geometry of a) recording and b) reconstruction of a slanted grating fringes in a diffractive optical element.

The variation of the diffraction efficiency with angle of incidence in the zero and first diffraction order was measured. In the recoding step, the sample holder was rotated (7°, 10.5° and 14°) away from unslanted positions and at each angle one grating was recorded. The recorded grating have a slant angles of (7°, 10.5° and 14°) respectively. The angle of the two recording beams in respect to the photosensitive sample was also varied.

The experimental results are shown in figure 6.3. The slant angles and the angle of two recoding beams outside medium (figure 6.2 A) and inside medium (figure 6.2 B) were calculated using Snell's law for the relevant wavelengths as shown in Table 6.1.

Table 6.1: Slant angles and incident angle outside and inside medium for recording and reconstruction wavelength

Wavelength	Slant angle	Angle (In air)	Angle (Inside medium)
532 nm	$\varphi = 7^{\circ}$	$\theta_1=2.42^{\circ}, \theta_2=11.58^{\circ}$	$\theta_1'=1.61^{\circ}, \theta_2'=7.69^{\circ}$
	$\varphi=10.5^{\circ}$	$\theta_1=5.92^{\circ}, \theta_2=15.08^{\circ}$	$\theta_1'=3.94^{\circ}, \theta_2'=9.98^{\circ}$
	$\varphi=14^{\circ}$	$\theta_1=9.42^{\circ}, \theta_2=18.58^{\circ}$	$\theta_1'=6.26^{\circ}, \theta_2'=12.26^{\circ}$
633 nm	$\varphi = 7^{\circ}$	$\theta_{B1}=1.55^{\circ}, \theta_{B2}=12.45^{\circ}$	$\theta_{B1}'=1.03^{\circ}, \theta_{B2}'=8.26^{\circ}$
	$\varphi=10.5^{\circ}$	$\theta_{B1}=5.05^{\circ}, \theta_{B2}=15.95^{\circ}$	$\theta_{B1}'=3.36^{\circ}, \theta_{B2}'=10.55^{\circ}$
	$\varphi=14^{\circ}$	$\theta_{B1}=8.55^{\circ}, \theta_{B2}=19.45^{\circ}$	$\theta_{B1}'=5.68^{\circ}, \theta_{B2}'=12.82^{\circ}$

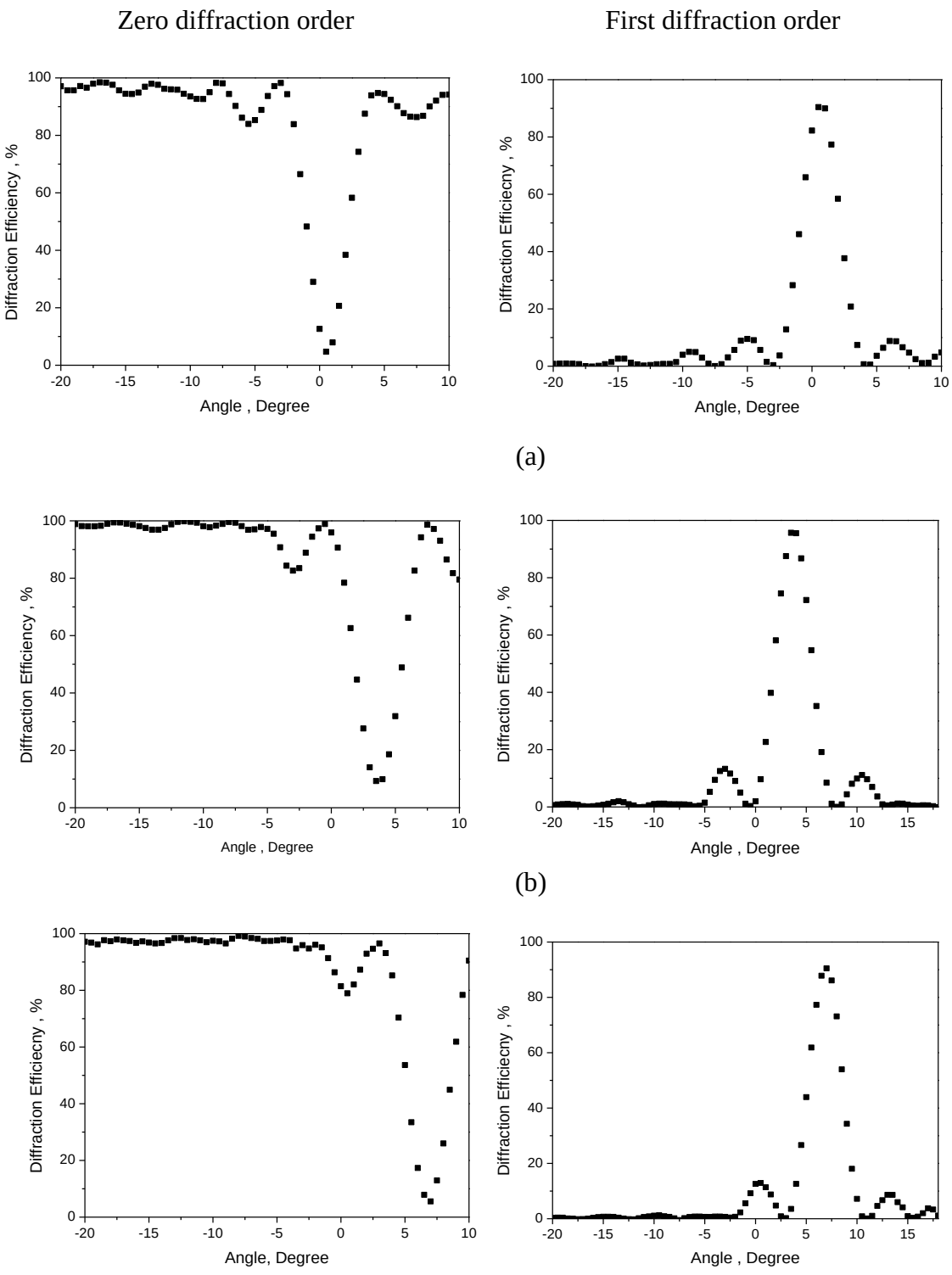

Figure 6-3 Angular selectivity curves for a grating with spatial frequency of 300 l/mm recorded in layers with thickness of 45±5 μm at range of slant angle: a) 7 degree, b) 10.5 degree and c) 14 degree before stacking.

The maximum diffraction efficiency peaks expected to be around 1.55°, 5.05° and 8.55° respectively at reconstruction wavelengths (633 nm) as shown in table 6.1. The experimental result shown in figure 6.3 verifies that the diffraction angles are as expected, and identifies any discrepancy. Any discrepancy that occurs can be explained by shrinkage of the photopolymer layer. It can also be observed that the diffraction efficiency of over 90% was achieved at spatial frequency of 300 l/mm for the layer with the thickness of 50 ± 5μm; the refractive index modulation of the layer (Δn) was calculated using equation 6.1:

$$\Delta n = \frac{\lambda \cos \theta_B \sin^{-1}(\sqrt{\eta})}{\pi d} \qquad \text{Equation 6.1}$$

where θ_B is the Bragg angle, λ is the reconstruction wavelength, d is the thickness of the photopolymer layer, η is the diffraction efficiency of the recorded grating at the Bragg angle. The refractive index modulation was found to be approximately 5.01 x 10^{-3} which is a high regime. The FWHM of the individual grating is approximately 3.0 ± 0.1 degrees.

After characterizing individual gratings, the next step was to stack three layers of gratings and compare their angular selectivity before and after stacking. However stacking the layers on top of each other require a carful control so that each grating/HOEs lies exactly on top of the other grating, there is no air gap between the layers and each element has the expected FWHM working range. In order to improve the quality of the stack device, range of flexible plastic and glass as well as rigid glass substrates was examined.

The results presented in figure 6.4 are for three layers, recorded as described previously, and then laminated into a single stack, with the grating area overlapping. They show the variation of diffraction efficiency with angle of incidence for the first order diffraction of the stack. Zero corresponds to perpendicular incidence on the top layer.

It can be observed that there is an apparent increase in the angular working range; however, we also observe an overall drop in diffraction efficiency to about 80% as well as a very significant fall-off in diffraction efficiency at certain specific angles and in the gratings after the stacking. This behavior can be explained by absorption and reflection losses at the multiple layers of substrate. Here they are laminated back to back (substrate side of one layer of grating was stacked on top of photopolymer side of second layer of grating and this was repeated for three layers). The refractive index of photopolymer and substrate are both very close to 1.5, nevertheless some losses at the boundaries must be expected.

The decrease in the diffraction efficiency after stacking the layers can be improved by investigating further methods of stacking and using different substrate (for example: flexible glasses) where the refractive index will be the same as the refractive index of photosensitive medium. In this study the optical power meter was kept at constant position relative to the incident beam to collect the light in first diffraction order.

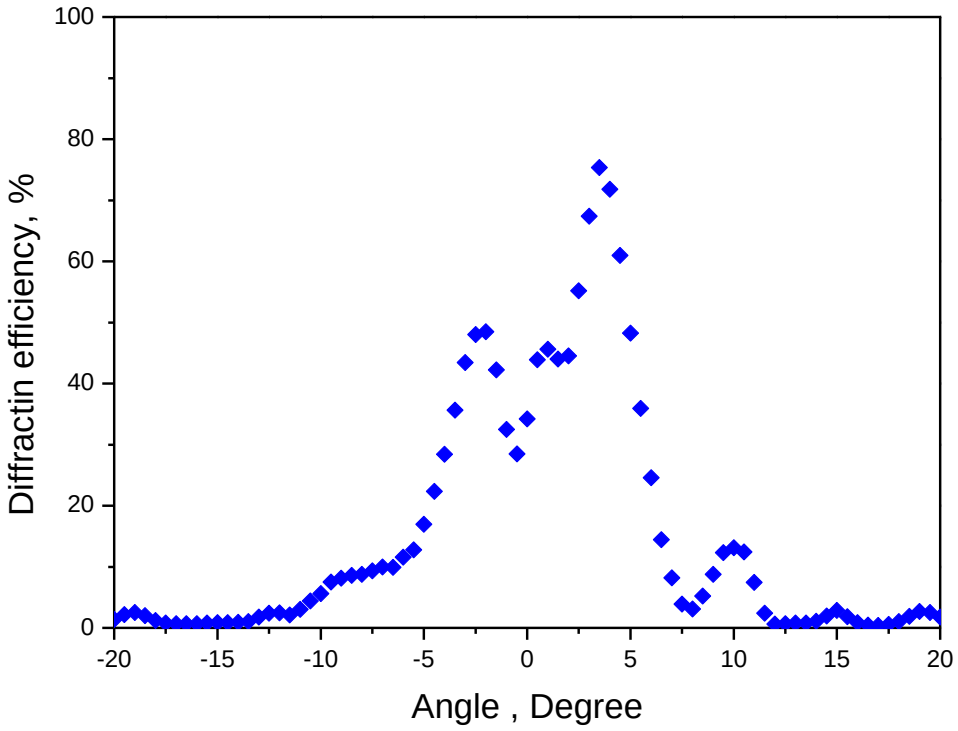

Figure 6-4 The angular selectivity curves for a three stacked gratings with spatial frequency of 300 l/mm recorded in layers with thickness of about 50 µm.

6.2.2 Experimental study of the acceptance angle of focussing elements (lenses) before and after stacking

This section reports results on the angular selectivity of stacked diffractive lenses. The diffractive focusing elements were recorded at a range of slant angles(7°, 10.5° and 14°) using optimum recording parameters as described in chapter 5. The sample holder was rotated (7°, 10.5° and 14°) away from unslanted position.

The variation of the diffraction efficiency with angle of incidence in the zero and first diffraction orders for holographic lenses is presented in figure 6.5. In this set of data, direction of rotation of the rotational stage at the recording step was opposite to the previous section; therefore the peak of the maximum diffraction efficiency was

expected to be around 12.45°, 15.95° and 19.45°.The experimental result verifies that the diffraction angles are as expected. The discrepancy at larger slanted angles is more observable and it can be explained by polymerization induced shrinkage. Assuming the shrinkage in photopolymer layer with the thickness of 50±5 μm is approximately 3% [4]. The slant angle after shrinkage, φ', was calculated by using equation 6.2:

$$\varphi' = Tan^{-1}\left(\frac{\tan\varphi}{1-\tau}\right) \qquad \text{Equation 6.2}$$

Where φ is the slant angle before shrinkage, τ is the coefficient of shrinkage (3% shrinkage correspond to $\tau = 0.03$).

The slant angles after shrinkage are 7.2°, 10.8° and 14.4° respectively. Therefore the diffraction angles are expected to be shifted slightly.

From the results presented in figure 6.5, it can also be observed that the maximum diffraction efficiency of about 80% was achieved for the sample with the thickness of 50 ± 5 μm while the FWHM was approximately 4.5 ± 0.1 degrees for each lens element. When interpreting the results it should be borne in mind that for such HOEs a range of spatial frequencies and slant angles are always present and the FWHM values of the lens element can be higher than the gratings as described in chapter 5.

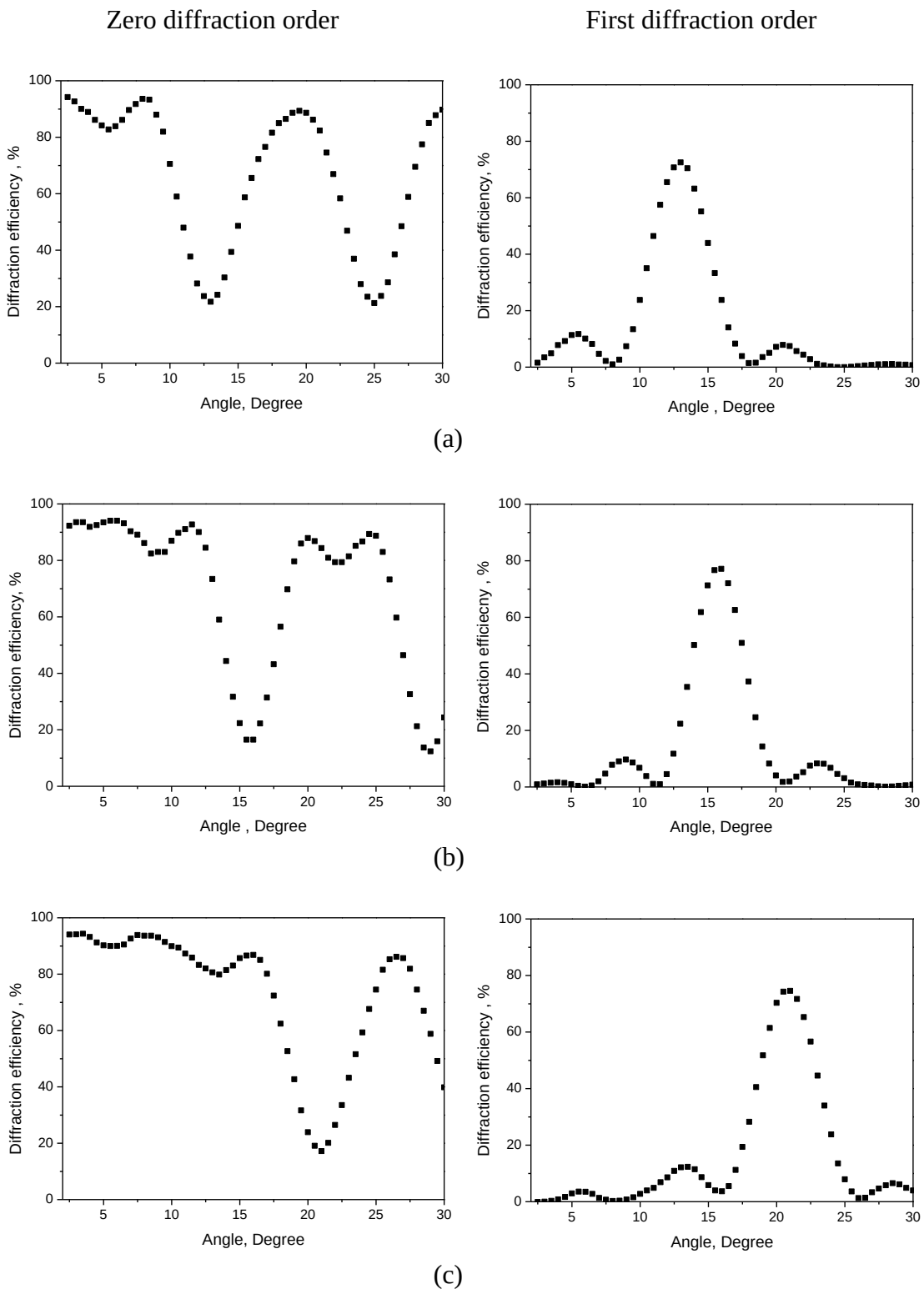

Figure 6-5 Angular selectivity curves for diffractive lenses with spatial frequency centered at 300 l/mm recorded in layers with thickness of 50 ± 5 μm on a plastic flexible substrate, at range of slant angles: a) 7°, b) 10.5° and c) 14° before stacking.

Figure 6.6 shows the variation of diffraction efficiency with angle of incidence for the first order diffraction of the stacked elements. It can be observed that the FWHM was increased to collect light from a working range of approximately 12°; however, losses in diffraction efficiency have occurred in the gratings after stacking as the diffraction efficiency has dropped to approximately 50%. Even though the layers appear to laminate together exceptionally well this reduction in efficiency may be caused by cumulative losses (scattering and reflection) at the multiple layer interfaces, since there are six interfaces in total including substrates. The decrease in diffraction efficiency after stacking the layers may be improved by using a different substrate where the refractive index will be better matched and moving to a thinner more transparent substrate with reduced birefringence, haze and scattering.

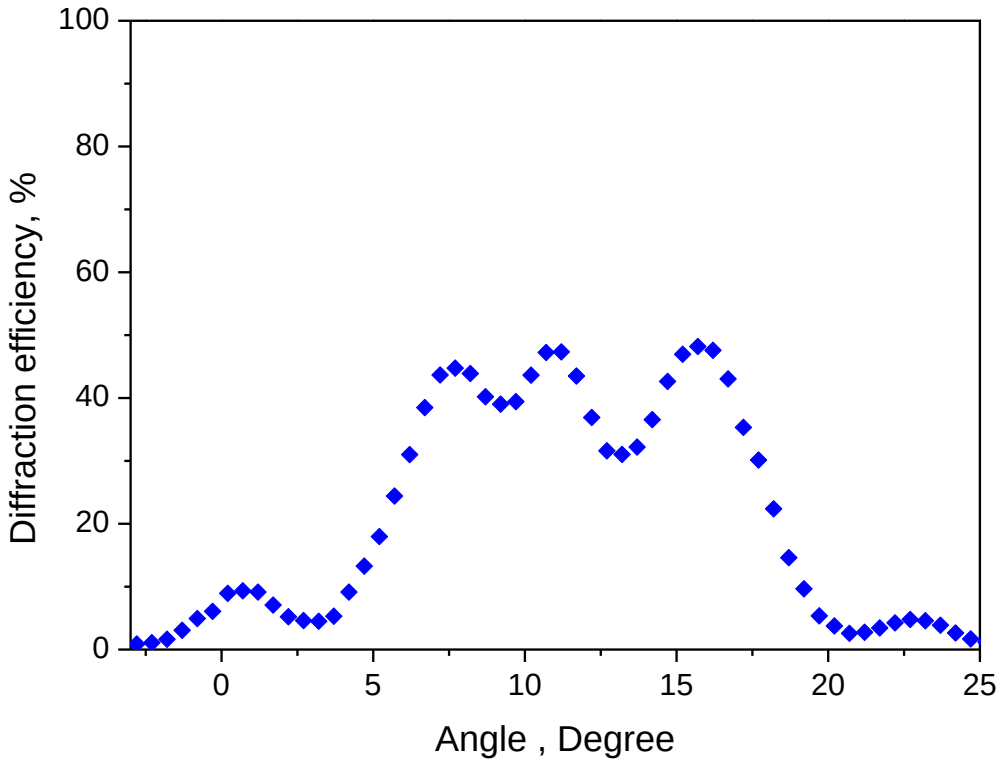

Figure 6-6 Angular selectivity curves for range of combined lens elements recorded with the exposure energy of 60 mJ/cm^2 at central spatial frequency of 300 l/mm.

6.2.3 Investigation of the acceptance angle of stacked gratings for diffraction toward a fixed location

In the above experiments, the common practice for analysis of Bragg diffraction in gratings/HOEs was used; where the angle of incidence is changed by rotating the grating/HOEs and keeping the source and detector fixed. However, in applications such as solar collection the angle of incidence will change during the day, without any relative motion between the grating and the detector or solar cell (assuming a non-tracking application).

In order to simulate this, the reconstruction step was repeated, but in this study the optical power meter (Newport 1830-C) was attached 1 cm behind the grating so that they remain fixed relative to one another. The aim of this study was to capture the total amount of incident light that would be concentrated by the holographic device in the case of a static grating and solar cell, but moving source.

In this case, to avoid any instability, the probe beam (He-Ne laser source) was kept in the constant position and sample with the attached detector were rotated around the source using rotation stage (Newport, ESP 300) as shown in figure 6.7.

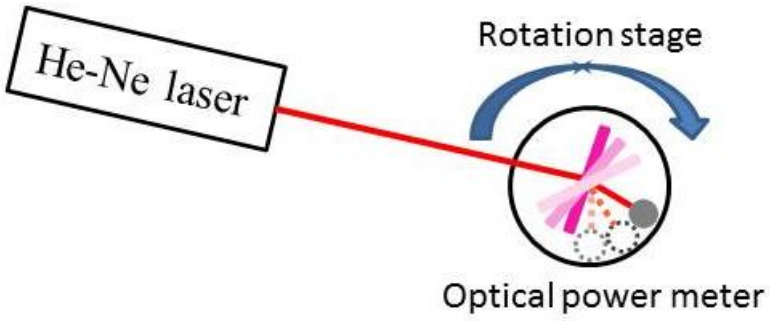

Figure 6-7 Schematic of proposed reconstruction set up

This method allows us to collect the light that is diffracted using holographic gratings/elements with a large range of angles and investigate the performance of the HOE for the various incident beam angles. In addition, it gives us the closest approximation of the efficiency with which the stacked layers will re-direct light to the fixed PV cell at wavelength of 633 nm. It brings the analysis a step closer to understanding how to design the holographic concentrator to be used in solar application.

The angular selectivity of the individual gratings, stack device and photopolymer layer with no gratings was measured using this method and results are presented below.

Figure 6.8 show plots of the % of light falling on the fixed detector as the angle of incidence of the light is varied of the three individual gratings before stacking. The 'no gratings' line shows the variation in intensity at the detector without the presence of any grating (just a layer of transparent polymer) for comparison from these results, redirection of the incident beam by the gratings can clearly be observed at the higher angles. Light incident at over 25 degrees, which would have otherwise missed the detector (or solar cell in a real application) is very efficiently captured using the gratings. However, a key issue is highlighted here. As well as directing light from higher angles to a lower angle each grating will also do the reverse. This issue was also discussed by Ludman in [5]. This is caused by the fact that each grating has two angles which the light is 'on Bragg' for diffraction (corresponding to the two beams which the grating was recorded).

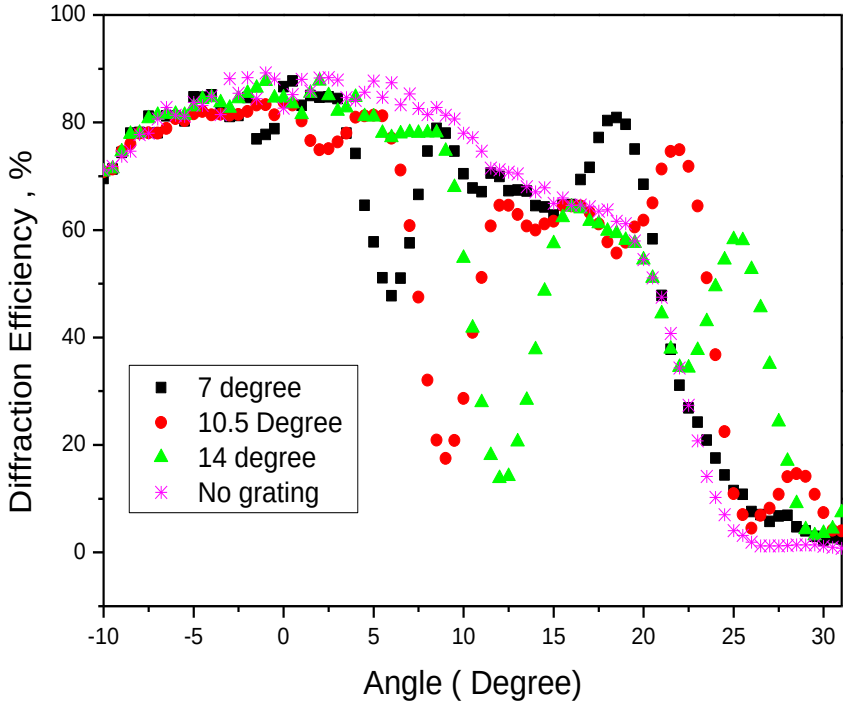

Figure 6-8 The angular selectivity curves of gratings recorded at different range of slant angles with spatial frequency of 300 l/mm in layers with thickness of about 50 µm; The recording intensity was 1mW/cm^2.

The angular selectivity of the stack of the three gratings was also measured using this method. The results are shown in figure 6.9. The same effect was observed for the stacked device. The results confirm that this method has improved the angular working range of the device. However; the increase gained at the higher angel is lost from the lower angles so that there is no net gain. Diffraction from higher angles would appear to be most useful in circumstances where grating is offset from the main path to the solar cell, such as off axis HOEs. In this way the direct light is unaffected, but the grating can usefully divert light from higher angles onto the solar cell.

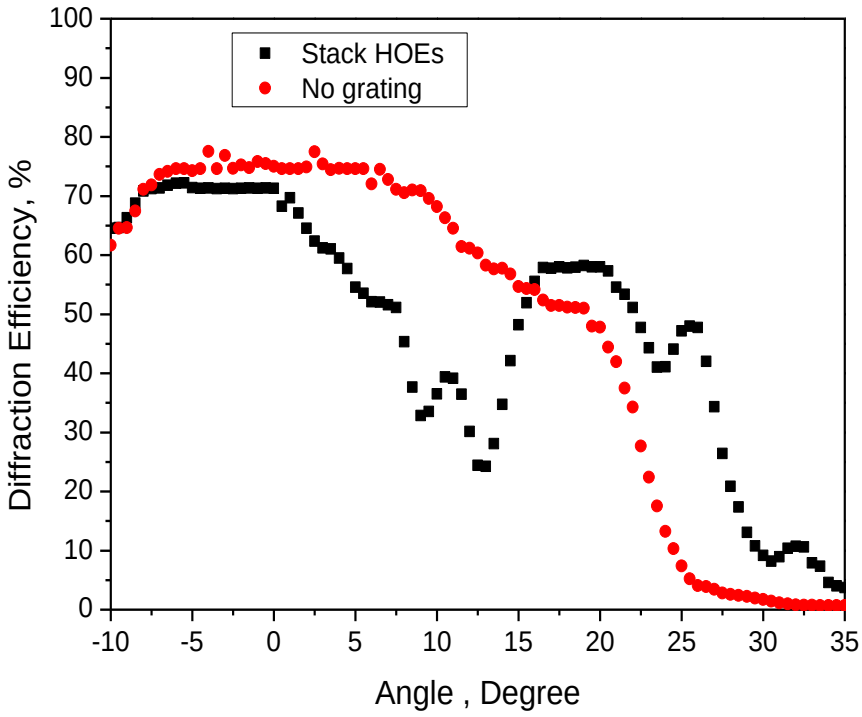

Figure 6-9 The angular selectivity curves for a three gratings stacked with spatial frequency of 300 l/mm recorded in layers with thickness of about 50 µm.

The optical properties of three substrates that have been used in this study are measured and shown in Table 6.2.The transmittance and reflectance of the three substrates available have been compared by using a laser with wavelength of 633 nm incident at 10.5 degree on the substrate and the results are shown in Table 6.2. Each transmittance and reflectance value is an average of 8 readings. The refractive index of the plastic and flexible glass substrates were measured using an Abbe refractometer (NAR-3T).

Table 6.2: The comparison of transmittance and reflectance of three substrates

Substrate	Transmittance	Reflectance	Refractive Index
Standard glass	90.1 ± 0.6 %	6.8 ± 0.5 %	1.500
Plastic	89.6 ± 1.6 %	9.7 ± 0.7 %	1.503
Flexible glass	91.9 ± 0.7 %	7.2 ± 0.9 %	1.504

6.3 Fabrication of arrays of lens

Given the issues identified with collecting light through gratings, the next stage of the research involved recording several holographic elements in proximity to one another but not overlapping. A gap of clear polymer directly above the detector/converter ensures efficient collection of direct and the holographic gratings are off-set from the centre. Using similar methodology as described previously, the study will be extended to the fabrication of arrays of HOEs side by side in order to achieve the optimum design for solar collection. The challenge here is to record arrays of high efficiency lenses in same recording layers while making sure Bragg angle is appropriate for all lenses, the focal length is constant and finally the diffracted beam hits the center of the solar cells. In order to fabricate the device, the following steps were carried out.

The first step was to record two cylindrical holographic lenses with the same focal length to focus the light with high efficiency using the optimum recording parameters and optical set up as described in chapter 5. Two sets of high efficiency cylindrical lenses with a focal length of 5 cm were recorded side by side in the same photopolymer layer with the thickness of 50±5 µm as shown in figure 6.10 A. The angular selectivity and diffraction efficiency of each element was then measured.

The second step was to make sure the diffracted beam of two lenses recorded close to each other, while there is a gap in between. In order to achieve this, first HOE was recorded using same method as previously described and then the recording medium was rotated by 180 degree and shifted slightly to the side to record the second HOE. So when the incident light passes through the center of the device, it can be collected by the solar cell as shown in figure 6.10 B. Simply, by using this method the light collected from the first HOE is focused with the off-axis to the right hand side with the focal

length of 5 cm on the center of solar cell. Then, second HOE can be designed to focus the beam in reverse direction with the same focal length. This step was not as straight forward as by adjusting the distance between the two HOEs recorded in layer, the position of the overlap of the diffracted beams was also varied. In order to avoid this issue, the angle of the diffracted beam was calculated for each element individually and the optimum distance between each element was found to be approximately 1.6 cm.

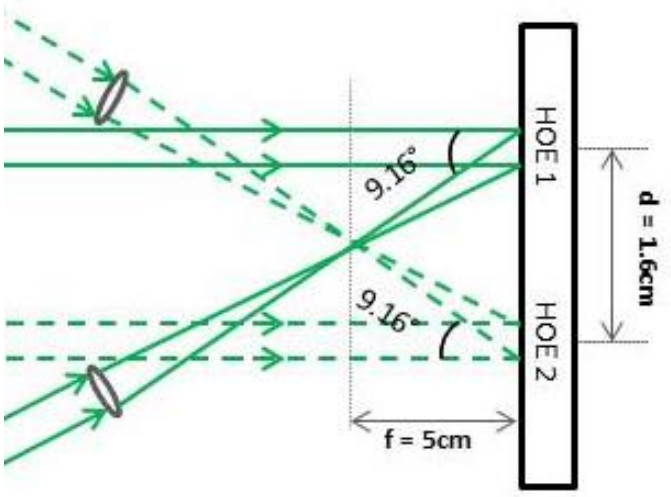

(a)

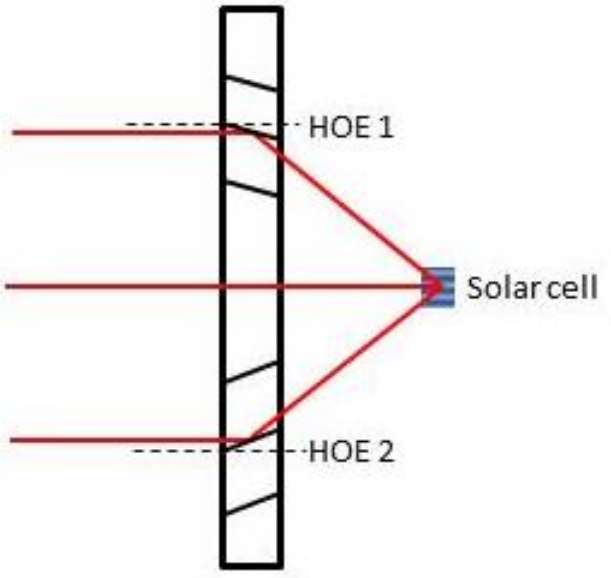

(b)

Figure 6-10 Schematic of the experimental arrangement a) recording, b) reconstruction geometry for recording arrays of lens.

The final step was to arrange the optical geometry so the two focusing elements will be on the Bragg angle when the incident light is normal to the gratings while the focal lengths of HOEs are kept at 5 cm. It was found that the HOEs recorded with slant angle of 2.66 degree (inside medium) would achieve a device which allows light to be directed to solar cells/detectors with the given specific conditions.

The performance of the recorded elements was characterised using solar simulator light source and the total current-voltage of the device collected by silicon solar cells will be presented in chapter 7.The photograph of arrays of photopolymer focusing elements recorded as described above under white light source is shown in figure 6.11.

Figure 6-11 Photo taken through holographic lenses recorded in acrylamide photopolymer reconstructed with solar simulator light source the central band of white is the diffracted, focussed light diverted by the two gratings , overlapping at the appropriate position.

6.4 Dependence of diffraction efficiency on S and P polarization of the incident beam (laser)

This section investigates one of the issues that arise when gratings are used with natural light rather than laser light, namely the polarization condition of the light source and tests the HOEs using polarized and unpolarized sources.

In this section the dependence of the diffraction efficiency of the gratings on S-polarization and P-polarization of the incoming beam at spatial frequency of 300 l/mm and 1000 l/mm is investigated. In order to achieve this, range of holographic gratings were recorded at two different spatial frequencies (300 lines/mm and 1000 lines/mm) and their performance is characterised by using unpolarised light.

The dependence of the first order diffraction efficiency of volume phase holographic transmission grating on the polarization of the incoming light has been discussed in detail by Baldry et al. [6].

The theoretical modelling for unpolarized light, S and P states for range of spatial frequencies are presented in chapter 3, section 3.4. The result shows that the lower spatial frequencies are less sensitive to polarization direction. In order to verify this experimentally, the HOEs recorded at spatial frequency of 300 lines/mm and 1000 lines/mm with the thickness of 50 ± 5 µm. This study explores the potential of HOEs in solar application with minimum sensitivity to polarization of the source.

The diffraction efficiency, η, of the recorded grating is defined here as the ratio of the intensity of the first diffraction order and the incident intensity of the probe beam. The diffraction efficiency of each HOE was determined by measuring the diffracted beam's

intensity close to the focal point. The laser was rotated 90 degree i.e. P polarized light and the experiment was repeated.

The results are presented in figure 6.12. From the result we can observe around 10% decreases in the peak diffraction efficiency for the HOE recorded at 1000 l/mm for S and P polarization at this thickness and parameters. In experimental results the percentage difference was about 16% for ± 1 diffraction order. However, a small decrease (about 6%) was also observed for the HOE recorded at 300 l/mm.

From the theoretical results presented in chapter 3, it was expected to observe about 10% and 2% decreases in diffraction efficiency between S and P polarisation for the spatial frequency of 1000 l/mm and 300 l/mm respectively for the sample with the thickness of 50 ± 5 μm.

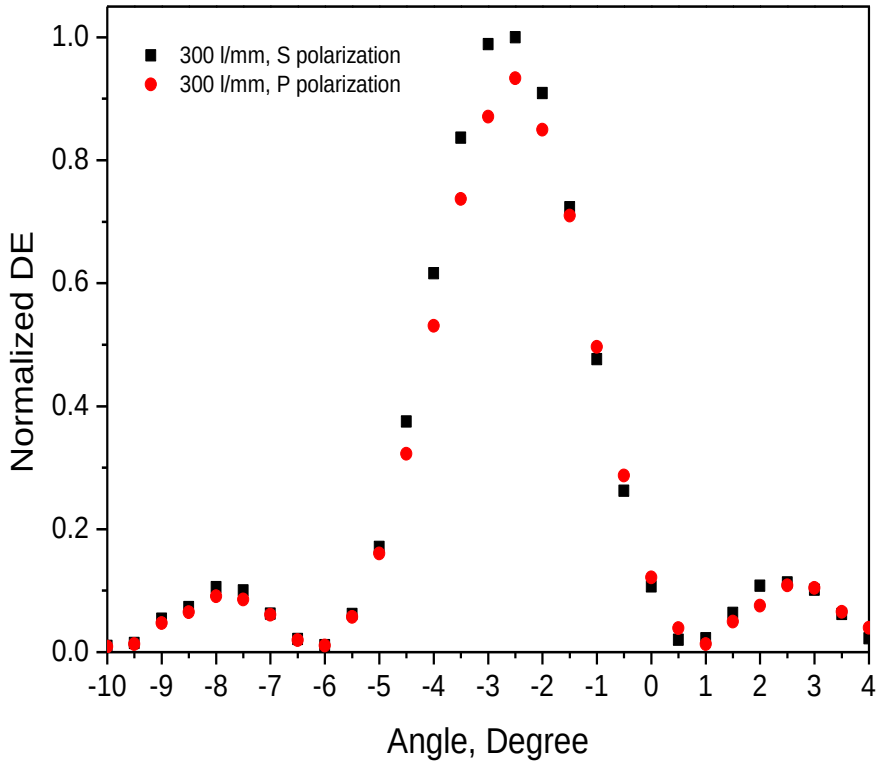

(a)

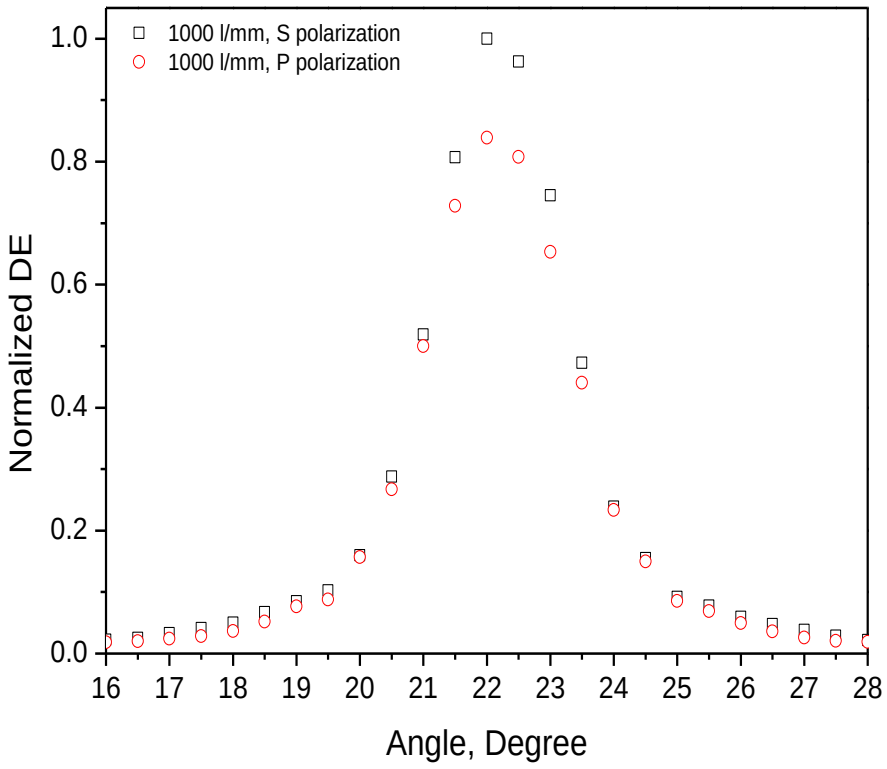

(b)

Figure 6-12 Dependence of first order diffraction efficiency on grating thickness for spatial frequency of a) 300 l/mm b) 1000 l/mm respectively. The experimental results are presented for S ▫ ▪ and P ○ • polarization.

6.5 Conclusions

The photopolymer materials used in this research can be laminated to other transparent plastics and/or multiple photopolymer layers, so implementation of stacking design is more straightforward than in other materials. The high diffraction efficiency is also important in order to minimize losses at multiple gratings. In order to increase the angular range further without reducing the diffraction efficiency of each element, a number of holograms can be stacked by laminating them together using flexible substrates. Off-axis holographic spherical and cylindrical lenses with large range of operation were successfully recorded in the photopolymer. The stacked devices were characterised in two ways: (i) the regular Bragg diffraction characteristics of the stack devices were measured. (ii) A set up was constructed to analyse their performance in a non-tracking system with a moving source and fixed detector/converter. The use of flexible substrates (such as plastic and flexible glass [7]) has significant advantages over conventional thicker glass as is flexible, conforms to the required shape, and has a reduced weight as well as thickness, implying lower losses for stacking devices. The results show significant improvement for the collection of light from the higher angles, and also highlight issues with unwanted diffraction directions in the stack. Light incident from higher angles will accumulate more losses because it is diffracted by more of the grating elements. The FWHM of the stacked device was increased to collect light from a working range of approximately 12°. The proposed method could be used in applications such as a solar collection and manipulation of beams in illumination systems.

A maximum diffraction efficiency of 90% was observed in photopolymer layers of 50± 5µm thickness at this spatial frequency. This means that over 90% of the incident light

was measured in the diffracted beam with no correction for reflection, absorption or other losses. At this spatial frequency, the HOEs with the thickness of 50 ± 5µmachieved diffraction efficiency of 80% and 50% in the single lens element and combined device, respectively.

The new approach introduced in section 6.2.3 dealt with the issue that arises with the non-tracking systems. This method has many advantages by directing light from higher angles to a lower angle; however each grating/HOE will simply undo the work of the previous one which can raise another issue.

Results confirmed that at the higher spatial frequency (Sf>1000 lines/mm), the variation in the diffraction efficiency with S and P state of polarization of the probe beam is significantly dependant on the spatial frequency and the thickness of the layer. HOEs with thickness and spatial frequency allowing for effective operation under illumination with unpolarised light were fabricated. The result confirms that our device recorded at central spatial frequency of 300 lines/mm works well for both S and P polarisation.

Reference:

1. S. Altmeyer, Y. Hu, P. Thiée, J. Matrisch MW and JS. Multiplexing of transmission holograms in photopolymer. DGaO Proceedings. ISSN: 1614-8436; 2013.

2. Mourey, D.A., Hoffman, R.L., Garner, S.M., Holm, A., Benson, B., Combs, G., Abbott, J.E., Li, X., Cimo, P., Koch, T.R. Amorphous Oxide Transistor Electrokinetic Reflective Display on Flexible Glass. IDW 2011, Nogoya. 2011;

3. Garner, S., Merz, G., Tosch, J., Chang, C., Lin, J., Kuo, C., Tseng, J., Chang, M., Lewis, S., Kohler, R., Tian, L., Simpson, L., Owens, M.,. Li, X., Huang, S., Shih, J., Wei, A., Lin, M.C., Huang, C.S., Lin, H.T., Lin, C.L., Chang, S.Y., Wang, C.T. S. Ultra-Slim Flexible Glass for Electronic Application. MRS Fall Meeting, Boston, Nov 28. 2012.

4. Moothanchery M. Studies of shrinkage in photopolymerisable materials for holographic applications. Doctoral. 2013. Available from: http://arrow.dit.ie/sciendoc/145

5. Ludman JE. Holographic solar concentrator. Appl Opt. Optical Society of America; 1982 Sep 1;21(17):3057–8.

6. Baldry IK, Bland Hawthorn J, Robertson JG. Volume Phase Holographic Gratings: Polarization Properties and Diffraction Efficiency. Publ Astron Soc Pacific. The University of Chicago Press; 2004 May 20;116(819):403–14.

7. Garner S, Glaesemann S, Li X. Ultra-slim flexible glass for roll-to-roll electronic device fabrication. Appl Phys A. 2014;116(2):403–7.

7 Enhancement of the performance of a solar cells device

7.1 Introduction

The aim of this chapter is to explore the potential of the recorded holographic elements for collecting sun light and use PV cell to convert it into electricity. The fabricated DOE devices are recorded with either spherical or cylindrical lenses as described in chapter 5.

A white light solar simulator was used as a light source; silicon solar cells used as a detector to convert the light from a solar simulator. The current-voltage characteristics of the solar cells were measured with and without the concentrating effect of the DOEs in place in front of the solar cell.

The recorded elements in this study are off-axis elements in order to make best use of direct illumination and avoid the problem of unwanted diffraction that has been highlighted in the previous chapter. Using off-axis focussing elements allows the direct light to pass through to the detector/solar cell and also gather the additional light from higher angles and redirects it into the solar cells.

In this chapter the characterisation of holographic devices in use with solar cells was carried out by comparing the I-V characteristics of the c-Si solar cell with and without the device. The experimental set up arrangements and results are described in detail below.

7.2 Theory

Measurement of the I-V curve is a standard measurement technique that quantifies any change in the current generated by the solar cell.The I-V curve shows the relationship between current and voltage in the solar when the condition of irradiation and temperature are held constant. The total current, I, for the circuit configuration shown in figure 7.1 is given by [1,2]:

$$I = I_L - I_0\left(e^{\frac{q(V+IR_S)}{nkT}} - 1\right) - \frac{V+IR_S}{R_{sh}} \qquad \text{Equation 7.1}$$

where I_L is current generated by the photoelectric effect, I_0 is the saturation current of the diode, q is the elementary charge, $1.6x10^{-19}$ Coulombs, k is a Boltzmann constant ($k=1.38x10^{-23}$ J/K), T is the cell temperature in Kelvin, n is the diode ideality factor, V is the measured cell voltage, and R_S and R_{SH} the parasitic resistances the series and shunt respectively. A typical circuit configuration that has been used is shown in figure 7.1 [3].

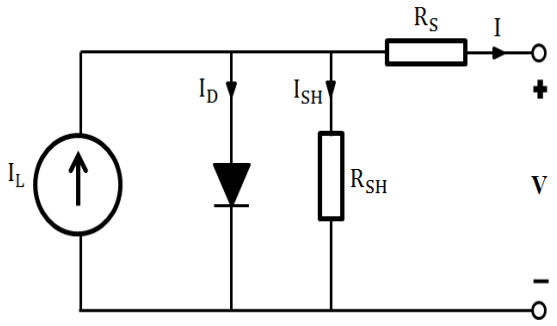

Figure 7-1 Equivalent circuit configurations used for the c-Si solar cells

Typical I-V (current-voltage) curve and P-V (power- voltage) curve of a photovoltaic device are presented in figure 7.2; these describe the capacity of the energy conversion at the specific intensity of light and temperature. It can be observed that the I-V curve ranges from the short circuit current (I_{sc}) at zero volts, to zero current at the open circuit voltage (V_{oc}).

The points which indicate the maximum power point (I_{mp}, V_{mp}), maximum electrical power is achieved and known as "knee'' of the curve. The flow of electrical charge to the external load becomes independent of output voltage when it reached the voltage well below V_{mp}. However, this behavior changes at knee point of the curve. This is simply due to the percentage increase of the charges within the solar cells instead of flowing through the load. Finally all the charges recombine internally at V_{oc}[4].

Several important parameters which can be used to characterise solar cells are as follow:

I_{sc} (Short-circuit current) - Is the maximum current value. It is produced when the cell impedance is low and is calculated when the voltage equals to zero: I (at V = 0) = I_{sc}.

V_{oc}(Open-circuit voltage) - Is the maximum potential difference across the solar cell. It occurs when the net current through the cell is zero: V (at I = 0) = V_{oc}.

J_{sc} (short circuit current density) – Since short circuit current is proportional to the area of the solar cell, the short circuit current density can be define as: J_{sc} = I_{sc}/Area of the cell.

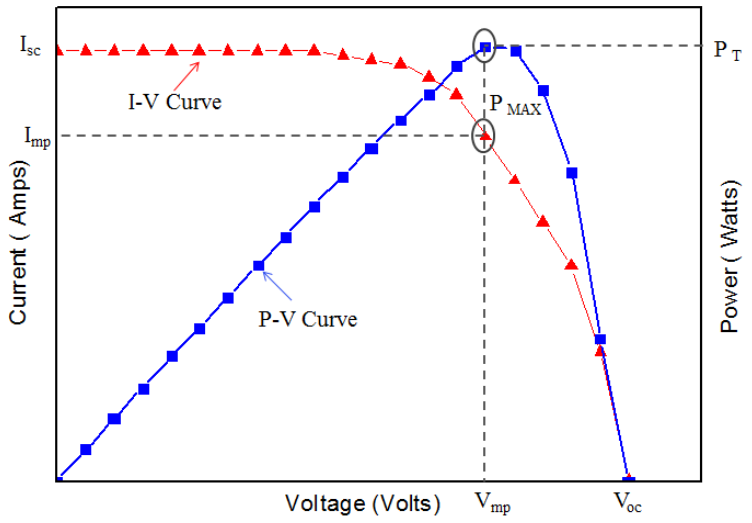

Figure 7-2 Typical Current-Voltage and Power-Voltage curves of a solar cell

7.3 Photovoltaic Technology

Photovoltaic conversion is the method of using semiconductor materials to convert solar energy into electricity, and was invented by Alexander Becquerel in 1839 [5].

In principle, absorption of a photon is by semiconducting materials such as silicon (Si), and Gallium Arsenide (GaAs) promotes an electron from the valence band to the conduction band which produces mobile electron-hole pair. The photons will not be absorbed by semiconducting materials if they don't have enough energy to overcome the band gap. When the energy of the incident photon is greater than the energy gap of the solar cell material, the photon is absorbed and thus the electron and hole can move freely through the lattice. The majority of the solar spectrum reaching the earth is composed of photons with energies greater than the band gap of silicon. In order to keep the electrons away from the hole, the silicon can be doped with other atoms to create p-n junctions. Where p-type doping adds different atom with fewer electrons and n-type doping adds an atom with more electrons in the crystal lattice of the silicon.

Adding p-type and n-type semiconductor together will lead to depletion region where the carriers in negatively charged p-type semiconductor and a positively charged n-type semiconductor are recombined as shown in figure 7.3. The difference in potential energy will separate the created charges and act as a diode [6].

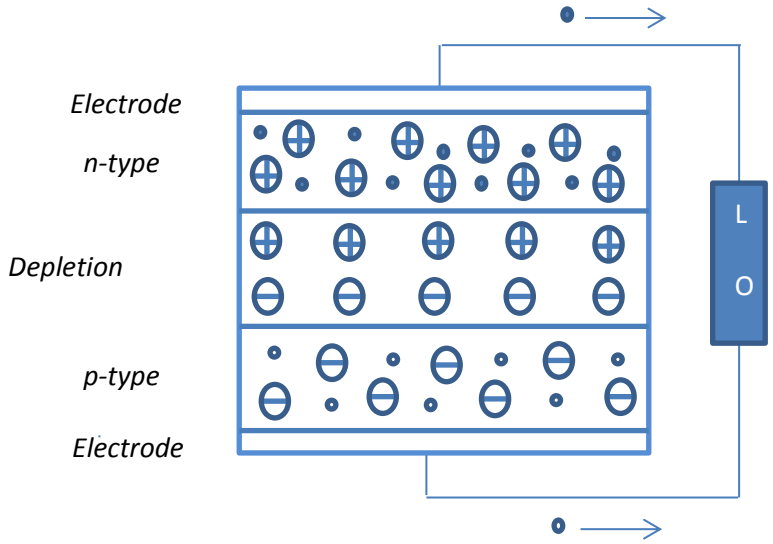

Figure 7-3 Schematic of a photovoltaic cell

7.4 Experimental

7.4.1 Solar cell preparation

In order to connect the solar cells to the source meter to measure the I-V curve, it was necessary to connect wires to the solar cells. One wire was attached to the base bar of the solar cell which is in front of the cell and the other wire was attached to the back of solar cells. The wires were secured using soldering irons and 3 mm solder wire. Then the solar cell was attached to a plastic holder in order to be able handle it safely and placed it in front of light source and diffractive elements.

In this study the area of the solar cells was controlled by using variable aperture on top of solar cells. Therefore only the specific area of the cell remains active to collect the incident light and the rest of solar cell is covered. The concentration ratio can be increased by using smaller size of solar cells compare to the size of diffractive elements. The photograph of the typical solar cells that has been used in this study is presented in figure 7.4.

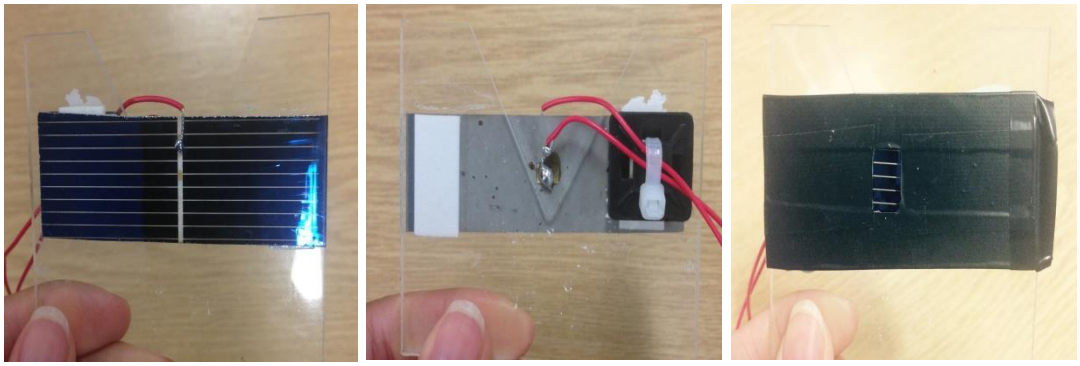

(a) (b) (c)

Figure 7-4 Photograph of the used solar cells, a) the front side of PV cell, b) the back side of PV cell, c) PV cell with the variable aperture

7.4.2 Electrical set up

The off axis elements were placed at a fixed position in front of the light source so that the diffracted beams from the higher angle was directed onto the solar cell while the direct beam is not blocked and can pass through into solar cells. The distance between the DOE and the silicon cells was arranged to be the same as the focal length of the DOEs which in this case was about 5 cm. In this study the size of the solar cells was varied between 3x3 mm^2- 8x8 mm^2.

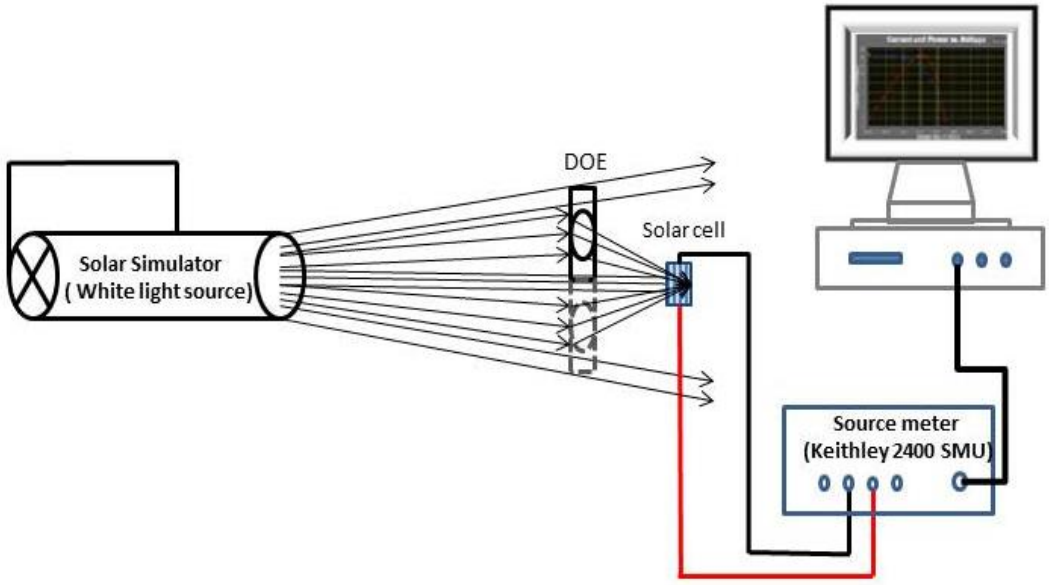

Figure 7-5 Diagram of the experimental setup for electrical measurements

I-V measurements were performed with a Keithley 2400 SMU (Source Meter Unit) as shown in figure 7.6 A with a Labview interface, using a set up described in figure 7.5. A metal halide discharge lamp (Griven, GR0262) was used as a light source which is shown in figure 7.6 B. The individual current and voltage output from each solar cell was read by a data acquisition card (DAQ). The measured current and voltage values were read into a computer using NI Labview for process and then the results were analysed.

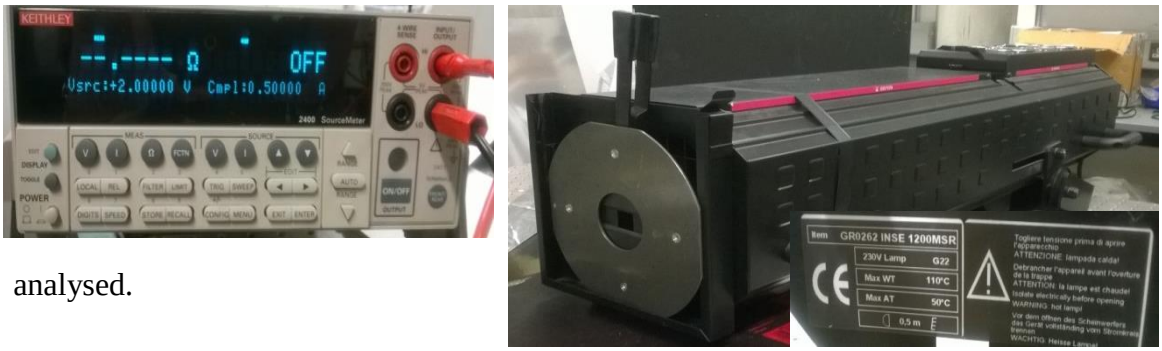

(a) (b)

Figure 7-6 Photograph of Halogen lamp solar simulator and the source meter unit

7.5 Results and discussion

7.5.1 Characterisation of the solar simulator and the c-Si solar cell

The solar simulator spectral irradiance was measured using an integrating sphere. An optical fiber. A CCD spectrometer (AVASPEC 2048-USB2) was used to monitor the photon count rate exiting at the measurement port of the integrating sphere. The results were compared to the standard solar spectrum (AM1.5G) given in [7]. The comparison is shown in figure 7.7. It was observed that the spectral irradiance of the solar simulator was very close to the standard solar spectrum.

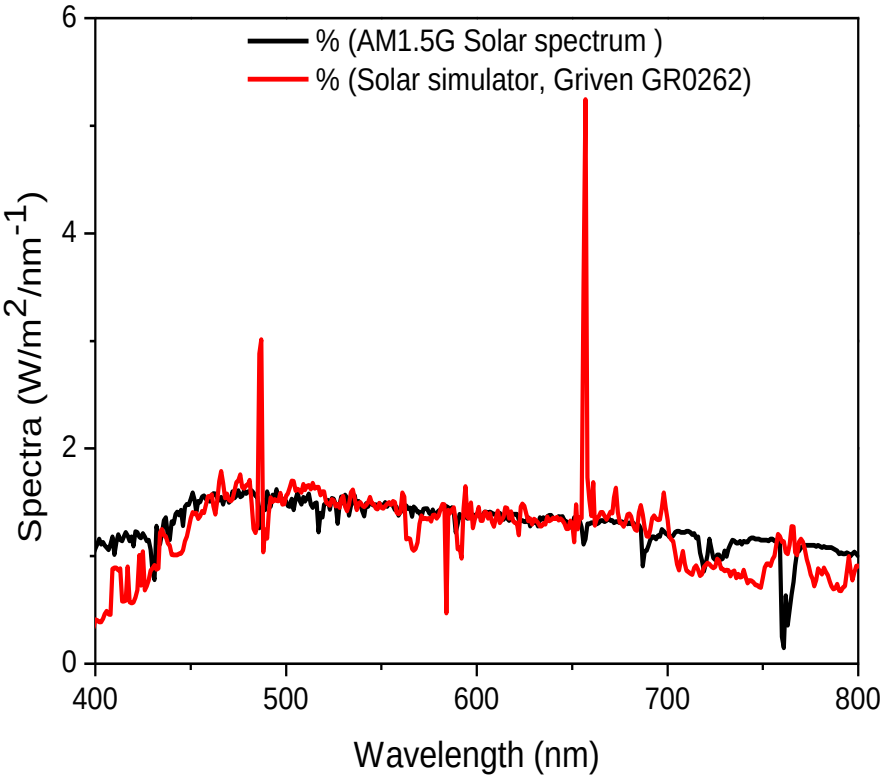

Figure 7-7 Spectral power distribution of the solar simulator and standard spectrum

In addition the silicon cell temperature was measured every 5 minutes in order to analyse the increase in temperature of the solar cells under the constant illumination from the solar simulator light source. The results are presented in figure 7.8. A rapid increase in the temperature was observed within the first 10 minutes and then the temperature remained constant at approximately 35 degrees.

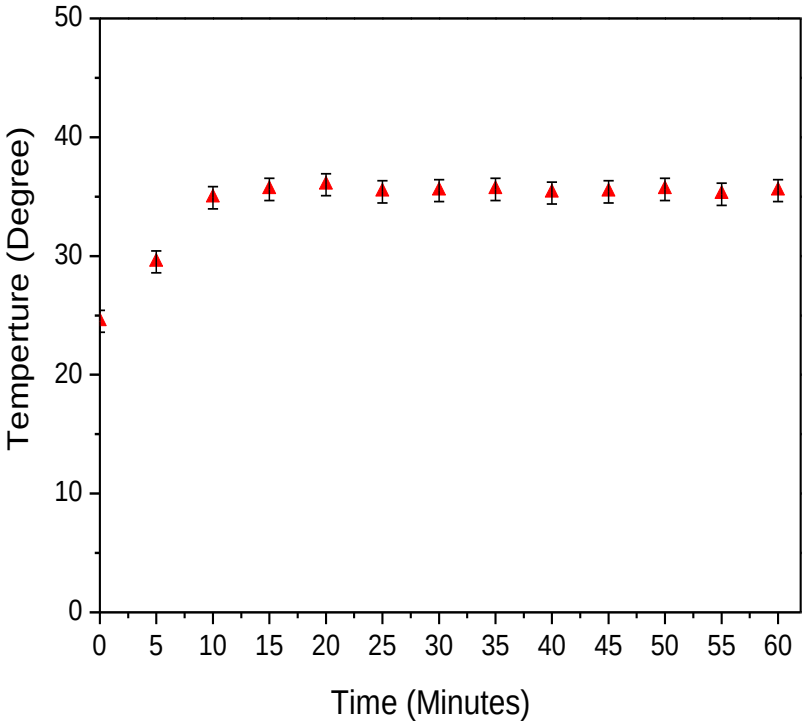

Figure 7-8 Temperature variation for Si cell under constant illumination from the solar simulator.

In order to characterise the performance of the solar cells at different intensity of the incident beam, the maximum current generated by the c-Si cell was measured for range of illuminance using digital lux meter as shown in figure 7.10. The results are presented in figure 7.9. It can be observed that there is proportional relation between output current and the illumination area. By increasing the light intensity, the current generated by the solar cells was also increased.

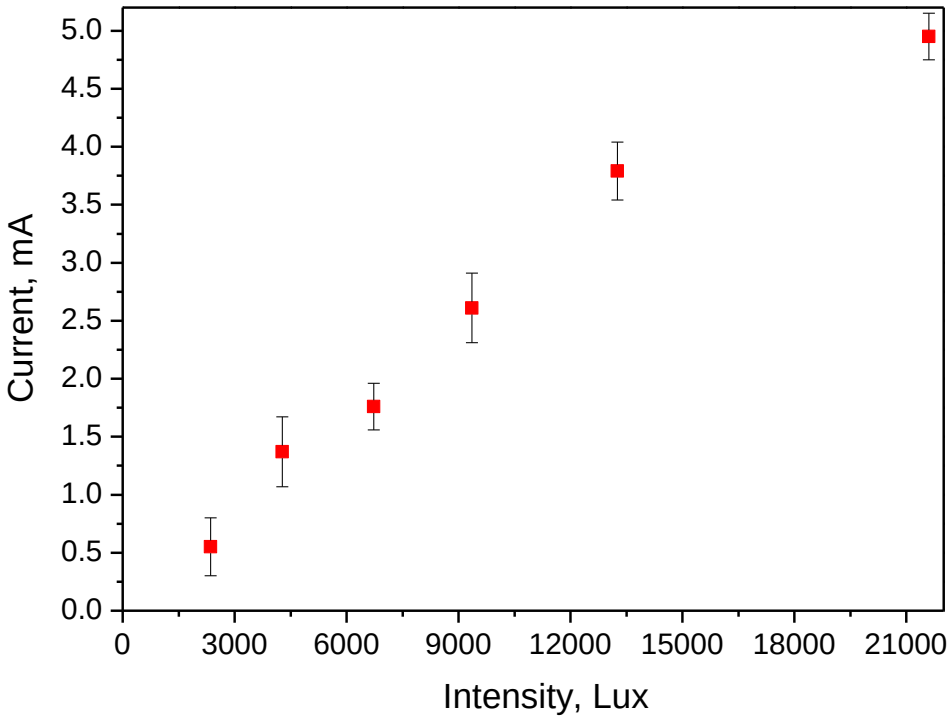

Figure 7-9 Current vs intensity for a c-Si solar cell

Figure 7-10 Lux meter

7.5.2 Characterisation and I-V curve measurement

The c-Si cells (3x3 mm^2- 8x8 mm^2, Solar capture technologies) were placed in a fixed position in front of the light source and the single/pairs of the DOE was placed in front of the solar cell in such a way as to re-direct and focus additional light onto the cell, while also focusing it (see experimental section).

The current vs applied voltages of the c-Si solar cell were measured using an electrical set up and the I-V curve was obtained as in Figure 7.11.In this study the area of the DOE was kept constant at 113 mm^2. The short circuit current (I_{sc}) output of the reference cell, i.e. without the DOE in place, is approximately 3.7 mA. When the cylindrical DOE is included, a relative increase in I_{sc} of 16 % is observed in comparison to the reference cell. When the spherical DOE is included, an increase of 32 % in signal is observed. This is a significant improvement, and is due to the fact that the light is focused in two dimensions instead of one. This measurement was then carried out for an array of two cylindrical DOEs, which resulted in an increase in the I_{sc} of 40 %.These results suggest that the use of larger arrays of cylindrical and/or spherical DOEs can achieve higher relative increase in I_{sc} for small areas of solar cells. The value for the short circuit current density (J_{sc}) of the Si solar cell was estimated using the I-V curves data for spherical/cylindrical DOE and pair of DOE relative to the solar cell area which in this case was 60 mm^2. The results are presented in Table 7.1.

Table 7.1. Calculated Jsc of the c-Si solar cell with range of DOE

	Isc mA	Δ Isc	Δ Isc % ±0.03	Jsc mA/cm^2
Bare Si	3.7			0.061
With Spherical DOE	4.9	1.2	32	0.081
With Cylindrical DOE	4.3	0.6	16	0.071
Array of two cylindrical DOE	5.2	1.5	40	0.086

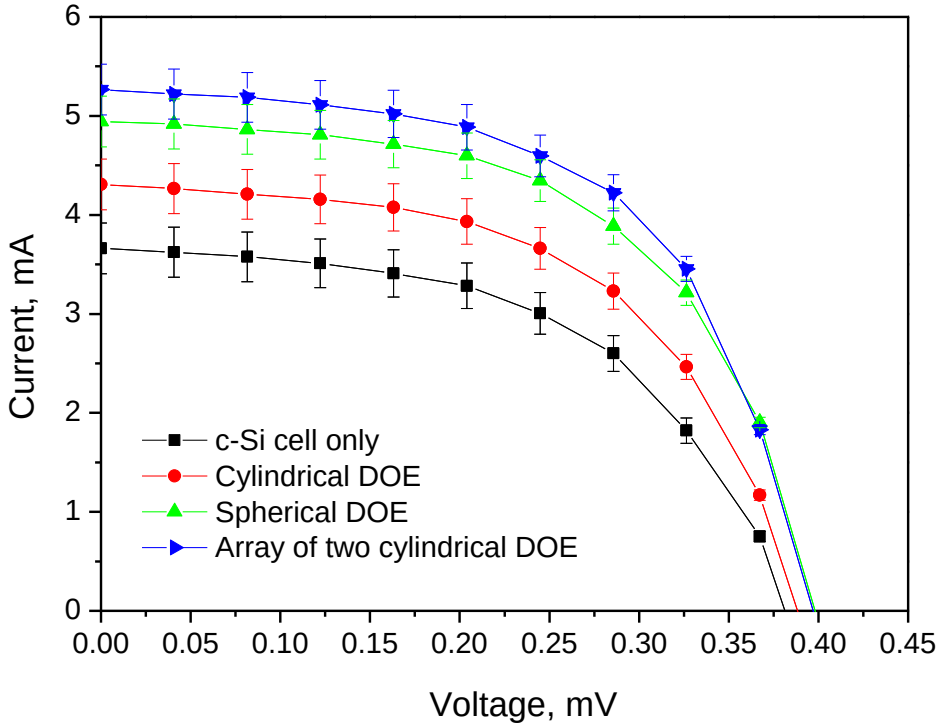

Figure 7-11 I-V curves for a c-Si solar cell (Area= 60 mm^2) without DOE, with cylindrical DOE, spherical DOE and array of two cylindrical DOE in place.

The results presented in figure 7.12 show the relative increase in the I_{sc} for the c-Si solar cells vs area of solar cells. The area of the DOE remained constant at 113 mm²

throughout the experiment while the solar cell area was varied between 9 mm^2- 100 mm^2. In order to optimize the concentration ratio, the preference is to use solar cells significantly smaller than the DOEs. These results show that there is a significant improvement in the output current obtained when using the holographic focusing elements.

It has been observed that for solar cells with area of 9 mm^2, a 52 % increase in the output current is achieved for a single spherical DOE compared to 11% for 100 mm^2 solar cell. This is because the smaller cell area makes better use of the focusing effect. A similar trend was achieved using a single cylindrical DOE; however, the concentration ratio was lower. This is due to the fact that the cylindrical DOE focus light in one plane only, forming a line at the focus rather than a spot.

The relative increase was nearly double for an array of two cylindrical DOE compared to the single cylindrical DOE. The device is capable of collecting light from a large area and redirects it into small centre of the solar cell; this can be beneficial in solar energy applications.

During this research, we had advice and collaboration with the specialist in solar energy field Dr. Sarah McCormack, Dept of Civil, Structural and Environmental Engineering, Trinity College, Ireland. After discussions it was decided to investigate the final device made with arrays of cylindrical lens in order to collect the light from a large angle and redirect it to stripe shape PV cells rather than the solar cell with small rectangular shape. The PV cells with the dimension of 10 mm x1 mm is relatively cheaper compare to the PV cell with the dimension of 1mmx1mm.

.

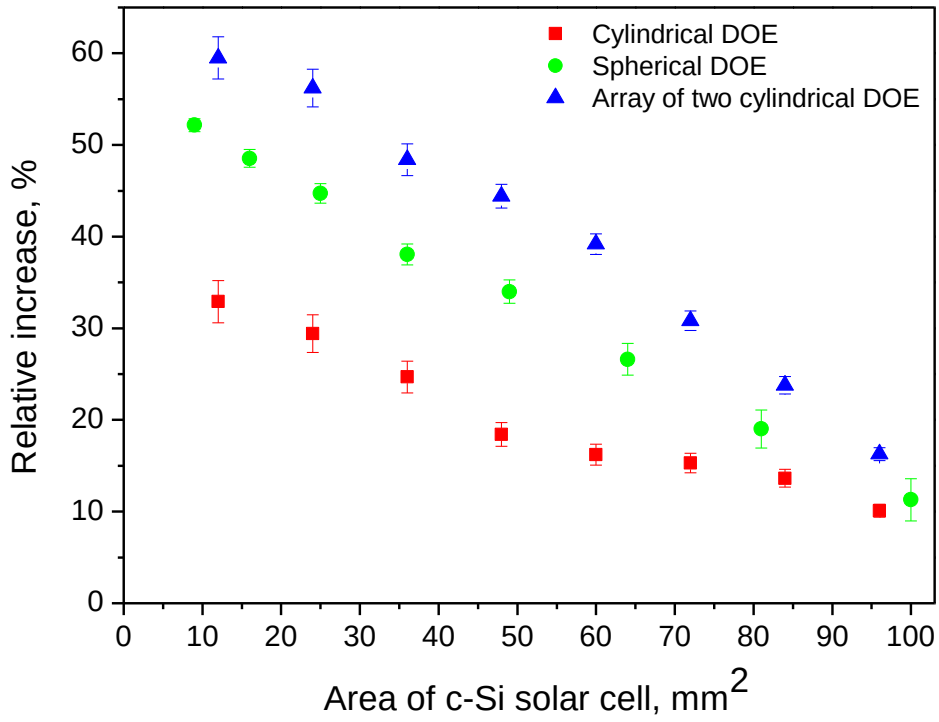

Figure 7-12 The percentage increase of output current of c-Si solar cells vs. area of the c-Si cells for spherical DOE, cylindrical DOE and arrays of two cylindrical DOEs.

This result compares very well with HOE systems reported in the literature, for example the concentrator demonstrated by Kostuk et al [8]. Their result shows that 25% increase was observed in the output from the cell over the output without the holographic element. Stacking multiple gratings or multiplexing several gratings in the same volume can extend the range of angles over which the devices are useful, as shown in previous chapters

7.6 Conclusion

A device was fabricated with the combine symmetrically arranged off axis lens elements in order to maximise the collection area and avoid unwanted diffraction of light away from the solar cell. The percentage increase achieved by using the device with c-Si solar cells and a solar simulator is reported. Relative increase of the output current of c-Si solar cells was measured for cylindrical DOE, spherical DOE and array of two cylindrical DOE to be approximately 16 %, 32 % and 40 % respectively for a cell with an area of around 60 mm^2. The results show that with arrays of DOE there is about 60% improvement in the output current obtained for the solar cells with area of 12 mm^2 when the incident light is within the acceptance angle.

Since the sun move 15 degree every hour, we would expect arrays of two to work about 30 minutes. This implies that several gratings will need to be stacked according to the protocol develop in chapter 6 in order to experience this increase for more hours. The collection area/ concentration ratio could also be further improve

Reference:

1. Earle MD. Electrons and holes in semiconductors. J Franklin Inst [Internet]. 1951 Jul [cited 2015 Oct 26];252(1):95. Available from: http://www.sciencedirect.com/science/article/pii/0016003251911027

2. Ghosh A, Norton B, Duffy A. Calculation of Colouration Voltage for a Multifunctional Glazing Powered by Photovoltaic [Internet]. Conference Papers. 2013 [cited 2015 Oct 26]. Available from: http://arrow.dit.ie/engschcivcon/66

3. Photong C. A current source inverter with series AC capacitors for transformerless grid-tied photovoltaic applications [Internet]. 2013 [cited 2015 Sep 1]. Available from: http://eprints.nottingham.ac.uk/13128/1/Thesis_Chonlatee.pdf

4. Ahmed H. Characterization of Luminescent Down-Shifting Materials and Applications for Enhanced Photovoltaic Devices.

5. Becquerel AE. Recherches sur les effets de la radiation chimique de la lumiere solaire au moyen des courants electriques. Comptes Rendus L´Academie des Sci. 1839;9:145–9.

6. Nelson J. The Physics of Solar Cells [Internet]. Imperial College Press; 2003 [cited 2015 Sep 1]. 363 p. Available from: https://books.google.ie/books/about/The_Physics_of_Solar_Cells.html?id=s5NN34HLWO8C&pgis=1

7. ASTM G173-03 Tables: Extraterrestrial Spectrum, Terrestrial Global 37 deg South Facing Tilt & Direct Normal + Circumsolar [Internet]. [cited 2015 Oct 26]. Available from: http://rredc.nrel.gov/solar/spectra/am1.5/

8. Kostuk RK, Castillo J, Russo JM, Rosenberg G. Spectral-shifting and holographic planar concentrators for use with photovoltaic solar cells. Proc SPIE. 2007;6649:66490I – 66490I – 8.

8 Conclusions and Future Work

8.1 The main achievements of the PhD research

In this thesis, the development and characterisation of recording holographic optical elements at low spatial frequency in photopolymer material for solar applications has been described. The main conclusions from this research are as follows:

- Theoretical modeling confirm that recording HOEs at low spatial frequencies is more suitable for solar application and larger angular and wavelength range of operation can be achieved with less number of elements to be multiplexed. It has been demonstrated that for the thicknesses most commonly used in acrylamide based photopolymers, spatial frequencies as low as a few hundred lines per millimetre are required in order to keep the number of multiplexed low for use in a solar collector.
- Detail study of the holographic recording at low spatial frequency was successfully carried out as well as intensity dependence in order to find the best recording conditions. It was found that the lower intensities achieved higher diffraction efficiency at spatial frequency range of 100-300 lines/mm. The maximum diffraction efficiency of over 85% was achieved with the recording intensity of 1mW/cm^2 in the layer with the thickness of 50±5 µm.
- For the first time, the HOEs were recorded in acrylamide based photopolymer at spatial frequency of few hundred line per mm.The diffraction efficiency of over 85% was achieved for recorded gratings/HOE on a layer with thickness of 50±5µm. In order to achieve high diffraction efficiency a full characterisation of the recording holographic grating in acrylamide based photopolymer was carried out at spatial frequency range of 100 lines/mm -300 lines/mm.

- Ranges of spherical and cylindrical off-axis focusing elements with focal length of 5 cm were successfully recorded in the acrylamide based photopolymer. A maximum diffraction efficiency of over 85% was achieved. The dependence of the diffraction efficiency on the diameter and position of the probe beam was determined in order to characterise the spatial frequency and slant angle of the grating component. Experimental results were compared with the theoretical results and it was found to be in good agreement with them.
- The wavelength selectivity of the recorded focusing elements was measured. Themaximum diffraction efficacy of over 85% at wavelength of 480 nm and 633 nm and about 70% at 540 nm was achieved. The results confirmed that HOEs recorded at optimum recording parameters are not very wavelength selective at these thicknesses. Therefore they are expected to perform well in solar applications.
- Off-axis holographic spherical and cylindrical lenses with large range of operation were successfully recorded in the photopolymer. This was achieved by stacking number of gratings and focusing elements on top of each other. The stacked devices were characterised in two ways: (i) the regular Braggs diffraction characteristics of the stack devices were measured. (ii) A set up was constructed to analyse their performance in a non-tracking system with a moving source and fixed detector/converter. The results show significant improvement for the collection of light from the higher angles, and also highlight issues with unwanted diffraction directions in the stack. The FWHM of the stacked device was increased to collect light from a working range of approximately 12°.

- The effect of polarization of the incident light on the diffraction efficiency of HOEs when they are used with natural light rather than laser light was investigated. The theoretical model predicted about 10% and 2% difference in diffraction efficiency between S and P polarisation for the spatial frequency of 1000 l/mm and 300 l/mm respectively for the sample with the thickness of 50 ± 5 μm. The experimental results and theoretical results confirm that our device recorded at central spatial frequency of 300 lines/mm works well for both S and P polarisation.
- A device was fabricated with the combine symmetrically arranged off axis lens elements in order to maximise the collection area and avoid unwanted diffraction of light away from the solar cell. The percentage increase achieved by using the device with c-Si solar cells and a solar simulator is reported. Relative increase of the output current of c-Si solar cells was measured for cylindrical DOE, spherical DOE and array of two cylindrical DOE to be approximately 16 %, 32 % and 40 % respectively for a cell with an area of around 60 mm^2. The results show that with arrays of DOE there is about 60% improvement in the output current obtained for the solar cells with area of 12 mm^2 when the incident light is within the acceptance angle.

  Since the sun move 15 degree every hour, we would expect arrays of two to work about 30 minutes. This implies that several grating will need to be stacked according to the protocol develop in chapter 6 in order to experience this increase for more hours. The collection area/ concentration ratio could also be further improved.

8.2 Future work

8.2.1 Further increase in working range

The next stage of the research should involve multiplexing several gratings within the HOE, since several gratings will be needed in one photopolymer -layer in order to allow light collection from a moving source. It would be interesting to explore other materials or formulations. Exposure scheduling will be used to equalize the efficiency of the gratings. Algorithms that the Centre for Industrial and Engineering Optics (IEO) group has previously developed for equalization of holograms in data storage systems will be adapted for this purpose. Our recent work demonstrates the feasibility of this approach when used in the acrylamide based photopolymer and outlines the need for optimisation of the schedule of recording[1].

The optimisation of the scheduling will involve characterizing the recording material by recording the growth of the diffraction efficiency of the grating during exposure of the photosensitive material to the laser-generated interference pattern, then devising an exposure schedule based on the results. The aim is to maximize diffraction efficiency across a range of angles. A series of holograms will be recorded using the devised schedule, and then studied for efficiency and selectivity. This would be compared to the theoretical predictions. Process will be repeated for a number of grating types and comparisons drawn. Efficiency will be measured using two methods: a) A laser source with photo detector; b) Solar simulator: [Light source (Griven GR0262) metal Halide Lamp]. The angular selectivity will be analysed using an additional rotation stage. Wavelength selectivity will be analysed with a broadband source (from an optical fibre) and a spectrometer. It would be beneficial to design and test the multiplexed device to redirect/focus the diffracted beam to a single location as described in chapter 7.

8.2.2 Development of holographic solar collectors for diffuse light

An important step in the characterisation of HOEs for solar applications will be to investigate the diffraction efficiency of HOEs for diffuse light sources.

The diffuse radiation from the sky has different properties in terms of wavelength and intensity compare to the direct radiation from the sun. And therefore it changes in wavelength, composition, intensity and direction, depending on if the weather conditions are stable over a longer period of time (clear sky or heavy overcast) or unstable in terms of fast-changing occasional cloudiness.

The percentage of the energy that can be collected from diffuse light depends on the weather conditions. The efficiency of fixed and adjustable orientation collectors has been investigated by a group in Serbia [2].

Currently Luminescent Solar Concentrators (LSC) are used as an alternative method to concentrate the diffused solar radiation, where a large transparent area of high refractive index material is doped with suitable inorganic or organic dopant material, and surrounded by a low refractive index material[3].

There are a number of researchers working to improve the efficiency of concentrators at lower cost; HOEs could provide a solution in order to concentrating the diffuse light which is challenging. Based on what has been learned from the current research, two approaches are worth further investigation.

The first will aim at the development of a HOE that directs diffuse light towards the photovoltaic cell in one step. The second approach will study the possibility of developing a more complex device that will consists of multiplexed optical elements that perform the same function in a multi-step/cascade manner.

8.2.3 Combination of HOE lens and photochemical upconversion layer in photovoltaic

HOE lenses can be developed - whereby a photochemical upconversion layer operates as the solar absorber, and is located at the focal distance of the HOE lens. The aim of using the HOE lens is to increase the localised incident photon flux and thereby increase the overall upconversion efficiency[4]. Long wavelength photons are transmitted through photovoltaic cell to an "upconversion layer". Upconverted photons are then converted to electrons at the PV cell, increasing the overall electrical power output of the PV cell. The upconversion quantum yield (photons emitted/photons absorbed) is known to increase at higher incident photon flux. Therefore, a lens array can be introduced between the PV cell and the upconversion layer. Also the upconversion layer can be directly attached to the lens (without air gap), or directly to a spacing layer used to position upconversion layer at a precise lens position (e.g. at the lens focal length). Due to their Bragg selectivity, HOE lenses have the potential to selectively diffract/focus specific wavelength regions of interest.

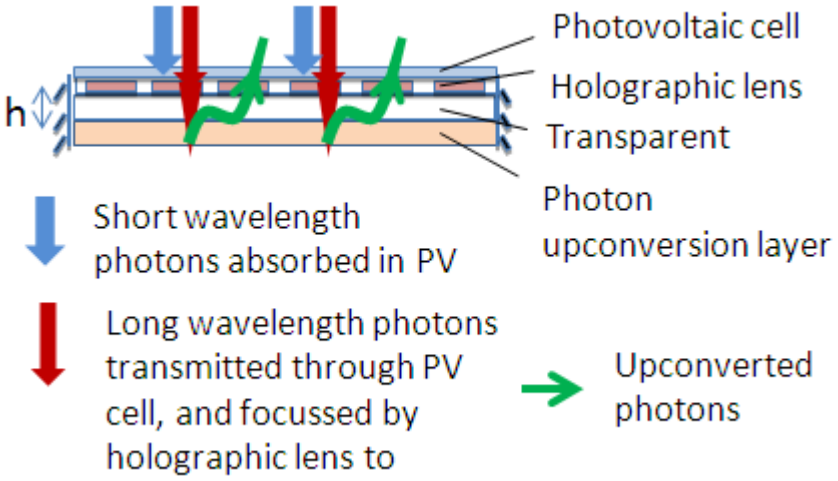

Figure 8-1 Configuration of the proposed cell

8.2.4 Combination of HOE lens in window

In this study the HOEs with high diffraction efficiency at low spatial frequency recorded in acrylamide based photopolymer and their performance were characterised. The results confirm that HOEs can be used to redirect and focus the incoming beam. It would be interesting to utilize the output of this thesis and the results of recent confidential work in IEO to make photopolymer couplers to design additional collection elements that can be applied to window glass so that semi-transparent gratings could re-direct light onto solar panels at the glass edge or window sill.

Reference:

1. Naydenova I, Akbari H, Dalton C, Pang C, Wei T, Toal V. Photopolymer Holographic Optical Elements for Application in Solar Energy Concentrators. "Holography - Basic Princ Contemp Appl. 2013;

2. Pucar M, Despic A. The effect of diffuse/indirect light on the energy gain of solar thermal collectors. Renew Energy. 2005;30(11):1749–58.

3. Verbunt PPC, Debije MG. Progress in Luminescent Solar Concentrator Research: Solar Energy for the Built Environment. World Renewable Energy Congress. 2011. p. 2751–8.

4. Baluschev S, Yakutkin V, Miteva T, Wegner G, Roberts T, Nelles G, et al. A general approach for non-coherently excited annihilation up-conversion: Transforming the solar-spectrum. New J Phys. 2008;10.

Dissemination of the PhD research

Journal publication

- Hoda Akbari, Izabela Naydenova, and Suzanne Martin, "Using acrylamide-based photopolymers for fabrication of holographic optical elements in solar energy applications," Appl. Opt.53, 1343-1353 (2014), Citation: 5

- Hoda Akbari, Izabela Naydenova, Lina Persechini, Sean M. Garner, Pat Cimo, and Suzanne Martin, "Diffractive Optical Elements with a Large Angle of Operation Recorded in Acrylamide Based Photopolymer on Flexible Substrates," International Journal of Polymer Science, vol. 2014, Article ID 918285, 7 pages, (2014).

- HodaAkabri, Izabela Naydenova, Hind Ahmed, Sarah McCormak, Suzanne Martin,"Acrylamide based photopolymer holographic concentrators for the enhancement of C-Si solar cell performance", Prepared for submission.

Book Chapter

- Naydenova I., Akbari H., Bade D., Dalton C., Yahya M., Ilyas M., and Pang V.T.C, Wei T., Martin S.,"Photopolymer holographic optical elements for application in solar energy concentrators", published online in InTech, (2013).

Conference proceedings

- Akbari H., Naydenova I., Kennedy M., Doran J., Martin S, "Design and Study of Acrylamide-based Photopolymer Holographic Optical Elements for Solar Application", 2nd International Conference on Sustainable Energy Storage, 19th-21st of June 2013, Trinity College Dublin, Ireland.

- Akbari H., Naydenova I., Martin S., "Diffractive optical elements with an increased angular and wavelength range of operation for application in solar collectors", Proc. SPIE 9508, Holography: Advances and Modern Trends IV, 95080J (May 8, 2015).

Oral presentations

- Akbari H., Kennedy M., Doran J., Naydenova I., Martin S., "Characterization of Holographic Optical Elements for solar collector application", DIT Annual Postgraduate Research Symposium, Dublin Institute of Technology, Dublin, Ireland, 2nd November 2012.

- Akbari H., Naydenova I., Martin S., "Fabrication of holographic optical focussing element for use in solar concentrator" Photonics Ireland, Queen's University Belfast, Northern Ireland, 4th- 6th September 2013.

- Akbari H., Naydenova I., Martin S., "Characterization of a holographic structure with an increased angular and wavelength range of operation for application in solar collectors'', COST MEETING, Advances in Optofluidics: Integration of optical control and photonics with microfluidics, Dublin Institute of Technology, Ireland, 24th-25th April 2014.

- Akbari H., Naydenova I., Martin S. "Characterization of a holographic structure with an increased angular and wavelength range of operation for application in solar collectors", II International Conference on Applications of Optics and Photonics , Aveiro, Portugal, 26th-30th May 2014.

- Akbari H., Naydenova I., Martin S; "Diffractive optical elements with an increased angular and wavelength range of operation for application in solar collectors", SPIE Optics + Optoelectronics, Holography: Advances and Modern Trends IV, Prague, Czech Republic, 13 - 16 April 2015.

Poster presentations

- Akbari H., Naydenova I., Martin S., "Study of acrylamide based photopolymers Holographic Optical Elements at low spatial frequency for solar application", 11th Mediterranean Workshop and Topical Meeting "Novel Optical Materials and Applications", Cetraro, Italy, 10th-15th June 2013.

- Akbari H., Naydenova I., Kennedy M., Doran J., Martin S, "Design and Study of Acrylamide-based Photopolymer Holographic Optical Elements for Solar Application", 2nd International Conference on Sustainable Energy Storage, Trinity College Dublin, Ireland, 19th-21st of June 2013.

- Akbari H., Kennedy M., Doran J., Naydenova I. , Martin S., "Advantages of the use of Holographic Optical Elements for solar concentrators", Institute of Physics Ross medal competition, Royal College of Surgeon, Dublin, Ireland, 30th March 2012.

- Akbari H., Naydenova I., Kennedy M., Doran J., Martin S., "Holographic Optical Elements for application in solar collector", 3rd Generation PV cells, European PV Cluster 3 Meeting &Ephocell: Luminescent Solar Concentrators Workshop, Barcelona, Spain, 2nd-3rdOctober 2012.